



---

**European Commission**  
**Research Programme of the Research Fund for Coal and Steel**

**INNOSEIS**

**Valorization of innovative anti-seismic devices**

**WORK PACKAGE 4 – DELIVERABLE 4.3**

**Volume on case studies for upgrading existing buildings**

Coordinator:

National Technical University of Athens - NTUA, Greece

Beneficiaries:

Universitatea Politehnica Timisoara - UPT, Romania

Politecnico di Milano - POLIMI, Italy

Universita Degli Studi di Napoli Federico II - UNINA, Italy

Universita di Pisa - UNIPI, Italy

Rheinisch-Westfaelische Technische Hochschule Aachen - RWTH, Germany

Instituto Superior Tecnico - IST, Portugal

Universitet po Arhitektura Stroitelstvo i Geodezija - UACEG, Bulgaria

Universiteit Hasselt - UHasselt, Belgium

Maurer Sohne Engineering GmbH & CO KG - MSE, Germany

Convention Europeenne de la Construction Metallique ASBL - ECCS, Belgium

Grant Agreement Number: 709434

05/03/2017

## **AUTHORS:**

NATIONAL TECHNICAL UNIVERSITY OF ATHENS – NTUA  
Institute of Steel Structures  
15780 Athens, Greece  
Chapter 2  
Authors: Kelly Kouniaki, Panagiotis Tsarpalis, Ioanis Vayas

NATIONAL TECHNICAL UNIVERSITY OF ATHENS  
Institute of Steel Structures  
15780 Athens, Greece  
Chapter 3  
Authors: Chatzimichail Michalis, Panagiotis Tsarpalis, IoannisVayas

POLITEHNICA UNIVERSITY TIMISOARA  
Steel Structures and Structural Mechanics department  
Ioan Curea Street, no.1, Timisoara, Romania  
Chapter 4  
Authors: Calin Neagu, Florea Dinu, Dan Dubina

UNIVERSITET PO ARCHITEKTURA STROITELSTVO I GEODEZIJA  
Department of Steel and Timber Structures  
1 Hr. Smirnenki blvd. 1046 Sofia, Bulgaria  
Chapter 5  
Authors: Tzvetan Georgiev, Lora Raycheva

UNIVERSITA' DI PISA – UNIPI  
Department of Civil and Industrial Engineering  
Largo Lucio Lazzarino 1, 56122, Pisa, Italy  
Chapter 6  
Authors: Caterina Buscaglione, Silvia Caprili, Francesco Morelli, Nicola Mussini, Walter Salvatore

UNIVERSITA' DI NAPOLI FEDERICO II – UNINA  
Department of Structures for Engineering and Architecture  
Via forno vecchio 35, 80134, Napoli, Italy  
Chapter 7  
Authors: Raffaele Landolfo, Mario D'Aniello

**MAURER SOHNE ENGINEERING GMBH & CO. KG - MSE**

Frankfurter Ring 193

80807 Munich, Germany

Chapter 8

Authors: Emanuele Gandelli, Christiane Butz, Francesco Morelli, Andrea Piscini

# CONTENTS

<b>CONTENTS .....</b>	<b>IV</b>
<b>1 INTRODUCTION .....</b>	<b>VIII</b>
<b>2 UPGRADING OF A SEVEN-STORY REINFORCED CONCRETE BUILDING IN ATHENS BY AN INERD-TYPE BRACING SYSTEM .....</b>	<b>1</b>
2.1 GENERAL .....	1
2.1.1 Introduction .....	1
2.1.2 Description of existing building.....	1
2.1.3 Description of upgrading measures.....	3
2.2 ANALYSIS OF THE EXISTING BUILDING.....	5
2.2.1 Linear modelling, analysis and safety checks for the existing building ..	5
2.2.2 Nonlinear modelling and analysis of the building .....	7
2.3 DESIGN OF THE UPGRADED BUILDING .....	9
2.4 CONFIRMATION OF BEHAVIOR OF UPGRADED BUILDING BY NON- LINEAR ANALYSIS.....	13
2.5 CONCLUSIONS.....	16
2.6 REFERENCES.....	16
<b>3 RETROFITTING OF A SIX-STORY REINFORCED CONCRETE HOTEL IN THE ISLAND OF RHODES BY A FUSEIS SYSTEM .....</b>	<b>18</b>
3.1 GENERAL.....	18
3.1.1 Introduction .....	18
3.1.2 Description of existing building.....	18
3.2 ASSESSMENT OF EXISTING BUILDING .....	22
3.2.1 Simulation .....	22
3.2.2 Model for the non-linear static analysis .....	23
3.2.3 Modal analysis .....	26
3.2.4 Non linear-static analysis .....	27
3.3 RETROFIT .....	27
3.3.1 Design of FUSEIS beam link systems.....	27
3.3.2 Modal analysis .....	31
3.3.3 Non-linear static analysis .....	33
3.4 CONCLUSIONS.....	34
3.5 REFERENCES.....	35

<b>4 SEISMIC RETROFIT OF AN EXISTING R.C. BUILDING USING STEEL SHEAR PANELS .....</b>	<b>36</b>
4.1 GENERAL.....	36
4.1.1 Introduction .....	36
4.1.2 Description of building.....	36
4.1.3 Retrofitting of the building .....	42
4.1.4 Conclusions .....	49
4.2 STRUCTURAL DETAILING .....	49
4.2.1 Longitudinal direction .....	49
4.2.2 In transversal direction .....	50
4.3 REFERENCES.....	51
<b>5 SEISMIC UPGRADING OF AN EXISTING INDUSTRIAL BUILDING USING CONCENTRICALLY BRACED FRAMES WITH MODIFIED BRACES .....</b>	<b>52</b>
5.1 CBF-MB .....	52
5.1.1 Introduction .....	52
5.1.2 Description of the building.....	52
5.2 BASIC ASSUMPTIONS AND DESIGN .....	57
5.2.1 Basic design assumptions.....	57
5.2.2 Preliminary selection of modified braces.....	57
5.2.3 Preliminary check of brace slenderness.....	59
5.2.4 Simulation .....	60
5.2.5 Design for static combinations .....	61
5.3 SEISMIC ANALYSIS.....	61
5.3.1 Seismic design situation.....	61
5.3.2 Response Spectrum Analysis .....	62
5.4 DETAILED DESIGN.....	63
5.4.1 Damage limitation – limitation of interstorey drift.....	63
5.4.2 Second order effects .....	64
5.4.3 Final verification of dissipative members.....	65
5.4.4 Transition stage .....	65
5.4.5 Capacity design of non-dissipative members.....	66
5.5 STATIC NONLINEAR ANALYSIS .....	68
5.5.1 Model for Static Nonlinear Analysis.....	68
5.5.2 Application of N-2 method.....	71
5.5.3 Comparison of results after SNA.....	73
5.6 BRACE SECTION DETAILING AND CONNECTION DESIGN.....	75

5.7	STRUCTURAL DETAILING .....	76
5.8	REFERENCES.....	77
<b>6</b>	<b>SEISMIC UPGRADING OF AN EXISTING R.C. INDUSTRIAL BUILDING IN ITALY THOROUGH STEEL-SELF CENTERING DEVICES .....</b>	<b>79</b>
6.1	GENERAL.....	79
6.1.1	Introduction .....	79
6.1.2	Description of case study building.....	79
6.2	ANALYSIS OF THE CASE OF STUDY.....	81
6.2.1	Linear modelling, analysis and safety checks .....	81
6.2.2	Nonlinear modelling and analysis of the building .....	83
6.3	RETROFIT OF THE EXISTING CASE STUDY BUILDING.....	88
6.4	CONCLUSIONS.....	92
6.5	REFERENCES.....	93
<b>7</b>	<b>SEISMIC REHABILITATION OF AN EXISTING R.C. BUILDING USING TRIANGULAR SHAPED HYSTERETIC DEVICES .....</b>	<b>94</b>
7.1	GENERAL.....	94
7.1.1	Introduction .....	94
7.1.2	Description of case study building.....	94
7.2	ANALYSIS OF THE CASE STUDY.....	97
7.2.1	Non-Linear modelling, analysis and safety checks of the original building.....	97
7.3	RETROFIT OF THE EXISTING CASE STUDY BUILDING.....	102
7.4	CONCLUSIONS.....	107
7.5	REFERENCES.....	108
<b>8</b>	<b>SEISMIC RETROFIT OF AN EXISTING INDUSTRIAL STEEL BUILDING USING MOON SHAPED HYSTERETIC DEVICES.....</b>	<b>109</b>
8.1	Introduction .....	109
8.2	Description of case study building.....	109
<b>9</b>	<b>ANALYSIS OF THE CASE STUDY .....</b>	<b>110</b>
9.1	Linear and non-linear modelling.....	110
9.2	Nonlinear static analyses .....	113
<b>10</b>	<b>RETROFIT OF THE EXISTING CASE STUDY BUILDING .....</b>	<b>115</b>
<b>11</b>	<b>CONCLUSIONS .....</b>	<b>119</b>
<b>12</b>	<b>REFERENCES.....</b>	<b>120</b>



## **1 INTRODUCTION**

This Volume presents six design examples of the seismic upgrade/retrofit of existing buildings adopting innovative seismic systems and devices. They have been developed within the activities of the European disseminating project INNOSEIS by six eight academic parthners. The Volume illustrates all the principal aspects of the seismic upgrade/retrofit design.

The examples cover different structural typologies, from residential to industrial buildings, consider both steel and reinforced concrete buildings, and the case studies analyzed are located in different seismic zones of the European territory.

The degree of the seismic upgrading (complete retrofit or upgrading) has been choesen, for each case study, on the base of the specific characteristic of the case study itself and of the dissipative device considered.

## **2 UPGRADING OF A SEVEN-STORY REINFORCED CONCRETE BUILDING IN ATHENS BY AN INERD-TYPE BRACING SYSTEM**

### **2.1 GENERAL**

#### *2.1.1 Introduction*

This case study refers to the seismic upgrade of an existing reinforced concrete building, located in Athens. The building was designed and constructed in the 1970s in accordance with old seismic regulations that did not include any dynamic analyses or special detailing provisions. Although the building was not damaged from previous earthquakes, an upgrade to comply with the current seismic regulations had to be performed in order to use it as an office building. This upgrade is carried out introducing vertical bracings connected to the structure with dissipative pin INERD type connections.

#### *2.1.2 Description of existing building*

The existing structure is a seven (7) story reinforced concrete building with two basement levels located in Athens. It has a rectangular shape of area 660,0 m<sup>2</sup>, plan dimensions 33,0x20m and an overall height 26,0 m (Figure 2.1 and Figure 2.2). The story heights range between 3,0 and 4,2 m, while the heights of the basement levels are 2,7 and 3,3 m.

Floors 1 to 5 are typical floors with identical plan dimensions, while floors 6 and 7 have reduced dimensions with re-entrant corners.

The columns are of rectangular cross section, that start with dimensions 70x70cm at the ground and gradually reduce over the height, ending to square shape 30x30cm at the top floor. The dimensions and the reinforcement of the internal columns are shown in Table 2.1.

The slabs in all floors are flat slabs resting on the columns, which have a widened capital (Table 2.1). The slabs at the top floor are conventional slabs resting on beams of dimensions 20x55 cm.

The basements are provided with full shear walls along their perimeter and are considered rigid in both lateral directions.

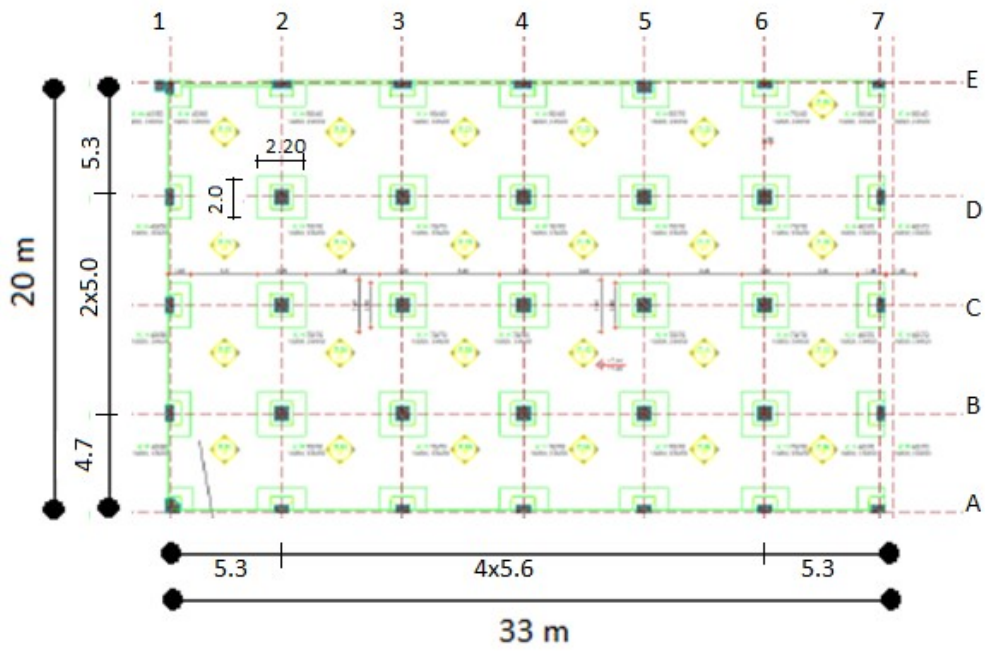


Figure 2.1 Dimensions in plan of typical floor

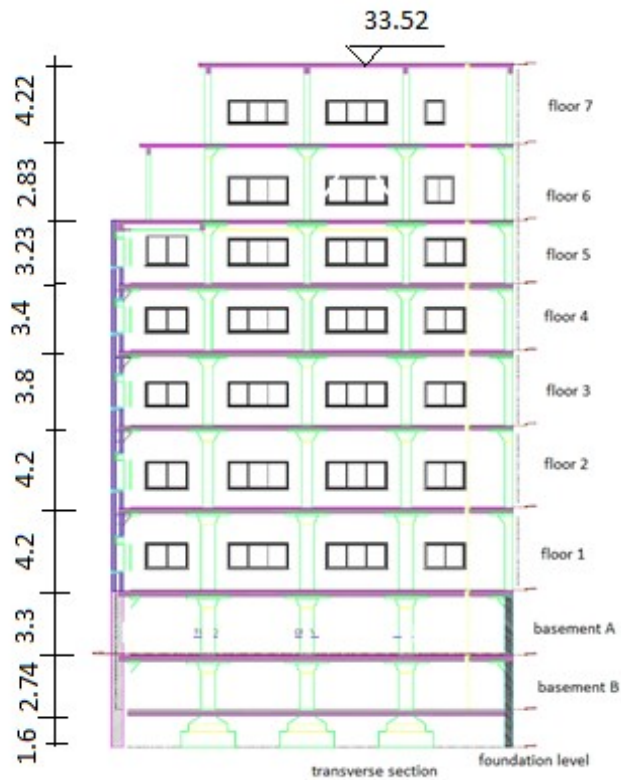


Figure 2.2 View in transverse direction

Table 2.1: Dimensions of typical columns with reinforcement and slab depths

Floor	Columns			Depth of slabs [cm]
	Dimensions [cm]	Longitudinal reinforcement	Transverse reinforcement	
Basement B	75x75	12Φ20	Φ6/20	30
Basement A	70x70	12Φ18	Φ6/20	30
Floor 1	70x70	12Φ20	Φ6/20	26
Floor 2	55x55	12Φ16	Φ6/20	24
Floor 3	50x50	8Φ16	Φ6/15	24
Floor 4	40x40	8Φ14	Φ6/18	24
Floor 5	35x35	4Φ16	Φ6/20	24
Floor 6	35x35	4Φ16	Φ8/20	10
Floor 7	30x30	4Φ16	Φ6/20	13

### 2.1.3 Description of upgrading measures

The building was designed and constructed in the 1970s, at a time where the Greek seismic regulations were based on a simple check to resist horizontal forces of some proportions of the vertical loads, but did not include any specific detailing measures for the flat slabs that are part of the seismic resistant system. The building had to be upgraded for office use to comply with current seismic regulations according to Eurocode 8, despite the fact that it was not damaged during past earthquakes in Athens.

The building is upgraded by providing vertical concentric bracings of inverted V-shape along its perimeter (Figure 2.3). The bracings are connected at their top to steel beams which are placed below the slabs and are simply connected to the columns. The connection between the steel beams and the brace was by means of dissipative pins of INERD type that protect the bracings from buckling and allow their replacement after a strong seismic event. At their bottom end the braces are connected conventionally to the columns, i.e. they are bolted to gusset plates. The overall bracing scheme is shown in Figure 2.4.

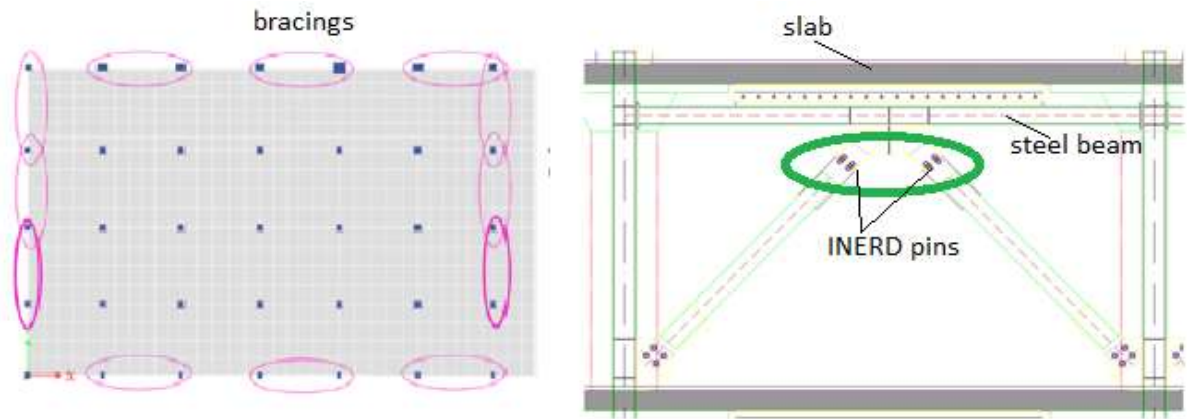


Figure 2.3 Bracings in plan and position of dissipative pins

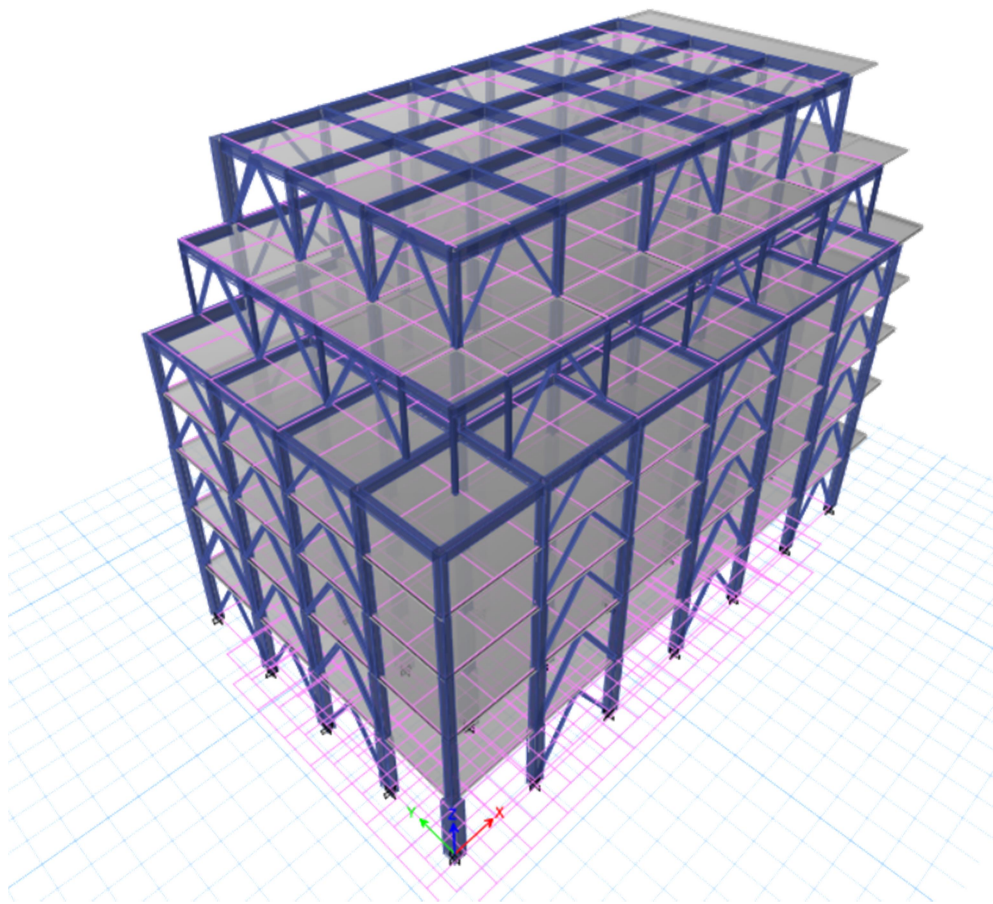


Figure 2.4 Upgraded building with concentric bracings

## 2.2 ANALYSIS OF THE EXISTING BUILDING

### 2.2.1 Linear modelling, analysis and safety checks for the existing building

The material properties for an existing building are determined as a function of the reliability level and the knowledge level. The reliability level for this building is assumed as “satisfactory”, so that the partial safety factors for resistance may be taken as equal to  $\gamma_c = 1,5$  for the characteristic strength of concrete,  $\gamma = 1,0$  for the mean strength of concrete and to  $\gamma_s = 1,15$  for the reinforcing steel. The mean strength of concrete was taken from the expression  $f_{cm} = f_{ck} + 8$  MPa. The construction materials are C/20/25 for the concrete and S400 for the reinforcement. Figure 2.5 shows the adopted material properties as introduced in the software.

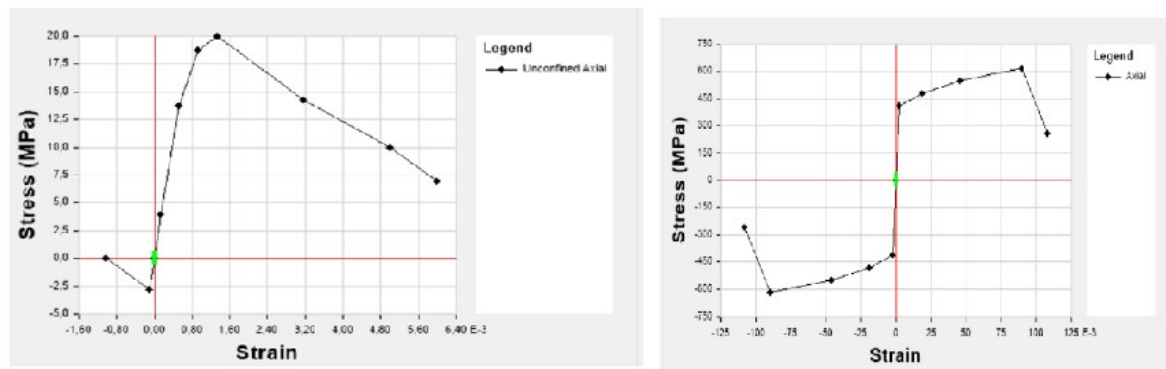


Figure 2.5 Stress-strain curves for concrete and steel

The existing building was modeled in the ETABS 2015 software. The overall analysis model, Figure 2.6, includes only the structure above ground, due to the fact that the basements have shear walls along their perimeter and are not subjected to substantial lateral displacements. The beams and columns are represented by beam elements, the slabs by shell element, while the diaphragm action of the slabs is accounted for by introduction of appropriate restraints. The columns are considered as fixed at the base due to the presence of the basement. The stiffness of all concrete elements is taken as 50% of the geometrical stiffness to account for cracking.

Following loads were taken into account:

Permanent loads G

Self-weight of r.c.:  $\gamma_c = 25$  kN/m<sup>3</sup>

Self-weight of structural steel:  $\gamma_s = 79$  kN/m<sup>3</sup>

Additional permanent loads:  $g_2 = 0,70$  kN/m<sup>2</sup>

Variable loads Q

Floors:  $q = 3,8 \text{ kN/m}^2$

Balconies:  $q = 4,0 \text{ kN/m}^2$

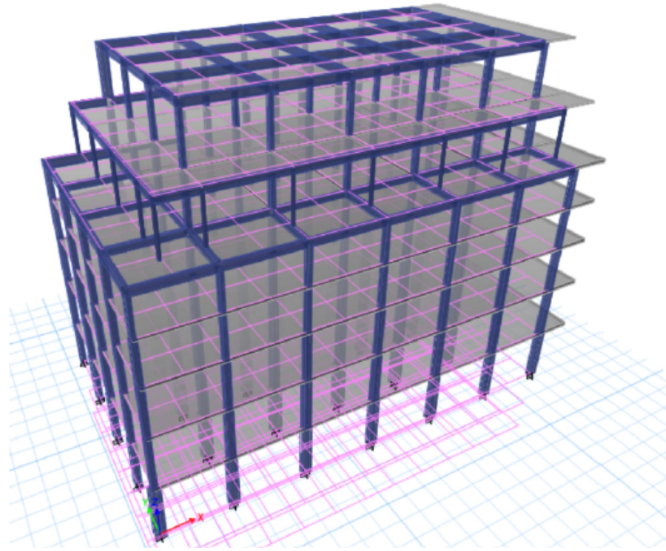


Figure 2.6 Analysis model of the existing building

Seismic action is defined according to Eurocoded 8 as following:

PGA = 0,16g,

Soil conditions B with corner periods  $T_1 = 0,15\text{sec}$ ,  $T_2 = 0,50\text{sec}$

Damping ratio 4%

Importance factor  $\gamma_I = 1,0$

q-factor = 1,5.

Figure 2.7 shows the modal shapes and the periods of the structure. It may be seen that the 1<sup>st</sup> modal shape corresponds to transverse vibrations, the 2<sup>nd</sup> to longitudinal, while the 3<sup>rd</sup> to rotations. 20 modes have to be taken into account in order to capture 90% of the total mass.

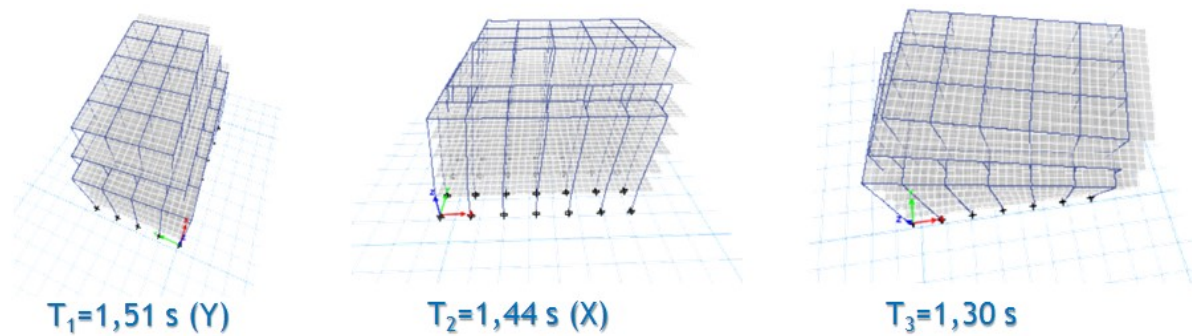


Figure 2.7 Modal shapes and corresponding periods, existing building

According to Eurocode 8, damage limitation is checked through the inter-story drift ratio. Figure 2.8 shows the calculated inter-story drifts, along with the Code prescribed limit value of 0,75%. It may be seen that the existing structure fails to comply with this criterion in both directions and at all floors. Accordingly, the building is susceptible to damage in case of frequent earthquakes.

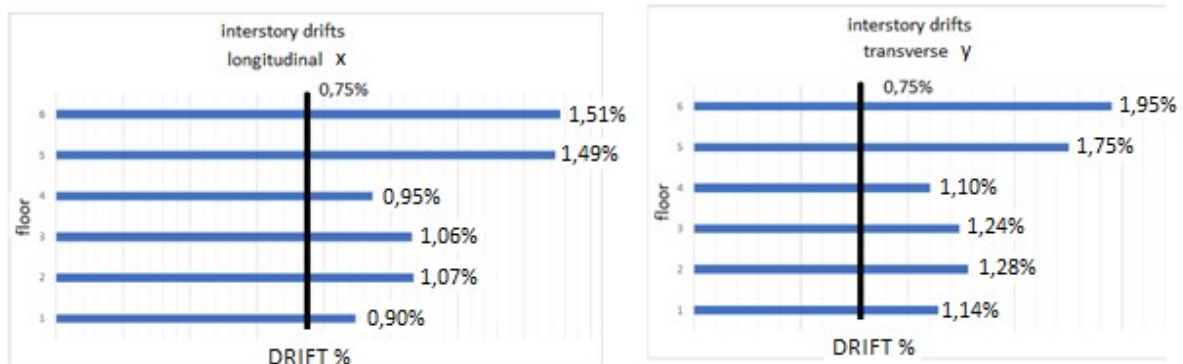


Figure 2.8 Interstory drifts for checking damage limitation

The ULS verifications for the seismic combination showed that the column capacities are not sufficient for both longitudinal and transverse direction of the seismic action.

### 2.2.2 Nonlinear modelling and analysis of the building

The structural assessment of the building was moreover executed through nonlinear static (pushover) analysis, determining the capacity curve of the building (base shear/displacement); the structural capacity was compared to the effective seismic demand, determining the effective performance of the structure and evidencing the eventual need of retrofit interventions.

A nonlinear lumped plasticity model of the building was elaborated, defining the moment/rotation relationships of plastic hinges at the ends of the columns. The

rotational capacity of plastic hinges was determined according to EN1998-3:2005 [5] for existing r.c. elements.

The static pushover analysis was performed for both main directions of the building, considering a uniform distribution of horizontal forces along its height. The control node was considered as the center of mass of the top story.

Figure 2.9 and Figure 2.10 show the pushover curves for the longitudinal (x) and transverse (y) direction, with indication of three performance levels for Immediate Occupancy (IO), Life Safety (LS) and Collapse Prevention (CP). On the same curve the achieved performance point for the considered seismic excitation is also shown.

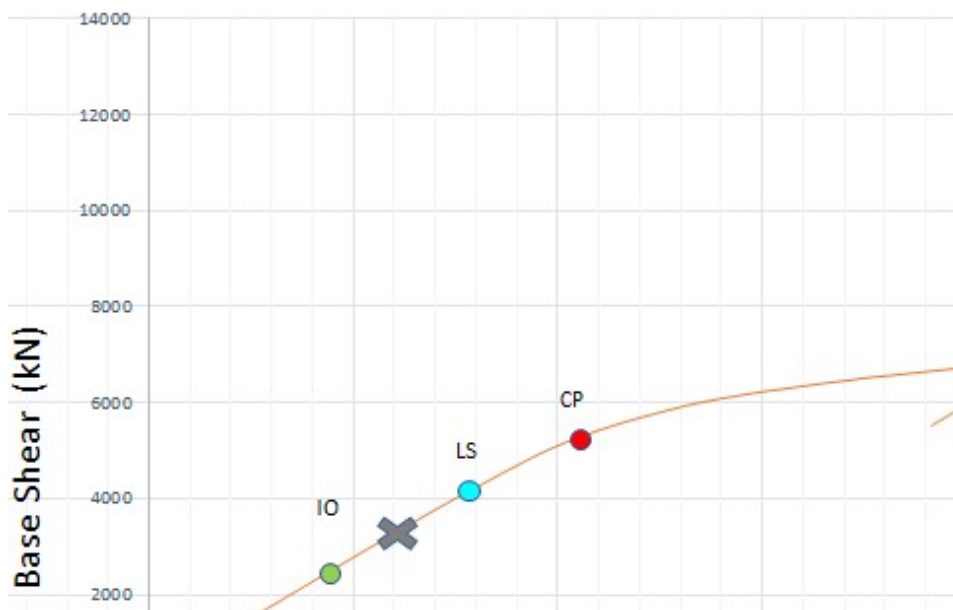


Figure 2.9 Pushover curve for the longitudinal direction

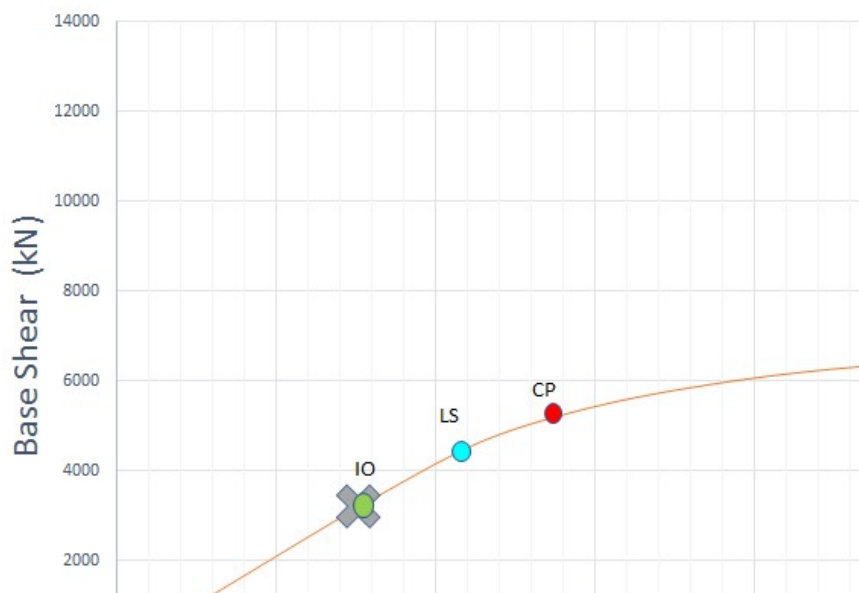


Figure 2.10 Pushover curve for the transverse direction

## 2.3 DESIGN OF THE UPGRADED BUILDING

The building is upgraded by introduction of vertical concentric  $\Lambda$ -bracings with dissipative INERD pin connections of the top. The upgraded structure is designed for the seismic combination, taking into account  $q=3$ . The design of the bracings and the pin connections is performed by an iteration procedure so that the upgraded building complies with Code requirements in respect to the limitation of inter-story drifts and the capacities for all structural members.

Table 2.2 presents the cross sections for the bracings in all four sides.

Table 2.2: Profiles for  $\Lambda$ -bracings, steel grade S355

Floor	South	North	West	East
1	HEA 120	HEA 140	HEA 120	HEA 180
2	HEA 180	HEA 180	HEA 200	HEA 220
3	HEA 160	HEA 180	HEA 180	HEA 200
4	HEA 140	HEA 160	HEA 160	HEA 180
5	HEA 120	HEA 140	HEA 140	HEA 140
6	HEA 120	HEA 140	HEA 140	HEA 160
7	HEA 120	HEA 120	HEA 140	HEA 140

The INERD connections, including internal and external plates and pins were determined using the relevant design guide. The steel grade for the plates and the pins are S355 and S275 correspondingly. The design was performed using appropriate software. In the following the design of a connection for one brace is presented as an example.

The pins are designed for the highest brace forces in the seismic design situations according to:

$$P_{Ed} \leq P_{u,Rd} \quad (3.1)$$

where  $P_{Ed}$  the design axial force of the brace and the connection  
 $P_{u,Rd}$  the ultimate resistance of the connection

The resistance of the connection due to bending and shear of the pin are defined in eq. (3.2a) and (3.2b) respectively. The factor  $\beta_{III}$  defines the percentage of the pin that has undergone significant plastic deformation on each side, with  $0 \leq \beta_{III} \leq 0.5$ . The ultimate resistance of the connection is found through an iterative process by

changing factor  $\beta_{III}$ , so that the two values of equations (3.2a) and (3.2b) become equal.

$$P_{u,M,Rd} = k_{pin} \cdot \frac{4 \cdot M_u}{a_{red,III} \cdot \gamma_{pu}} \quad (3.2a)$$

$$P_{u,V,Rd} = k_{pin} \cdot \frac{2 \cdot b \cdot (1 - 2 \cdot \beta_{III}) \cdot h \cdot f_y}{\sqrt{3} \cdot \gamma_{pu}} \quad (3.2b)$$

where  $M_u = W_{u,pl} \cdot f_{mid}$  the ultimate plastic resistance of the pin

$f_{mid} = f_y + (f_u - f_y) \cdot \lambda_f / 2$  the maximum normal stress of the pin

$\lambda_f = \left( \frac{a - h}{2 \cdot h} \right)^2$  a factor for the influence of shear with  $0 \leq \lambda_f \leq 1$

$W_{u,pl} = b \cdot h^2 \cdot \left[ \beta_{III} - \beta_{III}^2 + \chi \cdot (0.5 - \beta_{III})^2 \right]$  the plastic modulus of the pin, taking into account the reduction due to the shear stresses.

$$\chi = \sqrt{1 - (f_y / f_{mid})^2}$$

The connection may be modelled as an axil spring with spring constant for two internal plates:

$$K_{pin} = \frac{8 \cdot EI}{a \cdot \ell^2 \cdot \alpha \cdot (3 - 4 \cdot \alpha)} \quad (3.3)$$

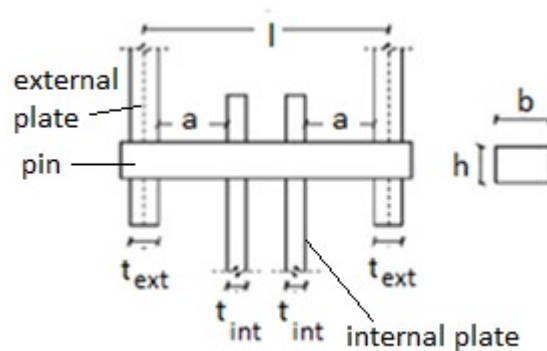


Figure 2.11 Dimensions of an INERD pin and corresponding internal and external plates

Overstrength of a pin  $i$  is defined by the expression:

$$\Omega_i = \frac{P_{u,Rd,i}}{P_{Ed,i}} \quad (3.4)$$

In order to achieve a homogeneous global dissipative behaviour of the structure, it should be checked that the maximum overstrength ratio  $\Omega_{max}$  over the entire structure does not differ from the minimum value  $\Omega_{min}$  by more than 25%:

$$\frac{\Omega_{max}}{\Omega_{min}} \leq 1.25 \quad (3.5)$$

Diagonal members shall be verified to yielding and buckling assuming the exhaustion of the capacity of the pins at their ends:

$$N_{Ed} = \Omega_{max} \cdot P_{u,Rd} \quad (3.6)$$

where  $\Omega_{max}$  is the maximum value of all the pinned connections of the diagonals  
Beams and columns connected to braces with flexible INERD connections should meet the following minimum resistance requirement:

$$N_{pl,Rd}(M_{Ed}) \geq N_{Ed,G} + 1.1 \cdot \gamma_{ov} \cdot \Omega \cdot N_{Ed,E} \quad (3.7)$$

Table 2.3 presents the dimensions of the INERD pins.

Table 2.3: Dimensions of INERD pins, steel grade S275

Floor	South	North	West	East
1	20x25	25x30	25x25	35x45
2	30x45	40x40	40x40	40x60
3	30x40	40x40	35x40	40x55
4	30x35	35x35	35x35	40x45
5	20x20	35x35	25x25	30x40
6	35x35	30x30	30x30	35x35
7	25x30	25x25	30x30	30x30

Figure 2.12 shows the modal shapes and the periods of the upgraded structure. It may be seen that the 1<sup>st</sup> modal shape corresponds now to longitudinal vibrations, while the 2<sup>nd</sup> to transverse. The upgraded building is much stiffer, with reduction of the two first fundamental periods from 1,51 to 0,903 sec and from 1,44 to 0,781 sec correspondingly. 2<sup>nd</sup> order effects may be ignored for the upgraded building due to the fact that the critical buckling factor is equal to  $\alpha_{cr} = 12,84 > 10$ .

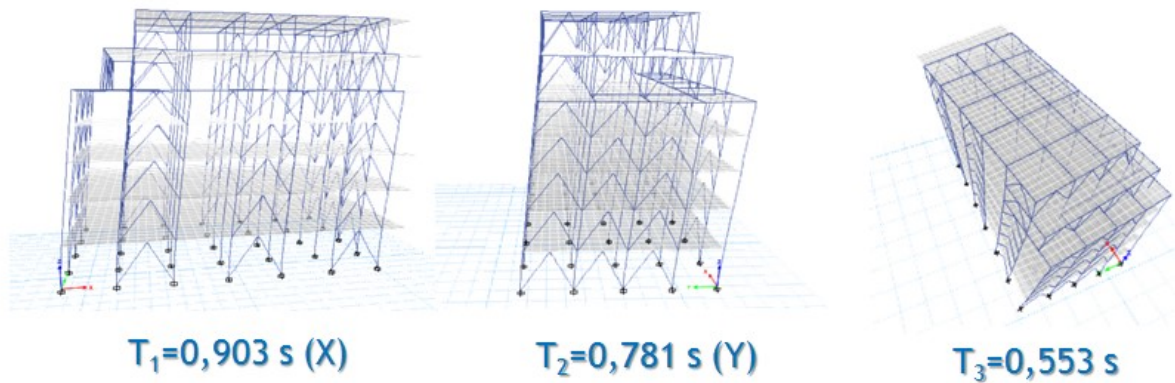


Figure 2.12 Modal shapes and corresponding periods, upgraded building

Figure 2.13 and Figure 2.14 show the inter-story for the existing and the upgraded building. It may be seen that inter-story drifts for the upgraded building are well within the Code limit of 0,75%.

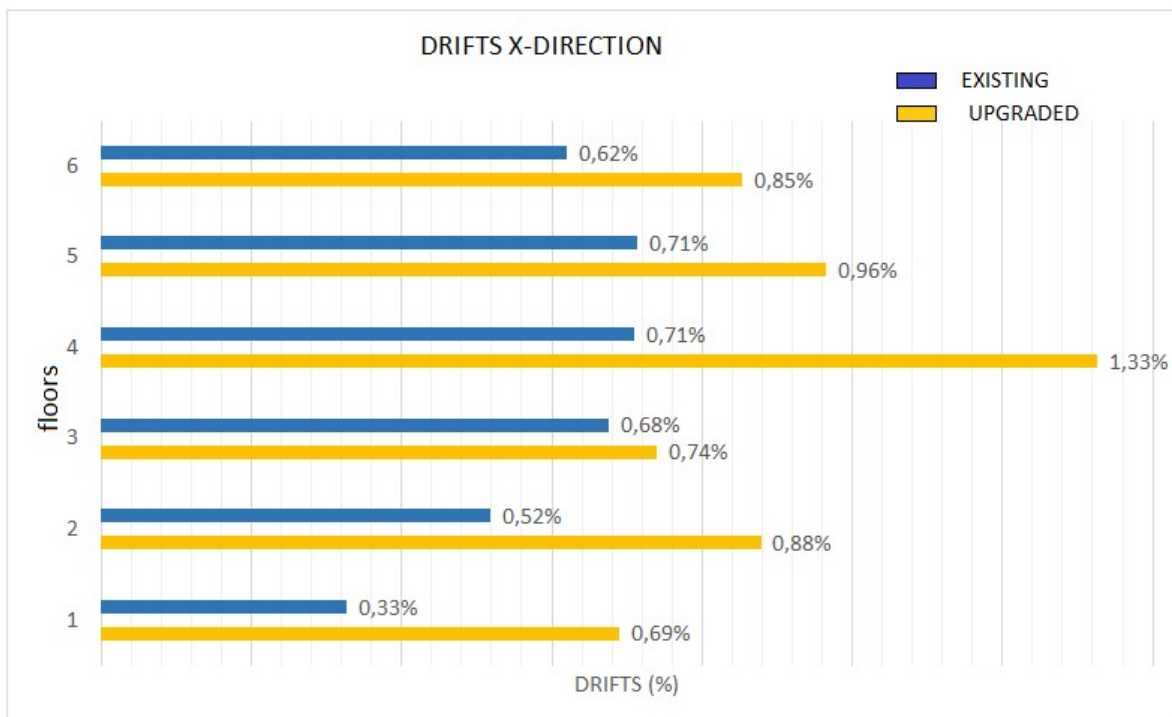


Figure 2.13 Inter-story drifts for the existing and the upgraded building in x-direction

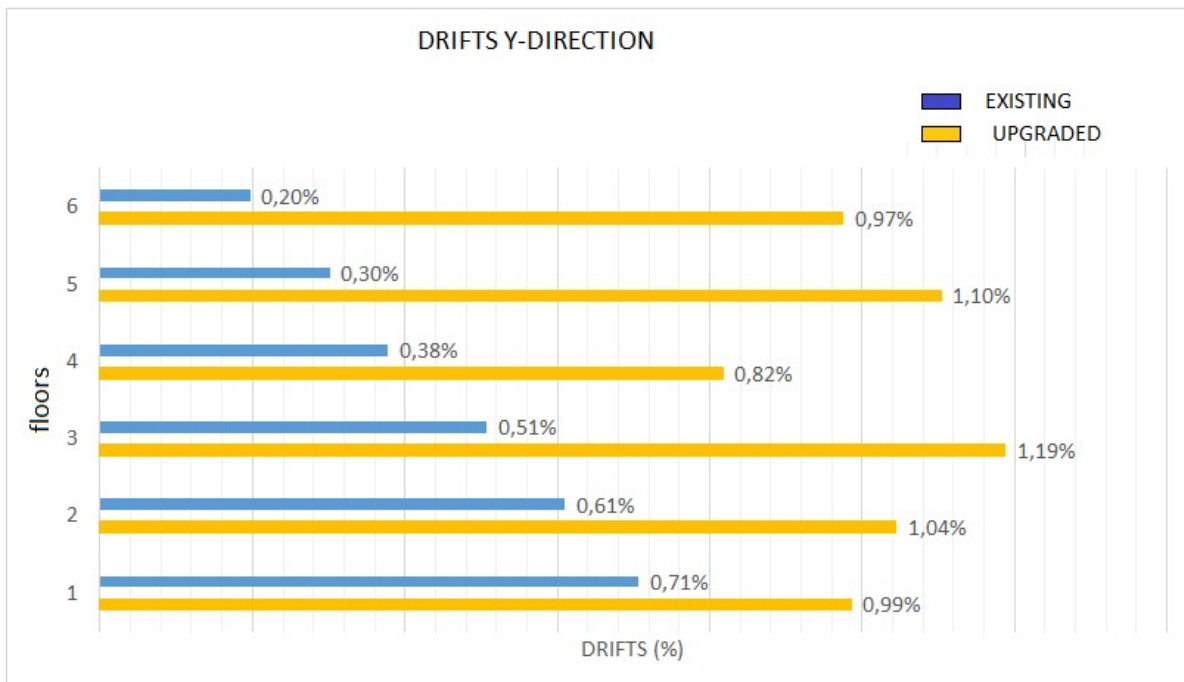


Figure 2.14 Inter-story drifts for the existing and the upgraded building in y-direction

## 2.4 CONFIRMATION OF BEHAVIOR OF UPGRADED BUILDING BY NON-LINEAR ANALYSIS

In order to confirm the dissipative behavior of the dissipative INERD pin connections, non-linear static (pushover) analysis was performed. The dissipative pin connection may be represented by a nonlinear axial spring at the diagonal's end. Characteristic points that define the axial spring properties are given in Figure 2.15.

Point	P	$\delta_{pl}$
A	0	0
B	$P_{yd}$	0
C	$P_{ud}$	$0.5 \cdot h$
D	$P_{ud}$	$a$
E	$0.5 \cdot P_{ud}$	$a$
F	$0.5 \cdot P_{ud}$	$1.5 \cdot a$
Acceptance criteria ( $\delta_{pl}$ )		
IO		$0.25 \cdot h$
LS		$0.6 \cdot h$
CP		$0.8 \cdot a$

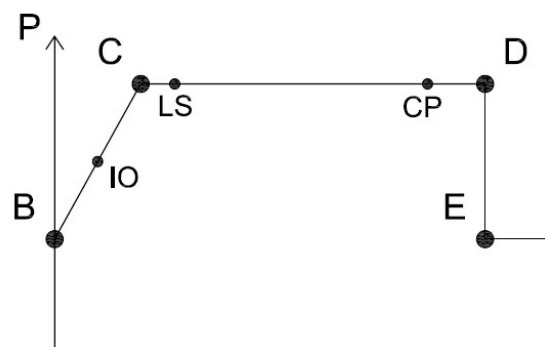


Figure 2.15 Nonlinear properties of the dissipative pin connection spring and performance levels

Figure 2.16 and Figure 2.17 illustrate the pushover curves of the upgraded and the existing building in both principal directions, as well as the performance points. It may be seen that the upgraded building has enhanced properties in respect to stiffness and strength. The new performance point is below the corresponding point for immediate occupancy level.

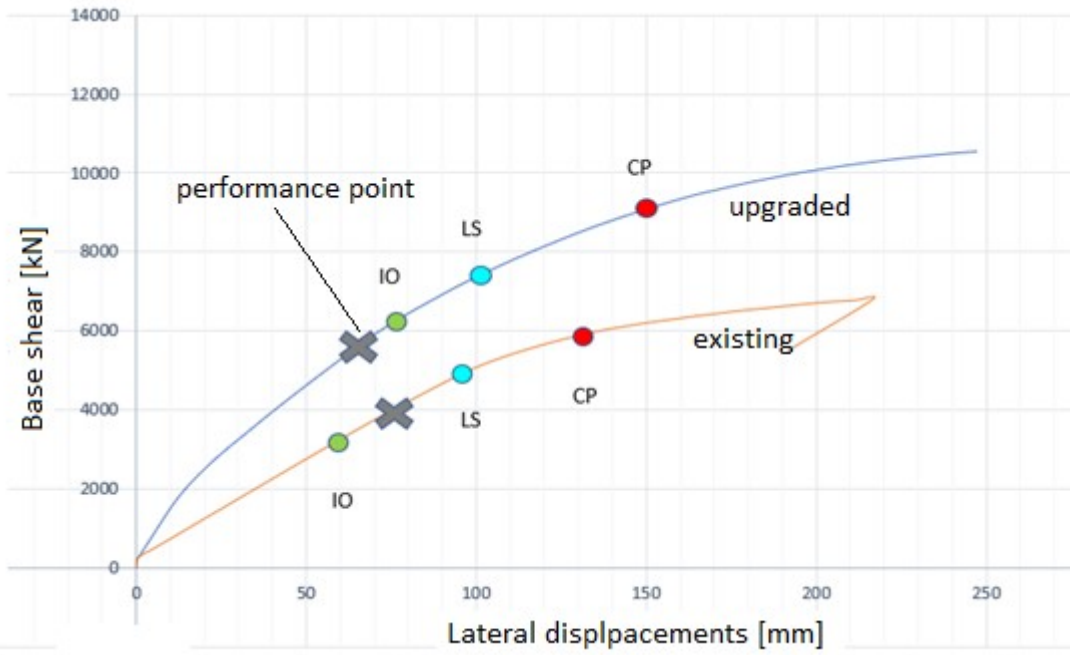


Figure 2.16 Pushover curve for the longitudinal x-direction

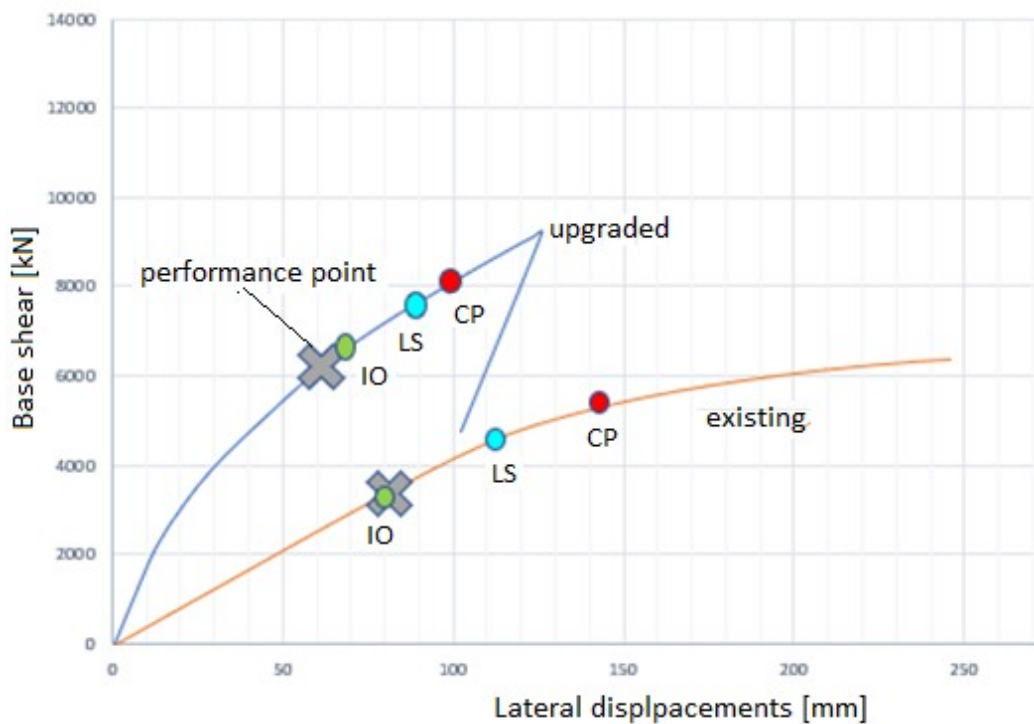


Figure 2.17: Pushover curve for the transverse y-direction

Figure 2.18 shows the deformation pattern and the distribution of plastic hinges at the performance point for the longitudinal x-direction. It may be seen that all inelastic activity concentrates on the dissipative pins. The same happens in the transverse direction as Figure 2.19 indicates.

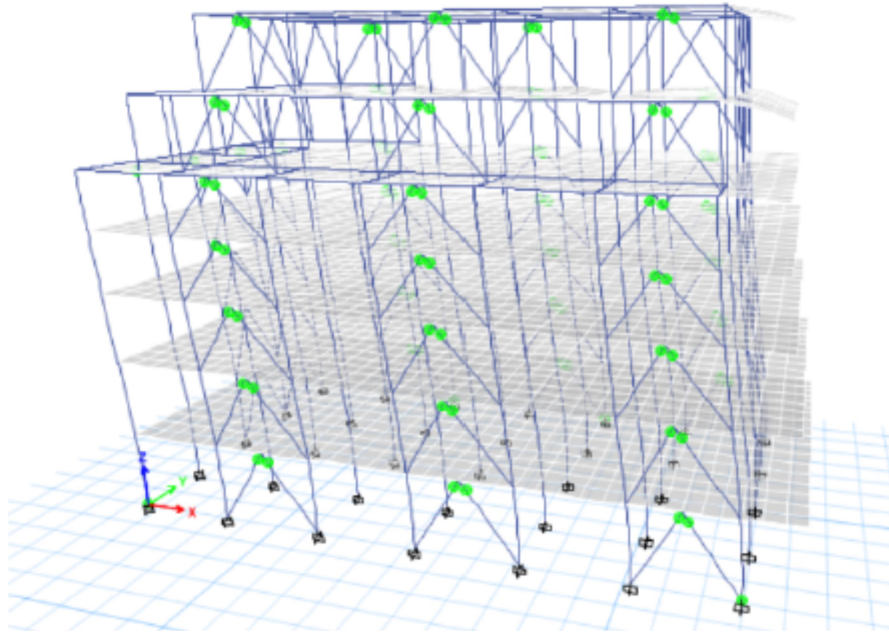


Figure 2.18 Deformation pattern and plastic hinges at performance point, upgraded building x-direction

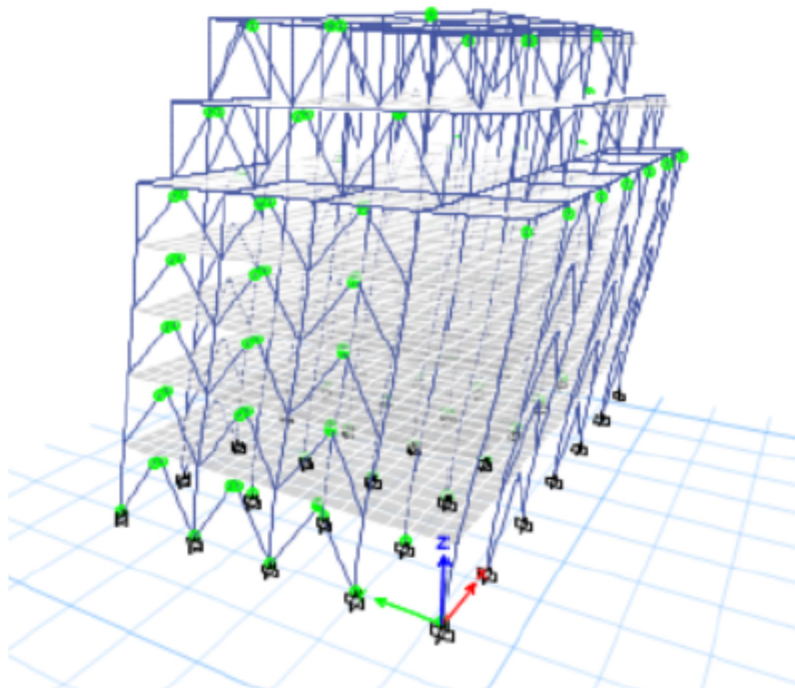


Figure 2.19 Deformation pattern and plastic hinges at performance point, upgraded building y-direction

## 2.5 CONCLUSIONS

An existing seven story reinforced building with two basement floors was upgraded. The building had flat slabs and was designed according to old seismic regulations with no specific detailing rules for provision of ductility. Code prescribed elastic analysis indicated that the existing building suffered in respect to lateral displacements and large inter-story drifts, as well as insufficient capacity of columns. Upgrading measures included the introduction of  $\Lambda$ -shaped bracings along the periphery, with dissipative INERD pin connections at their top end. All additional elements were designed in accordance with the rules provided by the design guide of this system. By elastic modal analysis and non-linear static pushover analysis it was shown that the building may be significantly upgraded to fulfill all Code requirements and perform well in case of both moderate and strong seismic events.

## 2.6 REFERENCES

- [1] I. Vayas (ed): Information brochures for 12 innovative devices, the INNOSEIS projects, ECCS, 2017
- [2] P. Thanopoulos: Seismic behavior of steel buildings with dissipative devices, PhD Thesis NTUA, 2006
- [3] Earthquake protection and planning organization (EPPO): Specific ations for interventions in reinforced concrete buildings, 2014 (in Greek)
- [4] EN1998-1:2005 - *Eurocode 8 –Design of structures for earthquake resistance, Part 1: General rules, seismic actions and rules for buildings*
- [5] EN1998-3:2005 - *Eurocode 8 –Design of structures for earthquake resistance, Part 3: Assessment and retrofitting of buildings.*
- [6] ATC-40, 1996 Applied Technology Council 1996, ATC40, Seismic evaluation and retrofit of concrete buildings, California Seismic Safety Commission, Proposition 122, Seismic Retrofit Practices Improvement Program, Report SSC 96



## **3 RETROFITTING OF A SIX-STOREY REINFORCED CONCRETE HOTEL IN THE ISLAND OF RHODES BY A FUSEIS SYSTEM**

### **3.1 GENERAL**

#### *3.1.1 Introduction*

This case study refers to the retrofitting of an existing reinforced concrete building, located in the island of Rhodes, Greece. The building was designed and constructed in the 1967 in accordance with old seismic regulations that did not include any dynamic analyses or special design or detailing provisions for reinforced concrete elements. The building was in need of retrofitting to comply with the current seismic regulations and to remove light damages, mostly due to aging and environmental actions. Retrofitting is carried out introducing dissipative FUSEIS beam link systems [9], using the provisions of the Hellenic Regulation for Assessment and Retrofit of Existing Buildings [11] and supplementary the provisions of EC8-3 [5], ASCE 41-13 [10] and ATC-40 [6].

#### *3.1.2 Description of existing building*

##### *3.1.2.1 Geometry and general assumptions*

Built at the second half of the 60's, Imperial Hotel is located in the city center of Rhodes, Greece. The building consists of a wall structured basement 2,90m high, an area of 755m<sup>2</sup> and five over ground floors of 725m<sup>2</sup> of which the first floor is 4,00m. high while the remaining are 2,90m. high. The hotel's floor plan approaches the shape of an isosceles trapezoid as it appears in Figure 3.1. In the basement there are the staff rooms, a wellness (spa) area and in ground floor there is the reception area, a conference hall, restaurant, café-bar, kitchen and offices. The guests' houses are located in the floors while at the terrace a café-bar and a restaurant are planned to be built.

At the time of the project's structural analysis the provisions of the Hellenic reinforced concrete code of 1954 were in force as well as the seismic design code of 1959. The horizontal seismic loads were determined by multiplication of the vertical loads of floors by a coefficient  $\epsilon$ , which was taken equal to  $\epsilon=0,12$ .

The structural system for provision of seismic resistance consists of individual walls, coupled walls and moment resisting frames. The frames and walls are distributed in the building's perimeter while in the position of stairs and elevators a core of coupled

walls is formed. The strong axis of columns is orientated towards axis Y of the floor plan while the columns of the east side of the building are inclining at  $12^\circ$  towards axis X. The fully rigid basement allows the assumption of complete fixed ground floor's columns at their base. The slabs are characterized as rigid diaphragms as there is intense presence of circumferential beams, there are no slabs that are not supported in beams as well as there are no height imbalances and significant openings.

The structural elements were designed at that time without consideration of capacity design rules, special detailing of the critical areas of structural members and confinement demands.

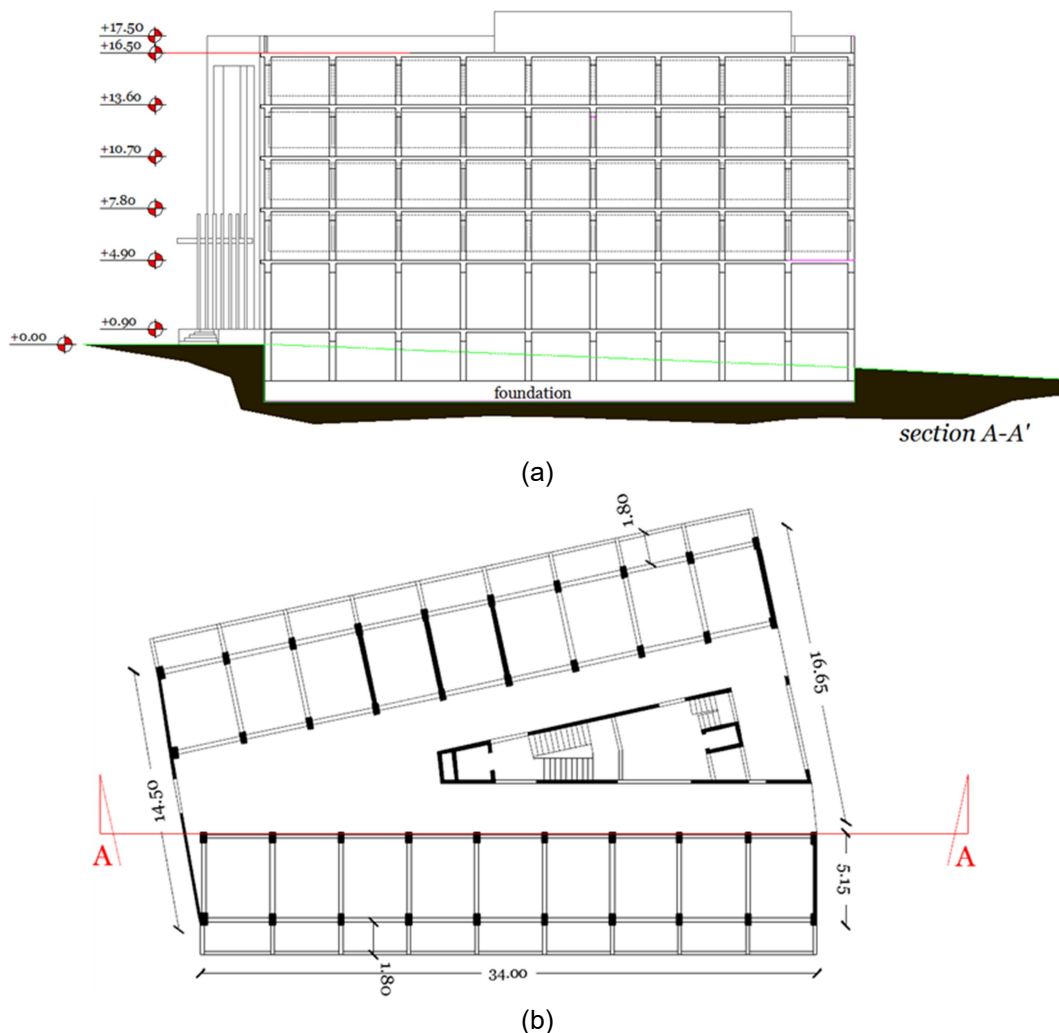


Figure 3.1: Overall building dimensions (a) Section A-A' (b) Typical floor plan

### 3.1.2.2 Current Condition

At the inspection performed in the building it emerged that the initial design has been applied without modifications regarding the geometry of the floors, the dimensions

and the structure of parts, as well as the uses of areas as they have been reported in paragraph 3.1.2.1. The exception is the construction of an additional floor which however was predicted and reported in the annotation of designs. The extent of the damages it suffered can be considered small and it includes mild or more severe cracking and delamination while no buckling or fracture of longitudinal and transverse reinforcement has been observed neither significant permanent deformations of edges in any member. The small extent of damages was maybe a fact that is predicted since the last strong earthquake that occurred in the city of Rhodes was reported in 1957 while the big cross sections of the current elements ensure a satisfactory resistance against the static vertical loads. For the assessment of the building's behaviour before and after the reinforcement there is the assumption that the damaged elements have been completely restored. At the Figure 3.2 and Figure 3.3 the most significant damages observed are presented.



Figure 3.2: (a) Concrete's delamination at a 1st floor balcony (b) Concrete's delamination of a wall in the building's rear view



Figure 3.3: Concrete's fracture of a wall in the building's rear view, Concrete's degradation of a column at its base without evident reinforcement buckling while at its top a delamination is noted

### 3.1.2.3 Materials

The concrete for columns and walls is B.300, equivalent of category C20/25, while for slabs and beams B.220, almost equivalent of category C12/15. For the longitudinal reinforcements of walls, columns, beams and slabs with span greater than 2,00m steel St IIIa was used, heat treated steel equivalent of S400 while for slabs with less span than 2,00m St I, mild steel equivalent of S220. For the transverse reinforcement of columns and walls steel St IIIa was used while for beams St.I. .

The average or typical values of materials are used depending on the method of analysis divided with the safety factor of the relevant material  $\gamma_m$ . The  $\gamma_m$  depends on the Data Reliability Level (DRL) which for the purposes of this thesis and provided that there are no significant deviations to the structure in relation to the initial design it is received as adequate. The materials' representative values  $f_c$ ,  $f_{s,y}$  or  $u$  are calculated from Annex 4.1 of the Hellenic Regulation for  $\gamma_{\text{concrete}} = 1,50$  and  $\gamma_{\text{steel}} = 1,15$  while for the average values of resistance the  $\gamma_m$  equals generally with 1,0. The average resistance value of concrete equals with  $f_{cm} = f_{ck} + 8$ , where  $f_{ck}$  is the characteristic resistance in MPa while the reinforcing steel is deemed equal with the characteristic  $f_{s,yk}$   $\eta$   $\rho$   $u_k$  . Their import in the software is made by modifying only the values of resistances of the already existing in the materials library C12/15, C20/25, S400, S220.

For the elastic dynamic analysis with the use of general behavior index  $q$  the calculation of resistances of all elements is made with the representative values of resistances. For the nonlinear static analysis with the representative prices the resistances of main elements are calculated that are examined in terms of forces (brittle) while with the average prices of elements controlled in terms of deformations (ductile) and secondary brittle.

### 3.1.2.4 Loads and load combinations

The actions enforced are determined according to the provisions of EC1 as shown in Table 3.1. The combination of vertical loads for earthquake conditions is the  $G + \psi_2 Q$ , with  $\psi_2=0.60$  for assembly areas.

Table 3.1: Vertical loads

Reinforced Concrete Weight	25.00 kN/m <sup>3</sup>
superimposed loads for intermediate floors:	1.50 kN/m <sup>2</sup>
superimposed loads for top floor:	1.00 kN/m <sup>2</sup>
Brick walls(0.12m):	0.22 kN/m
Brick walls(0.25m)	0.90 kN/m
Green roof(Extensive)	1.90 kN/m <sup>2</sup>
live loads on floors Domestic activities (Class A):	2.00 kN/m <sup>2</sup> :
live loads on balconies Domestic activities (Class A):	2.50 kN/m <sup>2</sup> :
live loads floors Susceptible to Large Crowds (Class C5)	5.00 kN/m <sup>2</sup>

For the elastic dynamic analysis, the design spectrum of EC8-1 was used for zone of seismic hazard II, ground C, damping  $\zeta=5\%$  and importance factor  $\gamma=1$ . The behavior factor  $q$  was assessed according to Annex 4.2 of the Hellenic Regulation for torsional sensitive building equal with 1,0. The same spectrum was used for the calculation of the target displacement at the non-linear static analysis.

## 3.2 ASSESSMENT OF EXISTING BUILDING

### 3.2.1 Simulation

With the use of ETABS 2015 software, for the modelling of beams and columns a beam element of six degrees of freedom in each node was used. The walls, the coupling beams and slabs were modelled with the use of shell elements. For modelling of the diaphragm action of slabs, appropriate restraints were used in each

floor. Due to the rigidity of the basement, the columns of the ground floor were considered as clamped. The stiffness of the structure elements was taken equal with 50% of their geometrical stiffness according to EC8-1 (cracked cross-section).

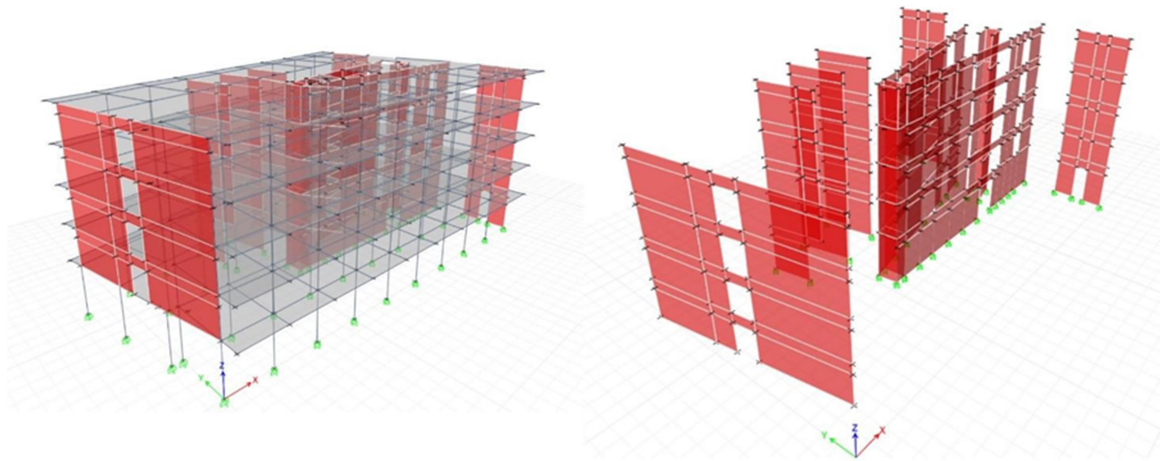


Figure 3.4: Model of the structure and wall system

### 3.2.2 Model for the non-linear static analysis

The non-linear behavior of ductile structural elements was described in accordance with the generic diagram of Figure 3.5. For the parts from RC the bending deformations coexist with the shear and fixed end deformations, therefore the appropriate selection of sizes F-d is the bending moment  $M$  and the chord rotation  $\theta$ , where the  $\theta$  will include the total of bending and shear deformations as well as the rotations in the element's fixed ends. At the compilation of diagrams  $M$ - $\theta$  it must be ensured that the failure in shear force occurs after the yield of element at bending as the part then is deemed brittle and is examined in terms of forces. The  $M$ - $\theta$  curve is modified to account for the presence of shear forces. Elements with brittle behaviour are considered those who fail in shear before their yield in bending, those whose index of available ductility of rotation  $\mu_{\theta} = \theta_u / \theta_y$  is less than 2,0 as well as those whose shear ratio  $a_s = L_v / h$  is also less than 2,0. For brittle elements the section forces  $F$  ( $M$  and  $V$ ) should not exceed the resistance of element  $F_u$ . Elements with brittle behaviour are considered those who failure in shear force before their yield in bending, those whose index of available ductility of rotation  $\mu_{\theta} = \theta_u / \theta_y$  is less than 2,0 as well as those whose shear ratio  $a_s = L_v / h$  is also less than 2,0. For brittle elements the section forces  $F$  ( $M$  and  $V$ ) should not exceed the resistance of element  $F_u$ . The resistances in bending and shear and the failure and yield deformations of the brittles of ductile elements are calculated in accordance with [11].

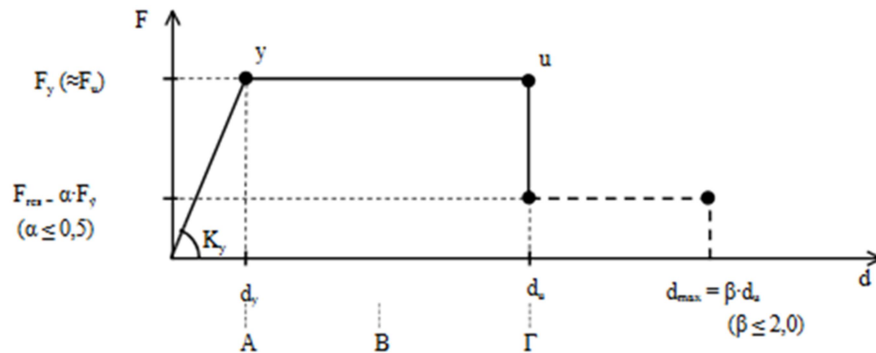


Figure 3.5: Diagram of the general behaviour of a ductile element

For the building analysed its members behave as follows:

- Moment Resisting Frames:** The parts that comprise the framed systems behave at their majority as ductile at X and Y. The exception is the thirteen columns of the first floor of a cross-section 25X55, which due to their small shear ratio at the direction Y ( $\alpha_s = 0,5 * 2,15 / 0,55 = 1,95 < 2,0$ ) behave as brittle. As limit states of the ductile elements the following chord rotations are defined on the diagrams M- $\theta$ . In the parts with brittle behaviour the performance levels are defined as percentage upon the resistance of a part for the current effect section force F (M or V), from the anticipated damages which are expected to occur in those. For level A we expect limited bending or shear cracking without concrete delamination or permanent deformations. For level B we expect delamination, cracking of greater extent and minor permanent deformations. For level C the deformations, degradation and cracking are significant retaining however the capacity of undertaking vertical loads. In Table 3.2 the performance levels are recorded as they were finally selected. Modelling of the elements behaviour in software is made by placing at the ends of the ductile elements Deformation Controlled Hinges (M- $\theta$ ) and Force Controlled Hinges (M and V) in the brittle ones.

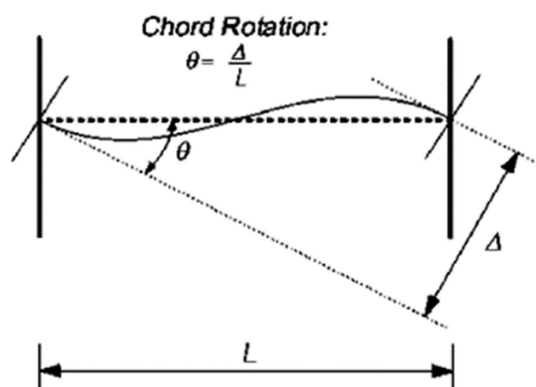


Figure 3.6: Determination of chord rotation (from ASCE 41-13)

Table 3.2: Element's Damage Levels

Damage Level/Behavior	Ductile (terms $\theta$ )	Brittle (terms $F$ )
Light Damage(A)	$\theta_y$	50%
Life Safety(B)	$1/2 (\theta_y + \theta_u)/\gamma_{Rd}$	80%
Collapse Prevention(C)	$\theta_u/\gamma_{Rd}$	100%

• Walls: The majority of walls presented  $\alpha_s < 2,0$  and were considered brittle except some of the walls of the core T8, T9, T10 and T11 the behaviour of which however was considered also as brittle due to the non-application of constructional provisions (formation of confined ends, minimum requirements of reinforcement, thickness etc.) which would provide enough ductility. The coupling beams, all of them at a cross-section 20/75, with net length ranging from 1,0 m up to 2,3m. are also characterized as brittle due to the small shear ratio while as ductile are considered only those that are approaching walls T1, T2 from the 1st up to the 4th floor. Due to the extremely poor reinforcement of the coupling beams, the increased resistance offered by the coupling in walls is ignored and they are examined as separate. For walls the damage limit states are defined equally with the other brittle elements and their possible exceedance is examined in every step of the inelastic analysis. For the cross-sections of the core (T3-T4-T15 and T10-T11-T5-T1) the resistances of walls at Y are calculated by applying effective width ( $b_{eff}$ ) upon the transverse at direction Y walls estimated by Pauley&Priestley [8] from the relation:

$$b_{eff} = 0.3 \cdot h_w + t_w \quad \text{Eq. (3.1)}$$

Where:

$h_w$             wall's height  
 $t_w$             wall's thickness

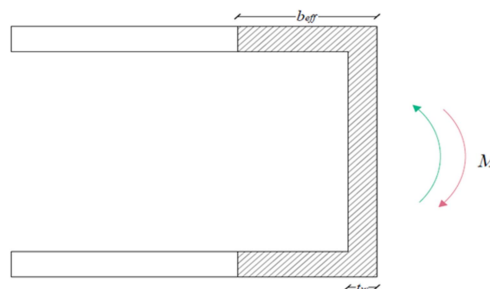


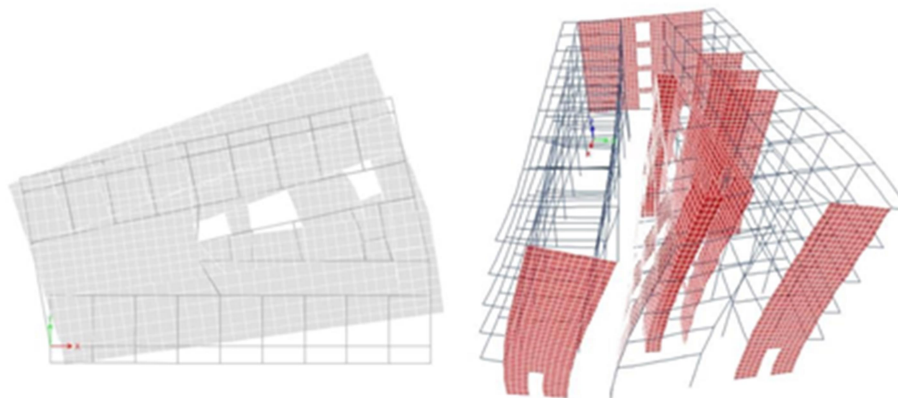
Figure 3.7: T shaped active of cross-section of wall

### 3.2.3 Modal analysis

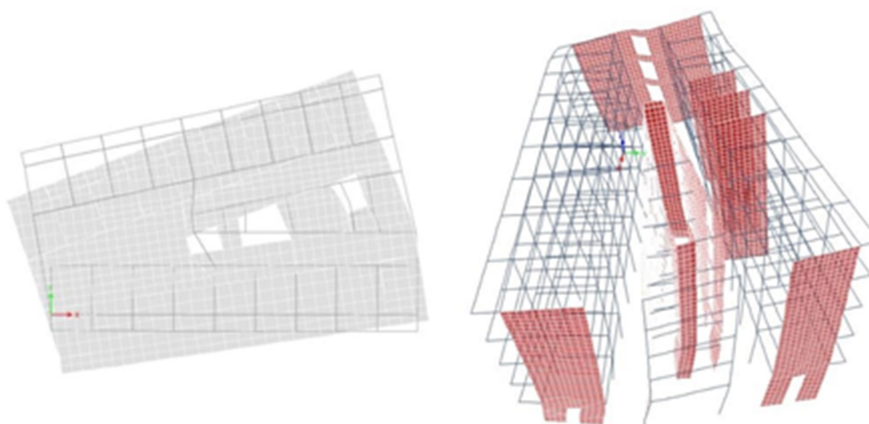
Table 3.3 shows the modes of vibration that provide more than 90% of the effective modal mass in the main directions of the building (displacement X, displacement Y, rotation at axis Z).

Table 3.3: Modes of vibration of the existing building

Mode No	Period T(s)	Effective modal mass on the total		
		X(%)	Y(%)	R <sub>z</sub> (%)
1	0,369	0,4	44,9	29,1
2	0,244	2,6	30,9	55,0
3	0,219	72,8	0,2	3,3
4	0,092	0,1	11,1	7,8
5	0,076	0,0	7,7	3,0
6	0,064	16,5	0	0,1
	SUM	92,4	94,8	98,3



(a)



(b)

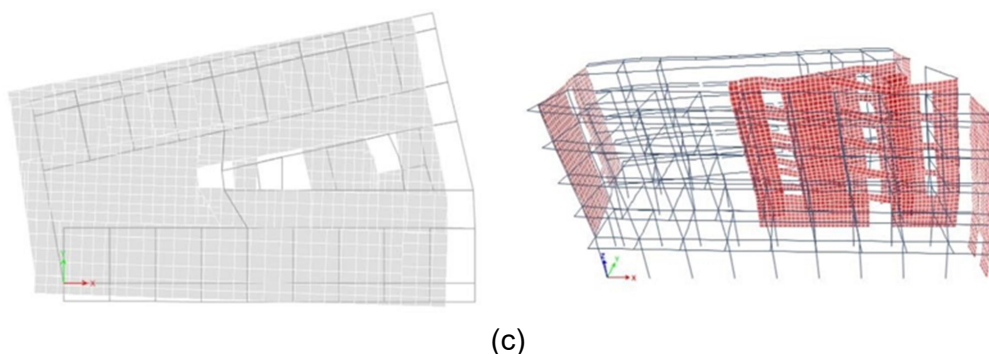


Figure 3.8: Modes of vibration of the existing building a) 1<sup>st</sup> b) 2<sup>nd</sup> c) 3<sup>rd</sup> mode

### 3.2.4 Non linear-static analysis

For the pushover analysis the building's mass center at top floor is selected as reference node. Two vertical distributions of lateral loads are applied, the "uniform pattern" and the "modal pattern". The influence of ( $P-\delta$ ) effects is taken into account as well as the accidental eccentricity. The targeted displacement or performance point for the elastic design spectrum of EC8 ( $q=1$ ) is directly calculated by the software with the equivalent linearization method of FEMA 440 [7] as well as with the coefficient method proposed by [11] and ASCE 41-13 [10]. The pushover curves and the yield patterns at the performance point indicate that many walls, i.e. principal structural elements, are beyond the Life Safe performance level in seismic excitation in y-direction, despite the fact that inter-story drifts are within the Code limits.

## 3.3 RETROFIT

### 3.3.1 Design of FUSEIS beam link systems

FUSEIS beam link systems were introduced in the building by evaluating the conclusions of the non-linear analysis for seismic action at direction Y, which also designates the necessity of the building's retrofit. The target set is the maximum possible exploitation of the system's absorption mechanisms of seismic action, offering the desired resistance, rigidity and ductility to the building in order to be able to overcome even greater seismic actions than those of the design. The systems are extended from the ground floor up to the building's roof. The beams are IPE cross sections steel S235, with reduced beam sections (RBS) at their ends, Figure 3.9. The columns steel S275, should behave elastically during the earthquake and thus larger cross sections are selected. The beam-to-column connections are welded. The systems are introduced in the most flexible region to limit the building's torsional sensitivity. Additionally, the intervention to the current structure must not "violate" the

area's functionality and aesthetics, particularly important criteria for a hotel. In the current building one main system in position 1 is introduced, as well as two similar ones in positions 2 and 3 shown in Figure 3.10. The main system is composed of two individual FUSEIS systems having as common the main column while the auxiliaries have the usual form. In the ground floor four beams are placed while in each floor three of them are placed with a distance of 30cm between them. The connection of the new FUSEIS systems with the existing structure is performed with the formation of a link between the columns of the system and the existing beams in positions 2&3 (Figure 3.11), while in position 1 it can be achieved also with its direct connection in the diaphragm. The RBS geometry follows the provisions of EC8-3 and the system's Design Guide. The proposed values for the formation of RBS presented in Table 3.4 and in Figure 3.9. The properties of the inserted systems is shown in Table 3.5 and Table 3.6.

Table 3.4: RBS suggested dimensions

	EC8-3	Fuseis Design Guide
a	$0,60b_f$	$50\text{mm}\sim 0.50b_f$
b	$0.75d_b$	$75\text{mm}\sim 0.65d_b$
g	$<0.25b_f$	$<0.25b_f$
r	$(4g^2+b^2)/8g$	-

Table 3.5: FUSEIS beam link system's characteristics in position 1 (Main)

Geometry		Beams		Columns		
Total length	6.25m	Cross section	IPE 500		Extreme	Central
Total height	15.60m	Material	S235	Cross section	HEM 700	HEM 800
Maximum width	0.40m	Class	1	Material	S275	S275
Weight		I	2.0m	Class	1	1
		$b_f$	0.20m	H	0,716m	0.814m
		$d_b$	0.50m	$b_f$	0.40m	0.40m
		$M_{pl,Rd}$	644.50 kNm	$M_{pl,Rd}$	3623kNm	4293kNm
		$V_{pl,Rd}$	838 kN	$N_{pl,Rd}$	10341kN	10914kN
		$a(0.50b_f)$	0.10m	$V_{pl,Rd}$	2818kN	3235kN
		$b(0.65d_b)$	0.325m			
		$g(0.20b_f)$	0.04m			
		R	0.35m			
		$L_{rbs}$	1.48m			
		$B_{f,rbs}$	0.12m			
		$M_{pl,rbs}$	462.50kNm			

Table 3.6: FUSEIS beam link system in positions 2 & 3

Geometry		Beams		Columns	
Total length	4.35m	Cross section	IPE 500	Cross section	HEM 700

Total height	15.60m	Material	S235	Material	S275
Maximum width	0.40m	Class	1	Class	1
Weight		l	2.0m	H	0.716m
		bf	0.20m	Bf	0.40m
		db	0.50m	Mpl,Rd	3623kNm
		Mpl,Rd	644.50 kNm	Npl,Rd	10341kN
		Vpl,Rd	838 kN	Vpl,Rd	2818kN
		a(0.50bf)	0.10m		
		b(0.65db)	0.325m		
		g(0.20bf)	0.04m		
		r	0.35m		
		l <sub>rbs</sub>	1.48m		
		bf <sub>rbs</sub>	0.12m		
		Mpl,rbs	462.50kNm		

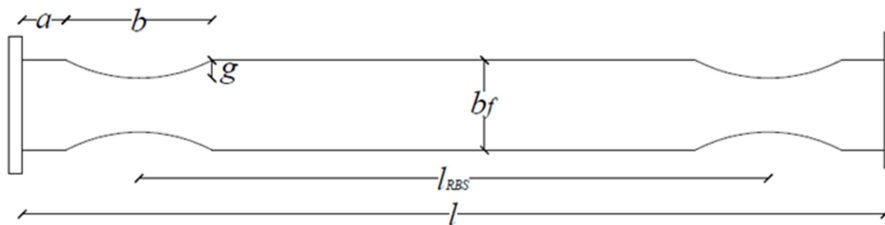


Figure 3.9: Typical beam of the system FUSEIS beam link

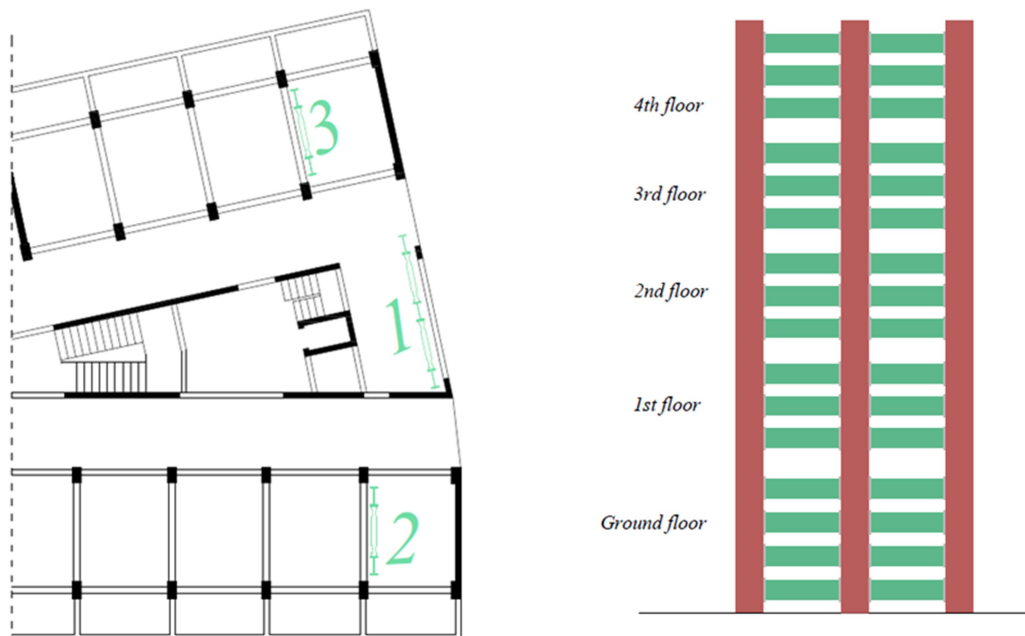


Figure 3.10: The positions of FUSEIS beam link systems in the building and view of the main system (position 1).

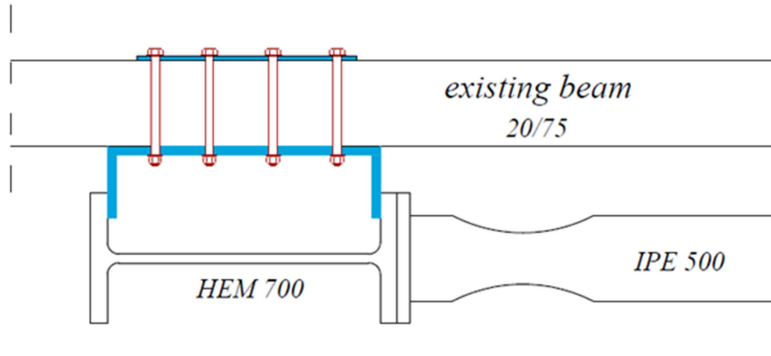


Figure 3.11: Section & view of a typical beam and the connection of system with existing structure in positions 2&3.

Beam elements are used for the system's modelling. The beams of the system consist of five parts which correspond to the complete cross-section at the ends and in the middle and to the reduced in RBS positions (Figure 3.12). The columns are pinned on their base. For the non-linear analysis M3 Hinges are placed to the RBS positions, with the properties proposed in the Design Guide as they are reported in Table 3.7, while P-M3 hinges are also placed in the columns in order to record any possible yield. The non-linear  $M-\theta$  diagram used is shown in Figure 3.13  $\theta_y$  is defined as equal to 2 mrad.

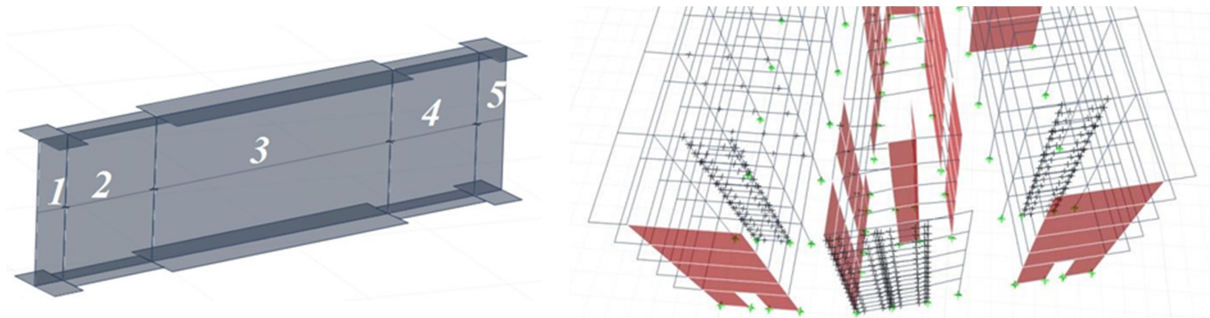


Figure 3.12: Retrofit system's modelling in software.

Table 3.7: Properties of non-linear hinges in RBS

Symmetric frame diagram of behavior			Performance Based Design	$\theta/\theta_y$
Point	$M/M_{pl,Rd-RBS}$	$\theta/\theta_y$		
A	0	0	IO	15
B	1	0	LS	25
C	$\alpha_{pl}=W_{pl}/W_{el}=1.18$	40	CP	35
D	0.60	40		
E	0.60	45		

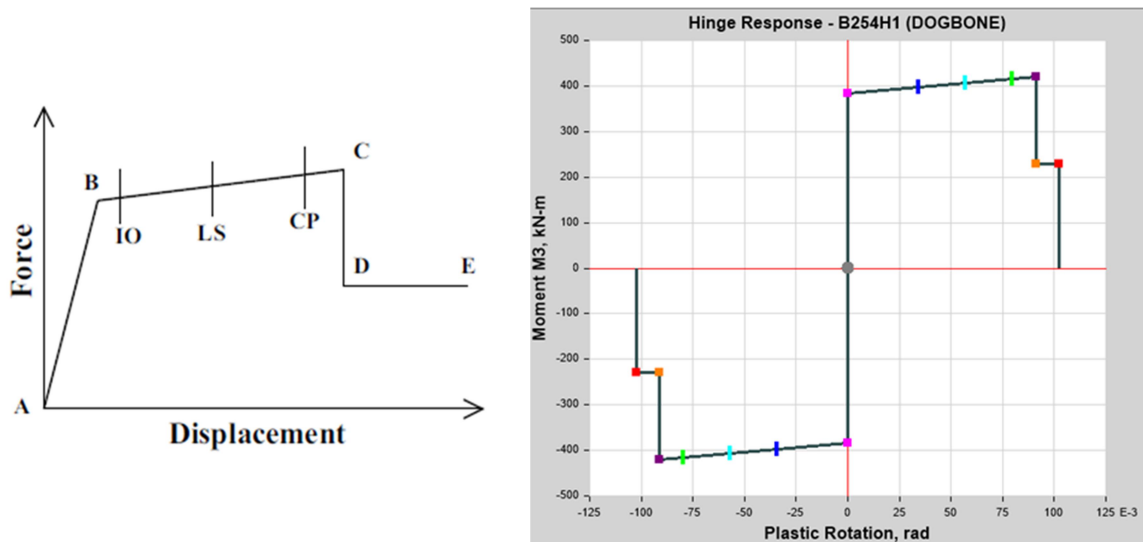


Figure 3.13: M- $\theta$  curve of reduced cross-section. Damage level IO is marked with blue, LS with light blue and CP with green.

### 3.3.2 Modal analysis

Table 3.8 shows the modes of vibration that provide more than 90% of the effective modal mass in the main directions of the building (displacement X, displacement Y, rotation at axis Z). The shapes of the first 3 modes are shown in Figure 3.14

Table 3.8: Modes of vibration of the retrofitted building

Mode no	Period T(s)	Active modal mass on the total		
		X(%)	Y(%)	R <sub>z</sub> (%)
1 <sup>st</sup>	0,315	2,2	51,4	25,0
2 <sup>nd</sup>	0,297	54,7	7,6	12,0
3 <sup>rd</sup>	0,268	16,0	17,2	49,0
4 <sup>th</sup>	0,089	0,2	1,2	12,2
5 <sup>th</sup>	0,081	1,5	16,5	0,2
6 <sup>th</sup>	0,074	18,3	1,3	0,3
	SUM	92,9	95,2	98,7

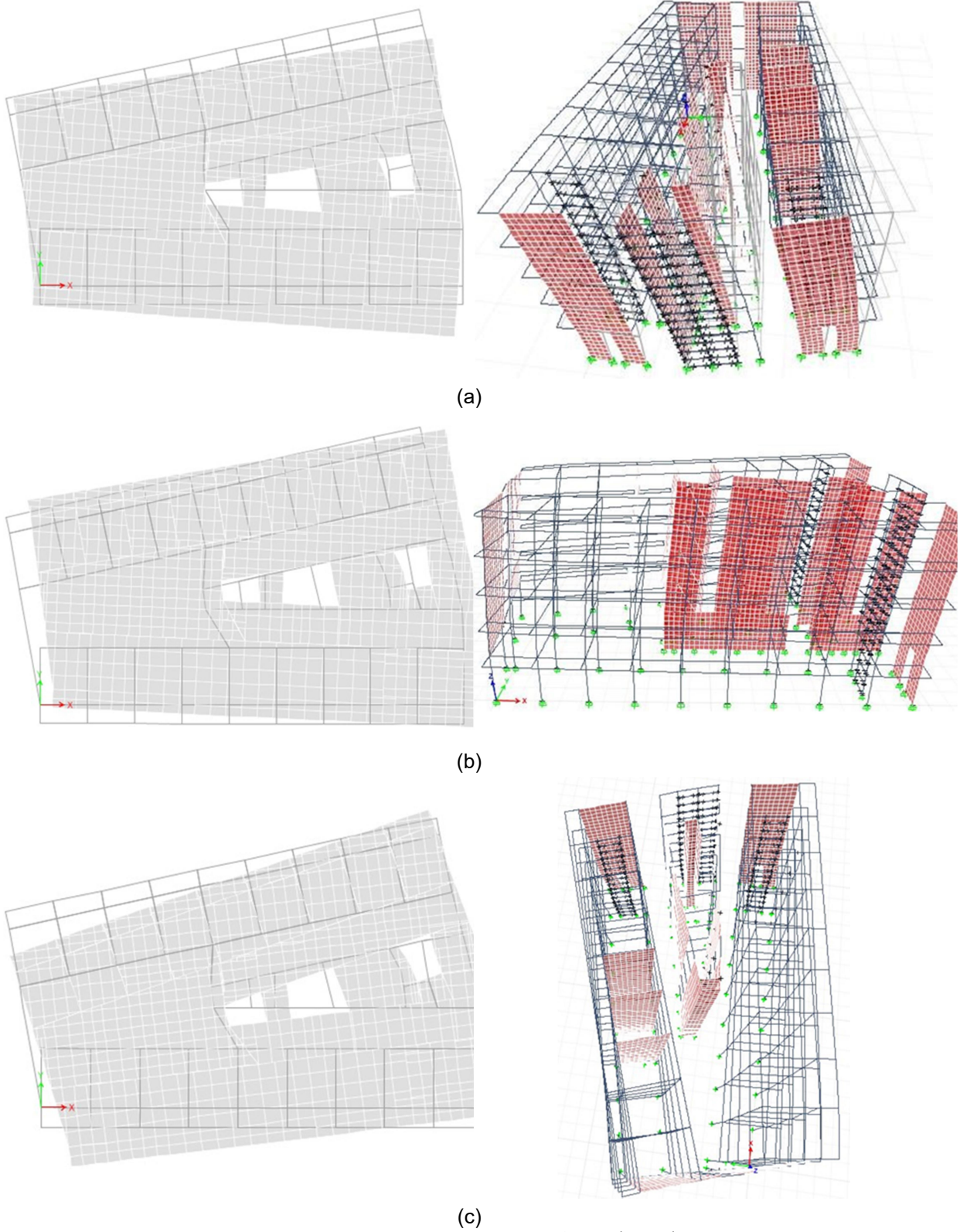


Figure 3.14: Modes of vibration of the retrofitted building a) 1<sup>st</sup> b) 2<sup>nd</sup> c) 3<sup>rd</sup> mode.

### 3.3.3 Non-linear static analysis

Figure 3.15 shows the pushover curves for the existing and the retrofitted building for the two main directions Y and X. Marked in the curves are the performance points for Life Safety (LS) and Collapse Prevention (CP), as well as the performance point that is achieved due to the design earthquake. It may be seen that the performance point for the design earthquake before retrofitting is close to the CP-point, while after the retrofit it is below the LS-point. Figure 3.16 shows the drifts before and after the intervention, indicating a substantial reduction due to the intervention.

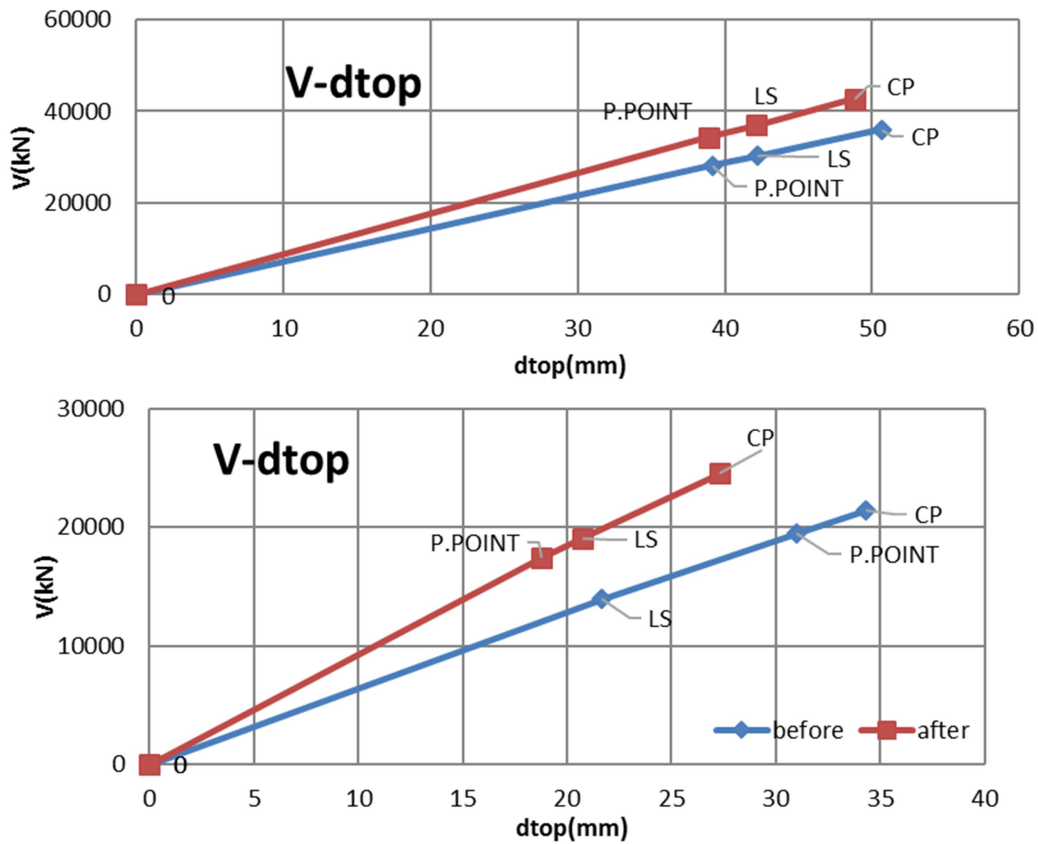


Figure 3.15: Capacity curves in X- and Y-direction, Modal Pattern.

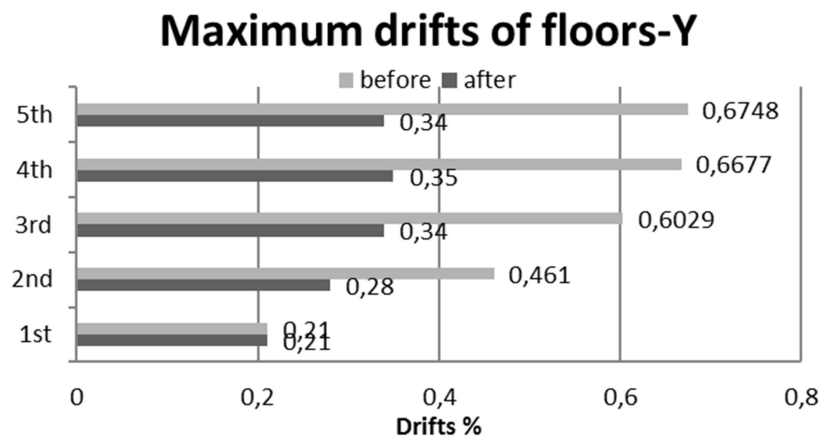


Figure 3.16: Displacements at performance Point - direction Y, modal pattern.

Figure 3.17 shows the plastic hinge formation at the performance point. It may be seen that the columns remain in the elastic area, as anticipated, while plastic hinges form in a number of system beams without exceeding LS damage level.

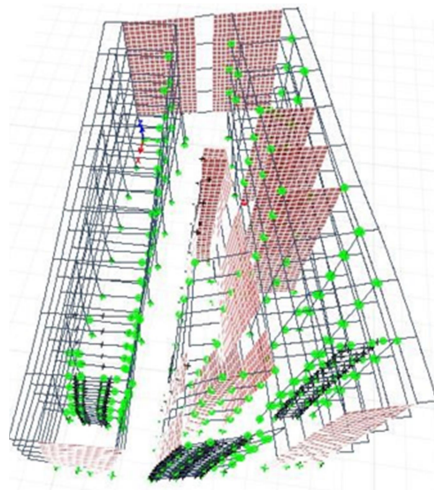


Figure 3.17: Plastic hinges (with green) at performance point.

### 3.4 CONCLUSIONS

It was found that the significantly reduced seismic demands of the old Greek seismic regulation compared to the contemporary ones may lead to the necessity to strengthen existing structures regarding. Due to the lack of morphological rules, lack of capacity design criteria and lack of specific detailing rules, older reinforced concrete structures do not have significant ductility. Structural retrofitting performed in this case study by means of insertion of FUSEIS systems proved to result in a structure that complies with all rules of modern Codes.

### 3.5 REFERENCES

- [1] Eurocode 0: Basis of structural design; EN 1990:2002 + A1:2005 + A1:2005/AC:2010.
- [2] Eurocode 1: Actions on structures - Part 1-1: General actions - Densities, self-weight, imposed loads for buildings; EN 1991-1-1:2002 + AC2009.
- [3] Eurocode 3: Design of steel structures - Part 1-1: General rules and rules for buildings; EN 1993-1-1:2005 + AC:2009.
- [4] Eurocode 8: Design of structures for earthquake resistance - Part 1: General rules, seismic actions and rules for buildings; EN 1998-1:2004 + AC:2009, 2010.
- [5] Eurocode 8: Design of structures for earthquake resistance - Part 3: Assessment and Retrofitting of buildings; EN 1998-3:2004.
- [6] Applied Technology Council(1996). "Seismic evaluation and retrofit of concrete buildings", ATC-40 Report, Applied Technology Council, Redwood City, California.
- [7] Applied Technology Council(2005). "Improvement of nonlinear static seismic analysis procedures", ATC-55 Project, prepared for the Federal Emergency Management Agency, Washington DC.
- [8] Pauley T., Priestley M.(1996) "Seismic design of reinforced concrete and masonry buildings", John Wiley & Sons, INC.
- [9] Vayas I., Karydakis Ph., Dimakogianni D., Dougka G., Castiglioni C.A., Kanyilmaz A. et al., "Dissipative devices for seismic resistant steel frames (FUSEIS)", Research Fund for Coal and Steel, European Commission, EU 25901 EN2013
- [10] American Society of Civil Engineers(2014). «Seismic Evaluation and Retrofit of existing buildings», Reston, Virginia.
- [11] Hellenic Organisation of Seismic Design and Safety(2013), "Regulation of Retrofits"

## 4 SEISMIC RETROFIT OF AN EXISTING R.C. BUILDING USING STEEL SHEAR PANELS

### 4.1 GENERAL

#### 4.1.1 Introduction

This case study refers to the seismic retrofitting of an existing concrete building. It aims at demonstration of implementation of the frames with replaceable shear panels in retrofitting of existing buildings. The case study elaborated refers to design and performance base evaluation procedures by non-linear analysis using finite element software SAP 2000 [[1]].

#### 4.1.2 Description of building

##### 4.1.2.1 Geometry of building

The building was designed in the early 1970's and completed in 1973. The building, with a total area of about 6700 m<sup>2</sup>, belongs to Politehnica University Timisoara and hosts classrooms, laboratories, office spaces, and computer rooms. The total width of the building is 16.5 m (two 7.0 m external spans - the classrooms and offices, and a 2.5 m internal span - corridor) and the total length of 64.0 m is composed primarily of 3.9 m bays. The first story is 3.8 m high, while the other three are all 3.5 m high. The last three bays in the northern part of the structure have been set back, having only two 7.0 m spans (see Figure 4.1). This reduction was made eccentrically, keeping the same frontline for the street side. The slabs were made of precast slab modules, while the steel columns were fully encased in concrete using concrete poured on site (Figure 4.2 ).

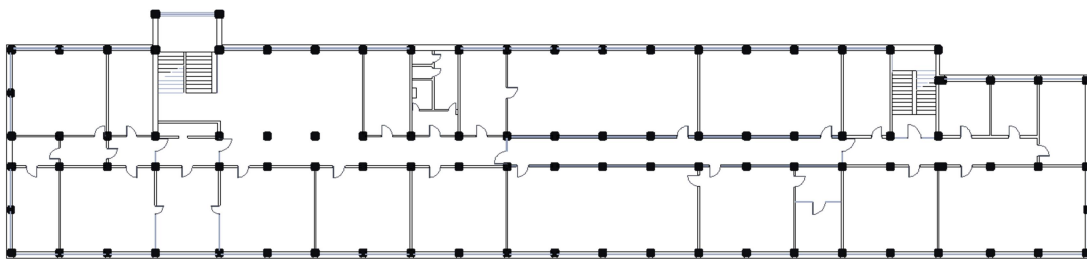


Figure 4.1: Floor view.

The concrete perimeter beam, which supports 1.0 m high brick exterior walls, is positioned eccentrically related to the column centerlines (Figure 4.2). Columns have cruciform sections made of two hot rolled IPN180 profiles (180x82x7x10 mm), grade

S235, encased in a 350 mm square reinforced concrete section with 4 D12 mm longitudinal reinforcement and D10 mm stirrups at 250 mm intervals. The steel profiles are rotated at 45 degrees with respect to their longitudinal axes (see Figure 4.3). The concrete class in the column is C12/15. The concrete class is below the minimum values required to consider the column as composite section column, see EN 1994-1 [[2]]. The precast concrete floors have a 50 mm thick deck and 350 x 110 mm (height by width) reinforcing ribs located approximately on the position plastic failure lines. The ribs are reinforced transversally and longitudinally, while the slab has a mesh wire reinforcement D6 at 160 mm on short direction and D4 at 200 mm on long direction (Figure 4.3).

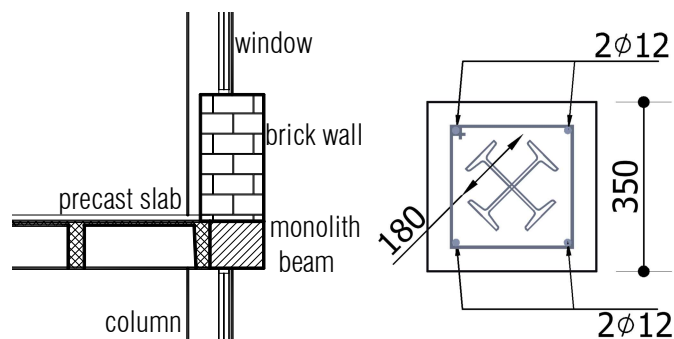


Figure 4.2: Section view for the exterior wall and column section.

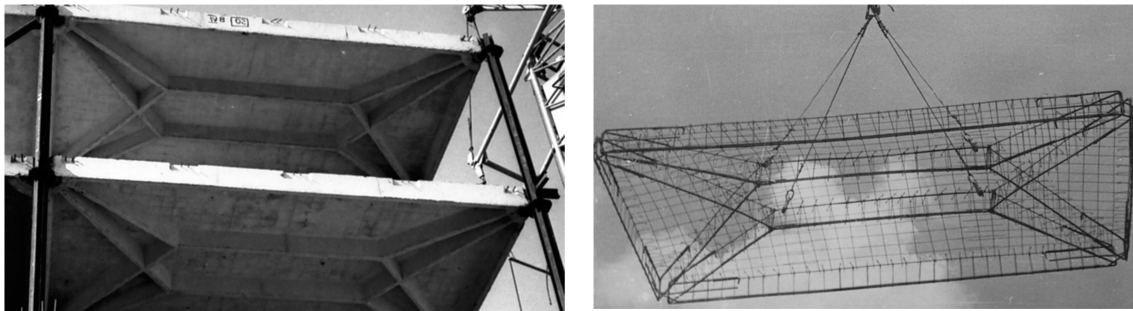
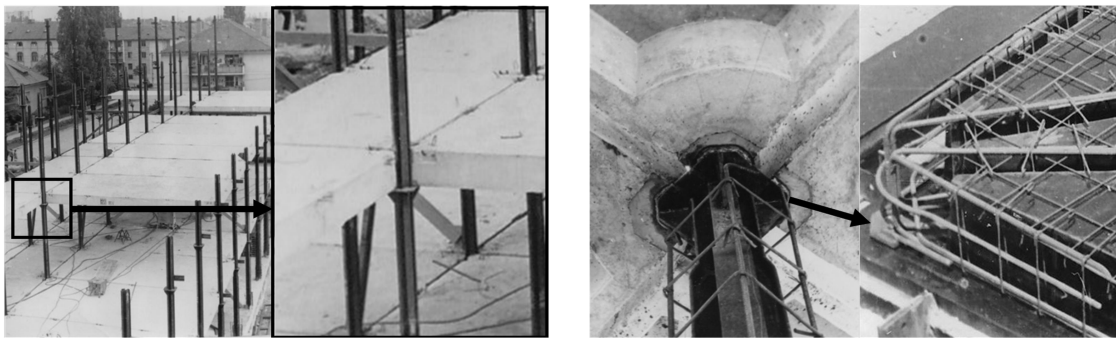


Figure 4.3: Precast slabs panels on site and the reinforcement cage.

On the sides of the precast concrete floors, reinforcement bars join the floor panels together and also provide the connection with the concrete perimeter beam. The panels have corner steel plates welded to the reinforcement cage before casting the panels. The steel plates are fixed with fillet welds to the columns steel brackets on which they rest before pouring the concrete in columns (Figure 4.4). At the top of the slabs, a 50 mm mortar was cast and then the floors were finished with parquet (mostly). In such conditions, rigid diaphragm condition is not fulfilled. Therefore, a conservative assumption has been made and diaphragm effect was not considered in the global analysis.



a) Views with the floor panels

b) Brackets on columns supporting the slab and detail with the reinforcement cage.

Figure 4.4: Precast concrete slab to column connection and details

#### 4.1.2.2 Seismic vulnerability of building

The building site is located in Banat region, well known as a moderate seismicity zone, and characterized by *near field* earthquakes. At the time of construction, the seismic design was covered by the Romanian Seismic code P13-63 [[3]], with additions in P13-70 [[4]]. Apart from other requirements and design provisions, the most important differences between these two codes and the P100-2013 code, which is in application today [[5]], are the seismic intensity and shape of the amplification spectrum, see Figure 4.5. As seen in Figure 4.5, the maximum amplification varied from 3.0 to 2.0 between first two editions, while in the latest seismic code the maximum amplification amounts 2.5. Probably more important, the parameter  $T_C$ , defined as the corner period at the upper limit of the constant acceleration region of the elastic spectrum, increased from 0.3 to 0.7 sec, while the design ground acceleration at the site increased from 0.025 g to 0.2 g, as the site changed the classification from low to moderate seismicity zone.

The structural performance of the existing building was evaluated using two analysis procedures, i.e. response spectrum analysis and nonlinear static procedure (pushover analysis). The loads considered in the evaluation were 2.0 kN/m<sup>2</sup> live load, 0.6 kN/m<sup>2</sup> wind pressure, and 1.5 kN/m<sup>2</sup> snow load. For response spectrum analysis, the following parameters were adopted:  $T_C = 0.7$  s,  $a_g = 0.2$  g, and  $q$  (reduction factor) = 1.0 (the structure has a low dissipation capacity).

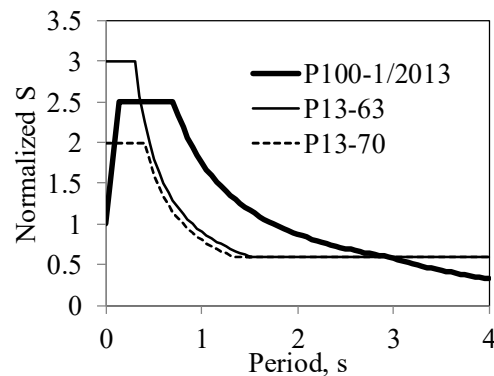


Figure 4.5: Evolution of elastic response spectra in seismic design codes.

In the longitudinal direction, in order to increase the lateral stiffness, eccentrically braces were used in some spans (Figure 4.6,a), while on the transversal direction, there are three inverted V braced frames and one eccentrically braced frame (Figure 4.6,b). The braces were welded on their lower part to the cruciform steel profiles of the column, while the upper part was welded to a horizontal IPN180 hot rolled steel profile. This horizontal beam is welded to the columns just below the precast slab's ribs, without any interaction with the ribs. Inverted V braces were made of 160 mm square hollow steel profiles, with 8 mm thick walls, while the eccentric braces were made of IPN180 profiles.

The analysis was performed using SAP 2000 [[1]]. The 50 mm deck of the precast slab was modelled with thin shell elements. The reinforcing ribs of the precast panel were modelled with bar elements that have common nodes with the shell (Figure 4.7). Gravity loads have been assigned directly to the shells. The columns were modelled as composite elements with equivalent homogeneous steel-concrete properties. Since the concrete floors provide a very limited diaphragm action, the diaphragm effect was not considered. Instead, a rigid element, aiming to connect the column with the corner of the individual precast panels, was applied to model the eccentricity of slab-to-column the connection. This rigid element is pin connected to the precast slab panel. The structure was considered clamped (e.g. rigidly connected) to the basement. The geometry of the braces is presented in Figure 4.6 and Figure 4.7.

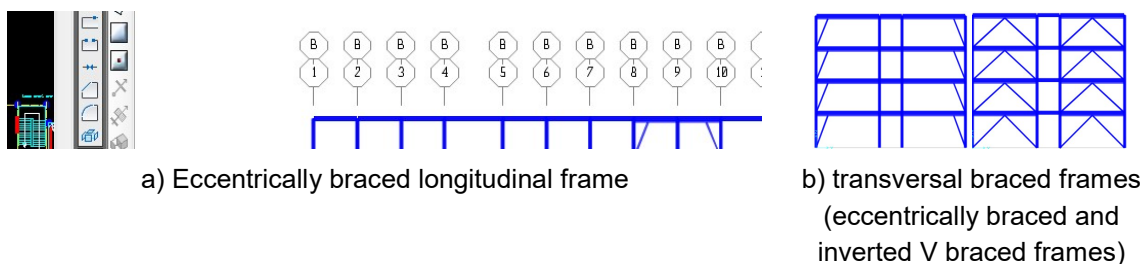


Figure 4.6: Longitudinal and transversal frames

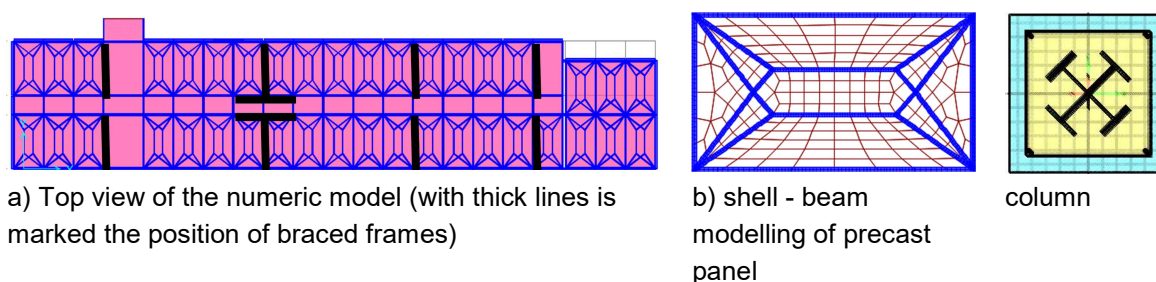


Figure 4.7: Building's numerical model

Additionally, the response of the structure under actions in permanent design situations was also verified using several combinations for both Ultimate and Serviceability Limit States. The actual structural system has adequate capacity under gravity and wind loads and all elements meet the safety requirements with some reserve of capacity.

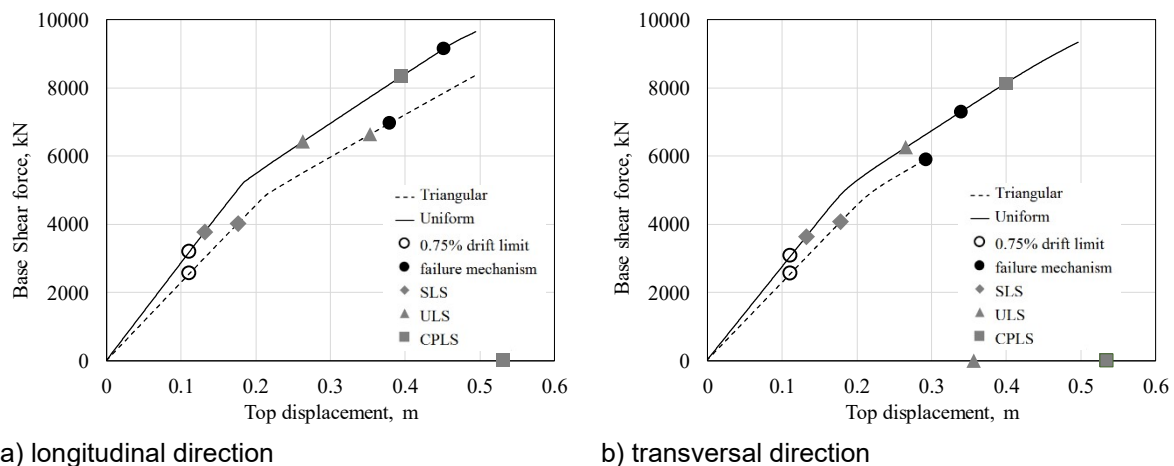
The first mode of vibration is translational (on longitudinal direction), with a period of  $T_1=1.28$  s. The next two periods of vibration are torsional with translational components on the transversal direction ( $T_2=0.69$ s;  $T_3=0.59$ s). The actual configuration of individual slabs that are eccentrically connected to the columns is slightly less rigid than considering a rigid diaphragm ( $T_1=1.28$  s instead of 1.23 s), without introducing any additional torsional effects. Nevertheless, in the seismic design combinations, steel braces and beams were severely overloaded. Therefore, due to the poor detailing and reduced capacity to transfer the lateral forces, the steel braces were no longer considered in the nonlinear static analysis. Columns are also inadequate in resisting the seismic action, especially due to large bending moments on both directions in comparison with moment capacities (corrected due to presence of axial force, N), i.e.  $M_{Ed}/M_{N,Rd} = 1.87 \div 2.93$ . The inter-story drift on the longitudinal direction is also 20% larger than the allowable limit, i.e.  $36 > 28.5$  mm.

In order to have an estimation related the change in the code provisions for the magnitude of the seismic action<sup>1</sup> within the past 40 years, the base shear force was computed for P13-1963 [[3]] and P100-2013 [[5]] codes. The force computed for P13-1963 [[3]] is 6.17 times lower than the one for P100-1/2013 [[5]].

The modal response spectrum analysis showed a poor seismic performance, with several weaknesses connected to global response but also weak structural elements and connections. Therefore, the response has been investigated using a non-linear static analysis on both transversal and longitudinal directions. The performance of the structure was assessed using the N2 method in accordance with EN 1998, Annex B [[6]]. Two distributions of the lateral loads were applied, i.e. first a “uniform” pattern, based on lateral forces that are proportional to mass regardless of elevation (uniform response acceleration), and second a “modal” pattern, proportional to lateral forces consistent with the lateral force distribution in the direction under

consideration (triangular distribution). The analysis was done independently on transversal and longitudinal directions.

Figure 4.8 shows the force-displacement curves for the existing structure, for transversal and longitudinal directions and both lateral load distributions. The three Limit States that were considered in the assessment are: (1) Serviceability Limit State, SLS; (2) Ultimate Limit State, ULS; (3) Collapse Prevention Limit State, CPLS. The earthquake hazard level for ULS corresponds to design earthquake level, while for SLS and CPLS the corresponding levels are 50% and 150% of the design one. For each limit state, the ability of the structure to attain the expected target displacement was calculated. The attainment of inter-story drift limit of  $0.0075h$  ( $h$  is the story height), and development of plastic hinges in columns (considered as a potential failure mechanism) were also marked on the pushover curves.



a) longitudinal direction

b) transversal direction

Figure 4.8: Force-displacement curves for existing structure

As seen from Figure 4.8, in all situations, the lateral stiffness is low and the inter-story drift limit is exceeded before the attainment of the expected target displacement for SLS. On longitudinal direction, the development of plastic hinges in columns before the attainment of the target displacement for ULS indicated a high risk to life safety, because the columns are not designed and detailed to sustain plastic deformations. On transversal direction, for the triangular distribution of lateral forces, the structure shows limited reserve capacity beyond ULS, due to formation of plastic hinges in columns. As a result, the seismic requirements for the un-retrofitted structure, even for low intensity ground motions, are not deemed to be satisfied. The excessive lateral flexibility and poor capacity of structure to dissipate the seismic energy require structural upgrading by and possible local retrofitting of some members. In the next section, two steel based solutions are analyzed and compared in terms of structural performance, taking into account also possibility of intervention.

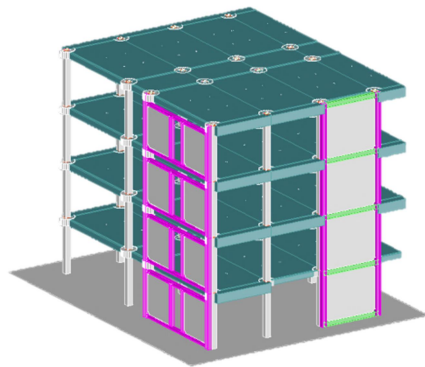
### *4.1.3 Retrofitting of the building*

Considering the structural and architectural constraints, as well as the ease of intervention, technical difficulties, time and cost of intervention, a solution has been analyzed for seismic upgrading. This solution is based on steel shear panels on both longitudinal (perimeter frames) and transversal directions (perimeter and internal frames). It provides high ductility, but it would obstruct the facade.

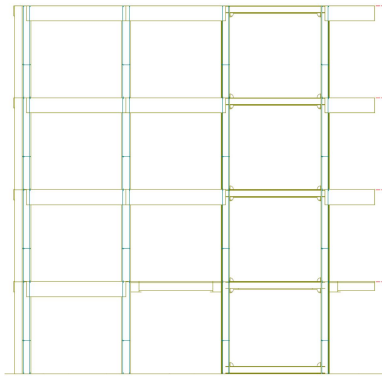
The adoption of upgrading solution only in the exterior frames is more convenient as it allows the minimisation of construction works inside the structure and certifies a certain level of reversibility of the intervention; moreover, placing the new elements, when possible, in the exterior frames guarantee a higher torsional stiffness in the retrofitted construction. However, architectural constraints may impose some limitations in placing the steel elements on the façades. Also, as the structure has a reduced width compared with the length, placing the steel braces on marginal frames only can reduce the stiffening effects for the intermediate transversal frames, and, moreover, induce high demands in foundations.

#### *4.1.3.1 Retrofitting solution*

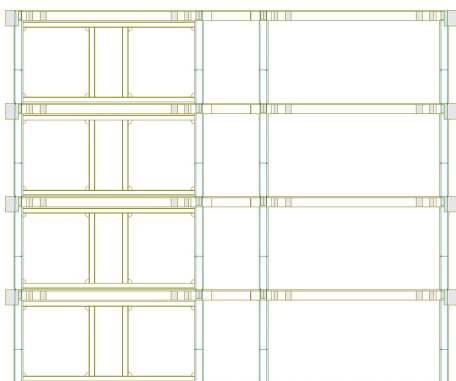
Shear panels are efficient lateral load resisting systems and can be chosen as an alternative solution to the traditional bracing systems. Typical shear panel systems include either singular system, where the shear panels is the only element resisting story shear, or dual systems, where panels are coupled with moment frames. A particular system, which consists of inserting shear panels inside moment frames, aiming at providing additional lateral rigidity [[7],[8]]. The shear panels bordered by additional vertical elements (stanchions) having simple connections to the beams. The beam outside the shear panel acts as a short, intermediate or long link, depending on the relative length of the shear panel and bay width. In this upgrading, both singular and coupled systems were used, see Figure 4.9. On the longitudinal direction, the perimeter frames were upgraded using shear panels, introduced in several spans. In the braced spans, the existing columns were strengthened using H profiles made from S355 steel. Additionally, longitudinal beams were also introduced at each floor level. The steel plates are bolted to the bordering elements (columns and beams) to avoid site welding. On the transversal direction, due to large span over height ration, two panels were used, separated by a link beam. Each shear panel is bordered by additional columns (to retrofit the existing concrete column) and a stanchion connected to the beams with simple bolted connections.



a) 3D view



b) transversal frame



c) longitudinal frame

Figure 4.9: Views with the upgrading system

#### 4.1.3.2 Structural assessment of the retrofitted building

The efficiency of the upgrading solution was investigated using nonlinear static analyses performed with SAP2000 program [[1]]. Detailed 3D Finite Element Models was built, see Figure 4.10. The beams and columns were modelled using conventional beam-column elements.

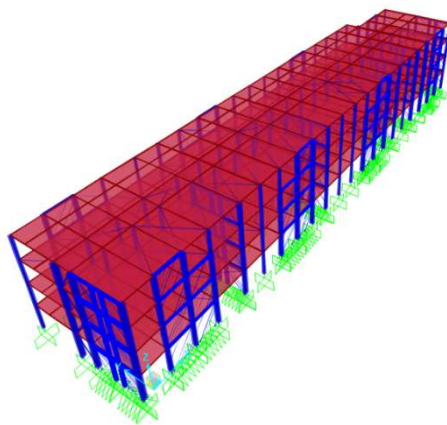


Figure 4.10: 3D models of SPSW system

Main parameters such as yielding displacement, initial stiffness, maximum shear capacity, and ultimate displacement were evaluated. Shear panels were represented by 10 equally spaced pin-ended strips, inclined at an angle  $\alpha$  with respect to the vertical [[9]]. To simulate strip yielding, an axial hinge was placed at the midpoint of each strip. The floors were not assumed as diaphragms because they are inadequate to provide such effect.

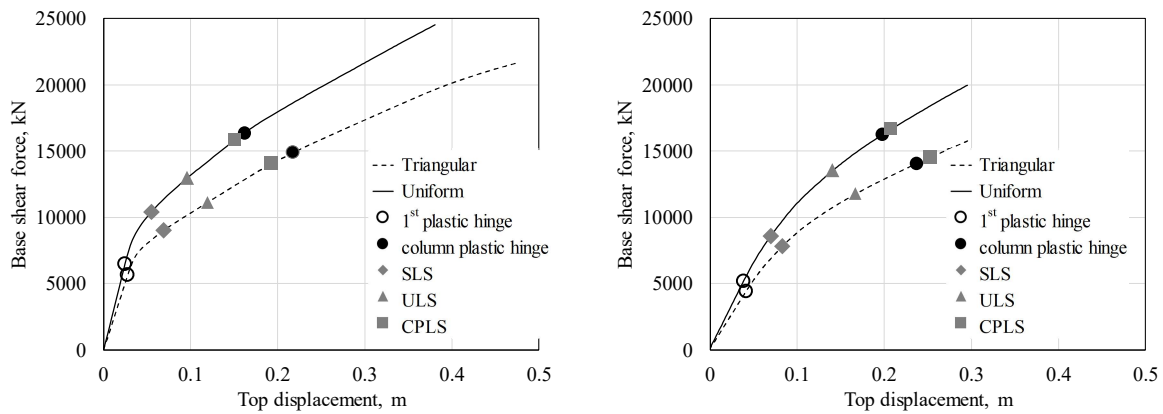
The modes of vibration for the retrofitted structure are presented in Table 4.1. Compared with un-retrofitted structure, the stiffness of the structure increases significantly. Also, the first two modes are translational, while the third mode is torsional.

Table 4.1: Vibration modes of retrofitted structure

Period (s)	Type
0.742	translational, transversal
0.580	translational, longitudinal
0.522	torsional

The response has been investigated using a non-linear static analysis on both transversal and longitudinal direction. The performance of the structure was assessed using the N2 method in accordance with EN 1998, Annex B [[6]]. Two distributions of the lateral loads were applied, i.e. first a “uniform” pattern, based on lateral forces that are proportional to mass regardless of elevation (uniform response acceleration), and second a “modal” pattern, proportional to lateral forces consistent with the lateral force distribution in the direction under consideration. The analysis was done independently on transversal and longitudinal directions. The deformation state of the structure was monitored for the target displacements corresponding to the three limit states. Due to deficient design and detailing of the columns, the failure of the structure was associated with the development of plastic hinges in columns. The development of first plastic hinge is also of interest and is marked on the force-displacement curves.

Figure 4.11 present the force-displacement curves for upgraded structure, for triangular and uniform distribution of lateral forces. Figure 4.12 present the distribution of plastic deformations (plastic hinges) at several performance levels on longitudinal frames, while Figure 4.13 show the same distribution but on transversal frames. Once plastic hinges develop in the un-retrofitted columns, it is assumed that the structure attains the ultimate capacity. The results are presented separately on longitudinal and transversal direction.

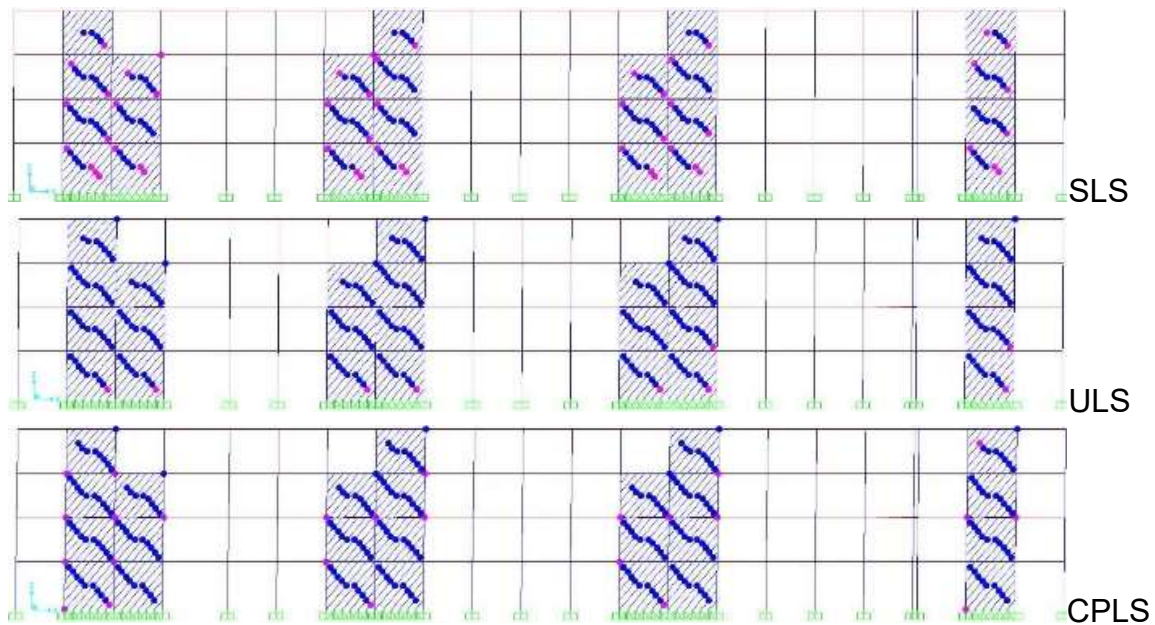


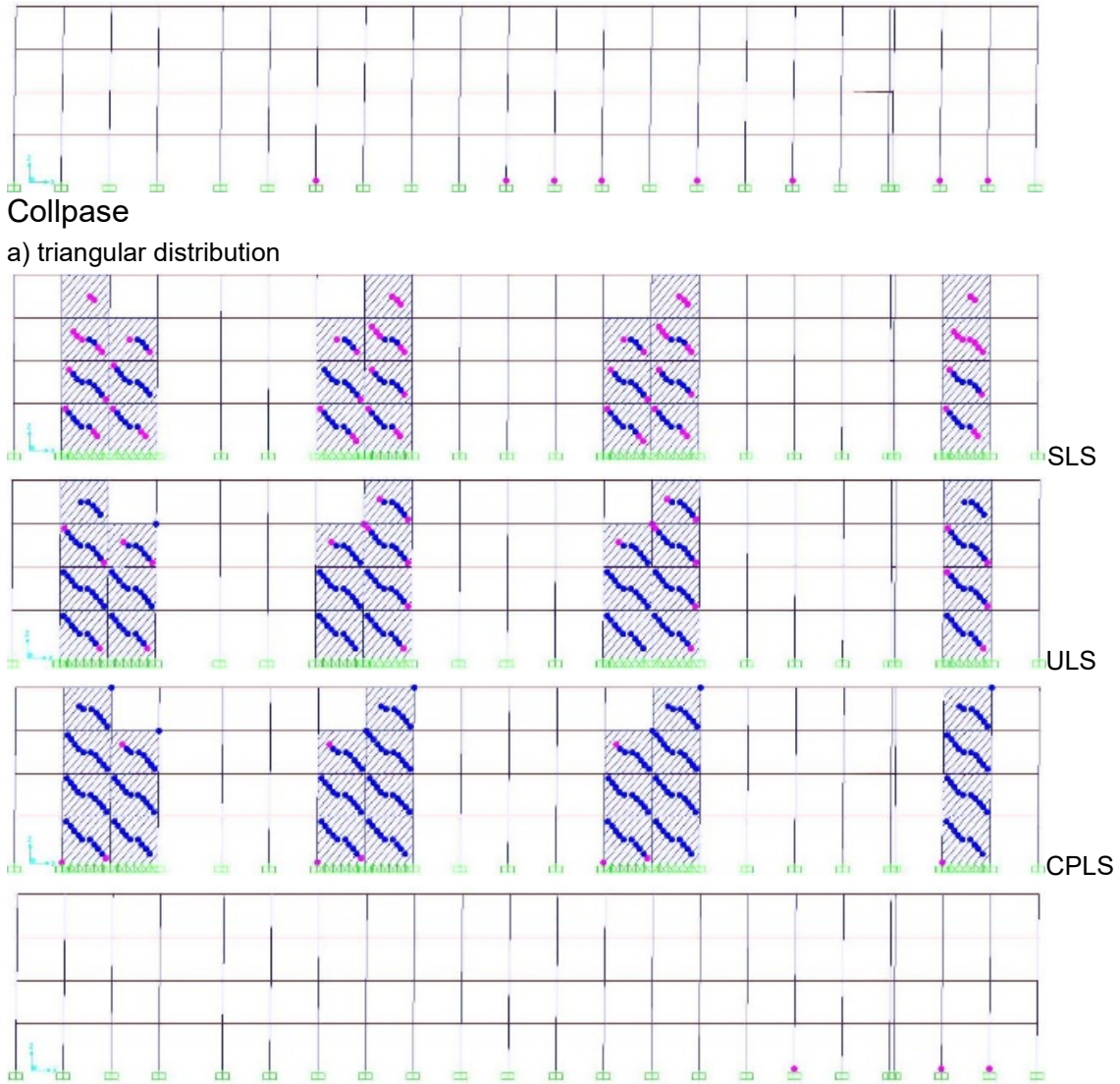
a) longitudinal direction

b) transversal direction

Figure 4.11: Force-displacement curves for SPSW upgraded structure, triangular and uniform distribution

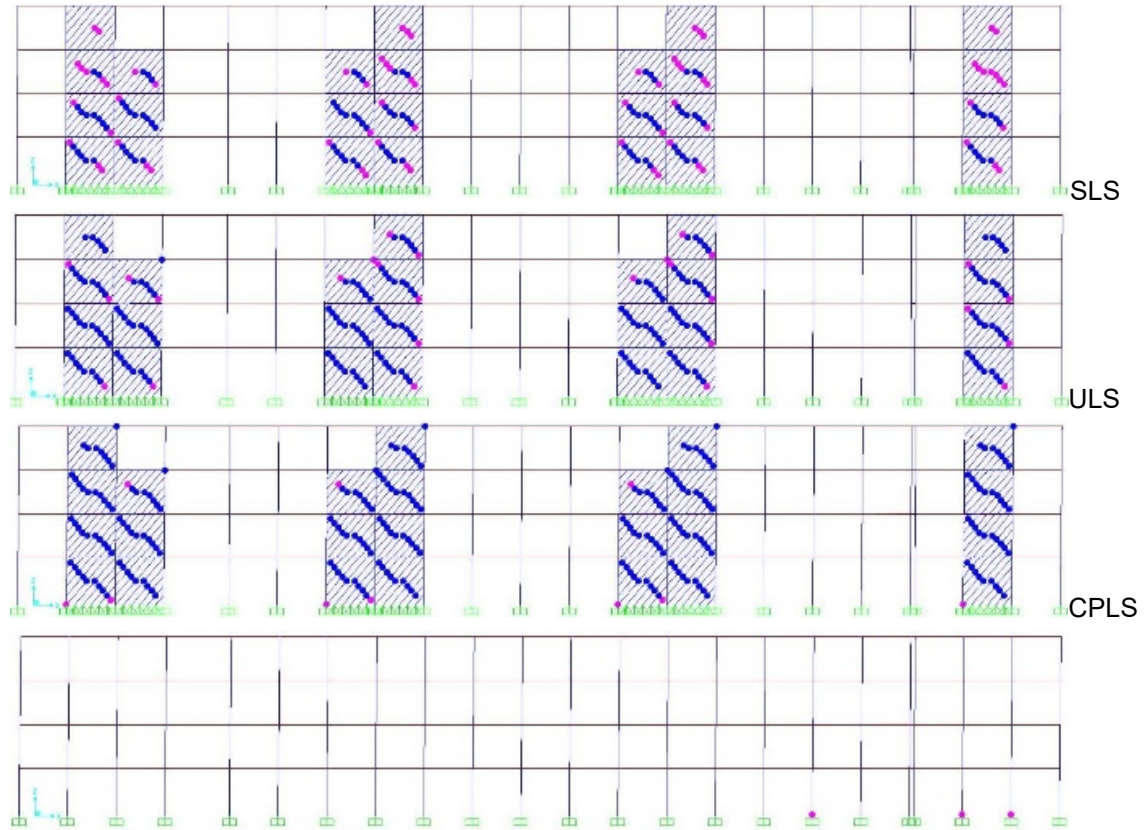
First plastic hinges develop before the attainment of the expected target displacement at SLS. With one exception, i.e. transversal direction, the expected target displacement for CPLS is attained before plastic hinges develop in un-retrofitted columns. This indicates the performance objectives of the upgraded structure are satisfied, and the risk of collapse is largely reduced. The structure shows a reserve of capacity after the attainment of the ULS displacement on transversal direction. The plastic mechanism is global, and the level of plastic deformation requirements is moderate.





Collapse

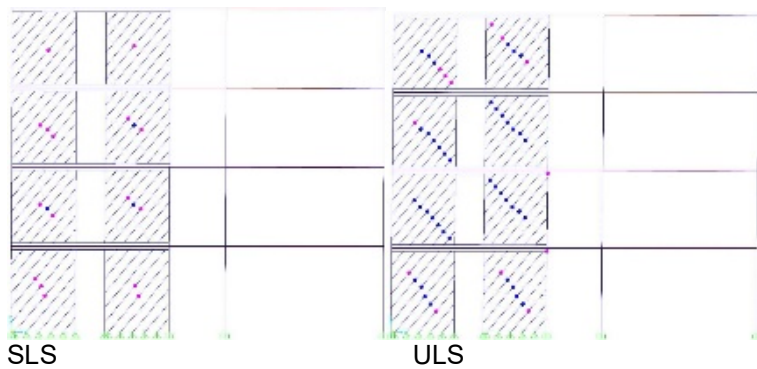
a) triangular distribution



Collapse

b) uniform distribution

Figure 4.12: Plastic hinges at the three limit states and collapse for SPSW structure, longitudinal direction



SLS

ULS

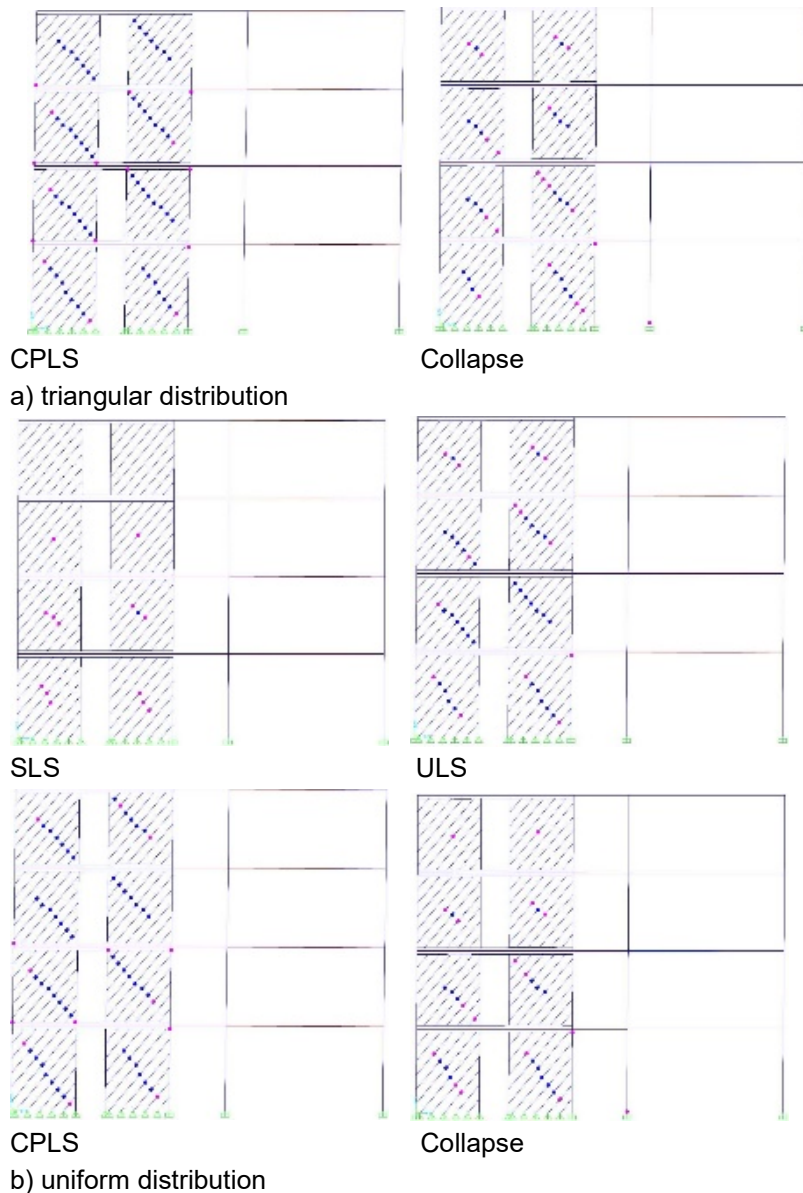
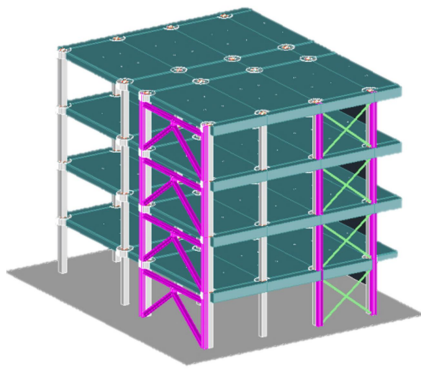


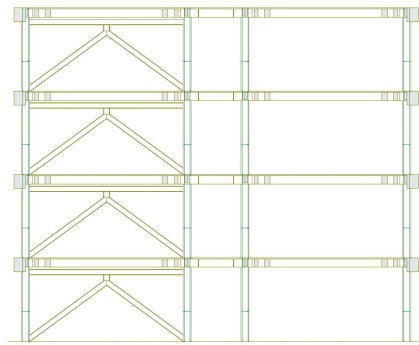
Figure 4.13: Plastic hinges at the three limit states and collapse for SPSW structure, transversal direction

Just for comparison, another structural system that was used to upgrade the existing concrete building is centrally braced frames + eccentrically braced frames [[10]]. In the following this system will be presented shortly.

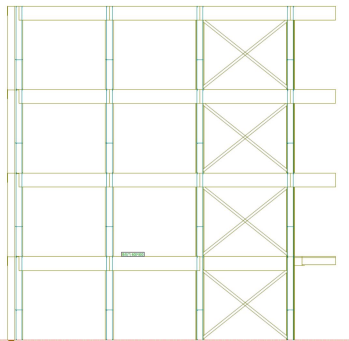
Figure 4.14 shows views and details of distribution for this upgrading system. On the longitudinal direction, the perimeter frames are upgraded using concentrically braced systems (CBF), introduced in several spans. On the transversal direction, an inverted V brace system and short vertical link has been adopted (EBF). Figure 4.15 the detailed 3D Finite Element Model and Figure 4.16 present the force-displacement curves, for triangular and uniform distribution of lateral forces, for CBF+EBF upgraded structure.



a) 3D view



b) transversal frame



c) longitudinal frame

Figure 4.14: Views with the upgrading CBF+EBF system

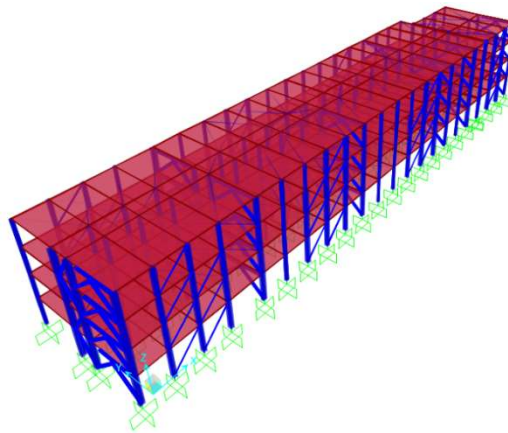
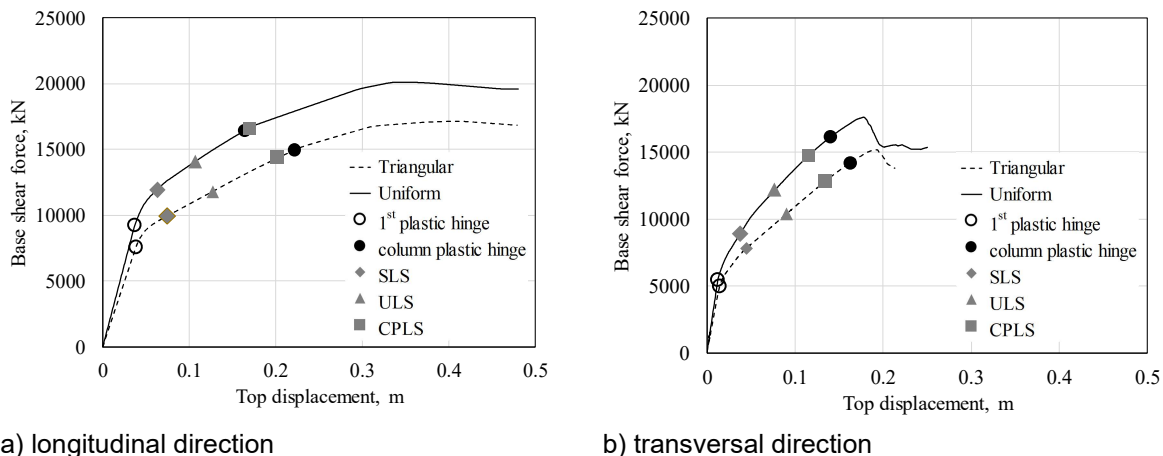


Figure 4.15: 3D models of CBF+EBF system



a) longitudinal direction

b) transversal direction

Figure 4.16: Force-displacement curves for CBF+EBF upgraded structure, triangular and uniform distribution

#### 4.1.4 Conclusions

The intervention requires the addition of lateral load resisting elements and possible local retrofitting of some columns. Fiber-reinforced polymer (FRP) techniques might be applied on this purpose. Also, since the diaphragm capacity of the flooring system needs to be improved, possible by adding steel bar braces at the level of each floor. The results obtained using nonlinear static analysis showed that the requirements for ultimate limit state can be accomplished without any additional local retrofitting of columns, while for collapse prevention limit state, some local retrofitting of columns are needed if SPSW system is adopted.

For the time being, the foundations have not been yet evaluated. However, in case, due to the demands induced by the strengthening of superstructure - even the density of interventions provides a good enough distribution, lowering these demands - seismic equilibration steel beams in-between foundations might be introduced, to provide tying of infrastructure system. If necessary, steel micro-piles could be also applied to enhance soil capacity.

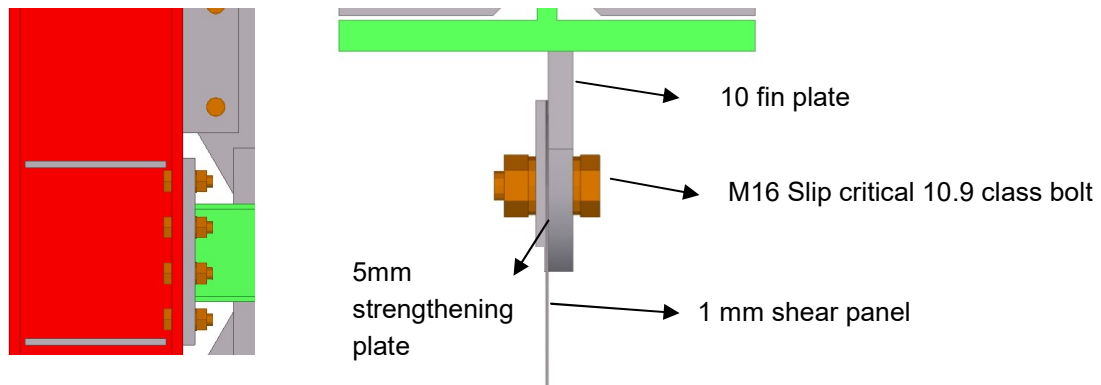
## 4.2 STRUCTURAL DETAILING

In the following are presented the detailing of the steel structure connections and the shear panel corner detail, Figure 4.17 and Figure 4.18. The detailing will be presented only for 1 story and frame in longitudinal and transversal direction, respectively.

### 4.2.1 Longitudinal direction

The main beam-to-column connection was designed using 24 mm extended end plate M24 10.9 class bolts (Figure 4.17,a). The connection between shear panel and boundary elements was designed using welded 10 mm fin plates to the boundary

elements and M16 slip-resistant 10.9 class bolts (Figure 4.17,b). 20 bolts were needed in both horizontal and vertical direction. An additional 5 mm strengthening plate is used on the bolted area of the shear panels in order to avoid failure by shear and bearing.



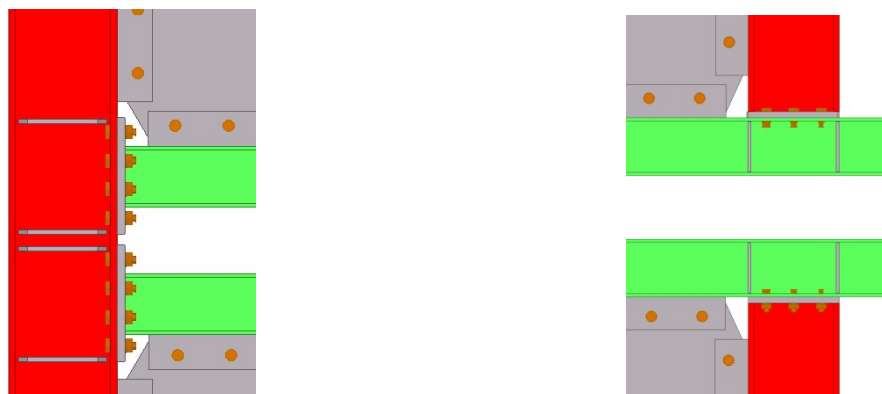
a) Shear panel beam-to-column connection

b) Shear panel to boundary element connection

Figure 4.17: Overview of joints in longitudinal direction

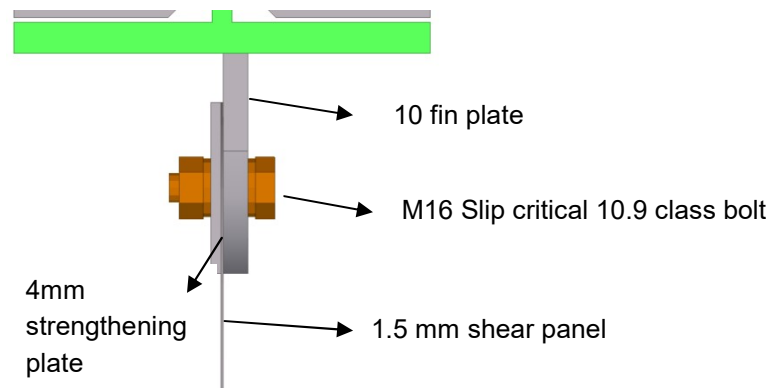
#### 4.2.2 In transversal direction

The main beam-to-column connection was designed using 27 mm extended end plate M24 10.9 class bolts (Figure 4.18,a). Stanchion-to-main beam connections were designed using 20 mm flush end plate and M20 10.9 class bolts (Figure 4.18,b). The connection between shear panel and boundary elements was designed using welded 10 mm fin plates to the boundary elements and M16 slip-resistant 10.9 class bolts (**Error! Reference source not found.c**). 22 bolts were needed for horizontal direction and 20 for vertical direction. An additional 4 mm strengthening plate is used on the bolted area of the shear panels in order to avoid failure by shear and bearing (Figure 4.18,c).



a) Shear panel beam-to-column connection

b) Stanchion-to-beam connection



d) Shear panel to boundary element connection

Figure 4.18: Overview of joints in transversal direction

### 4.3 REFERENCES

- [1] Computers and Structures Inc. (CSI): SAP 2000 Advanced Structural Analysis Program, Berkeley.
- [2] CEN. EN 1994-1-1 Eurocode 4: Design of composite steel and concrete structures -Part 1-1: General rules and rules for buildings, Brussels, 2004.
- [3] P.13 – 63, Normativ conditionat pentru proiectarea constructiilor civile si industriale din regiuni seismice (in Romanian), Bucharest, 1963.
- [4] P.13 – 70, Normativ pentru proiectarea constructiilor civile si industriale din regiuni seismice (in Romanian), Bucharest, 1970.
- [5] P100-1. Seismic Design Code. Part 1: Earthquake Resistant Design of buildings (in Romanian, Bucharest), 2013.
- [6] CEN. EN 1998-1 Eurocode 8: Design of structures for earthquake resistance-part 1: general rules, seismic actions and rules for buildings, Brussels, 2005.
- [7] Dubina, D and Dinu, F, "Experimental evaluation of dual frame structures with thin-walled steel panels". Thin-walled structures, 78, 57-69, 2014.
- [8] Neagu, C, Multi-Storey Building Frames Stiffened with Dissipative Shear Walls. 2011, Ph.D. Thesis: Politehnica Timisoara.
- [9] Driver R.G., Kulak G.L., Kennedy D.J.L. and Elwi A.E. "Seismic behavior of steel plate shears walls", Structural Engineering Rep. No. 215, Dept. of Civil Engineering, Univ. of Alberta, Edmonton, Alberta, Canada, 1997.
- [10] Dubina D., Dinu F., Neagu C., Marginean I. and Dan D. "Structural upgrade of reinforced concrete building frames using replaceable hysteretic steel-based fuse elements", 3<sup>rd</sup> International Conference on PROTECTION OF HISTORICAL CONSTRUCTIONS, Lisbon, Portugal, 12 – 15 July, 2017.

## **5 SEISMIC UPGRADING OF AN EXISTING INDUSTRIAL BUILDING USING CONCENTRICALLY BRACED FRAMES WITH MODIFIED BRACES**

### **5.1 CBF-MB**

#### *5.1.1 Introduction*

This case study refers to the seismic upgrading of existing industrial building. It aims at demonstration of the implementation of the Concentrically Braced Frames with Modified Braces (CBF-MB) in rehabilitation of structures. The case study elaborated refers to modelling and analysis by q-factor approach based on linear response spectrum analysis methods (RSA) and N-2 method based on Static Nonlinear Analysis (SNA). It also demonstrates detailed design of the main dissipative and non-dissipative members and basic structural detailing of CBF-MB. The design and analysis of the rest part of the structure including the industrial frame, roof truss and RC columns are not presented in the current case study.

#### *5.1.2 Description of the building*

##### *5.1.2.1 Period of construction and type of the building*

The subject of the rehabilitation case study is an industrial building, built in the mid-sixties (1965) operating as raw material storage of metallurgy plant. It is a single storey, single span reinforced concrete industrial frame, accommodating a heavy overhead crane. Part of the building is covered by roof and enclosed by masonry walls while the rest part is open - Figure 5.1, a). Since environmental requirements do not allow spreading of dust, the owner of the plant has started renovation project including construction of new roof and walls that enclose the whole building in conjunction with the structural seismic upgrade. A supplementary objective of that case is to keep as much as possible from the existing reinforced concrete frame as well as the existing foundation Figure 5.1 b).



a) View from the warehouse before the renovation project

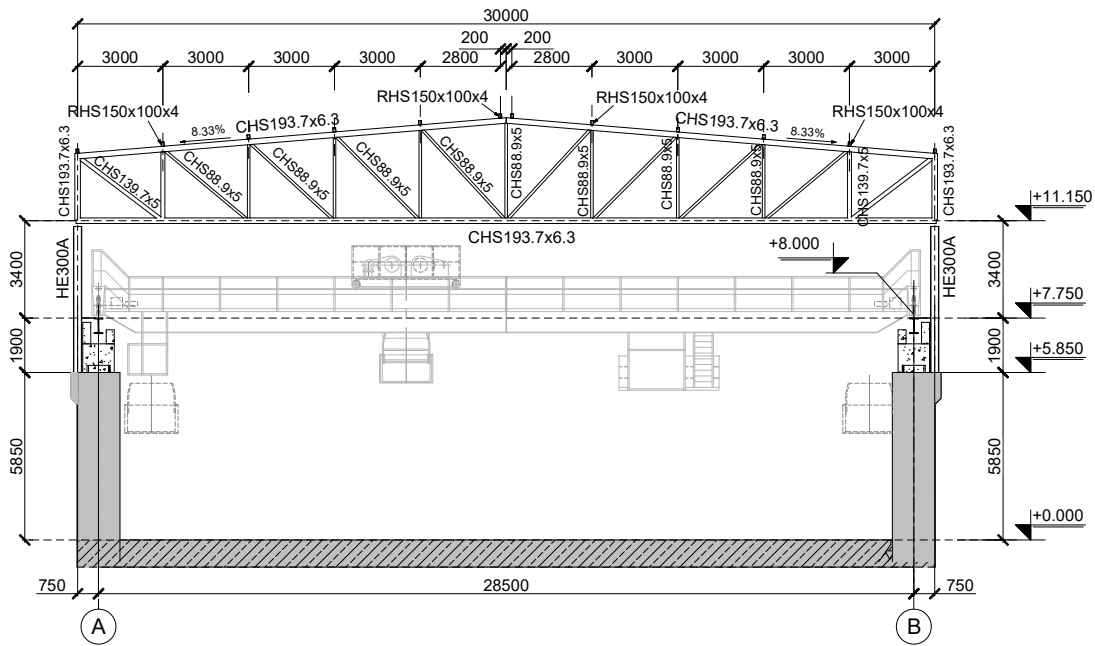


b) View from the warehouse after the renovation project

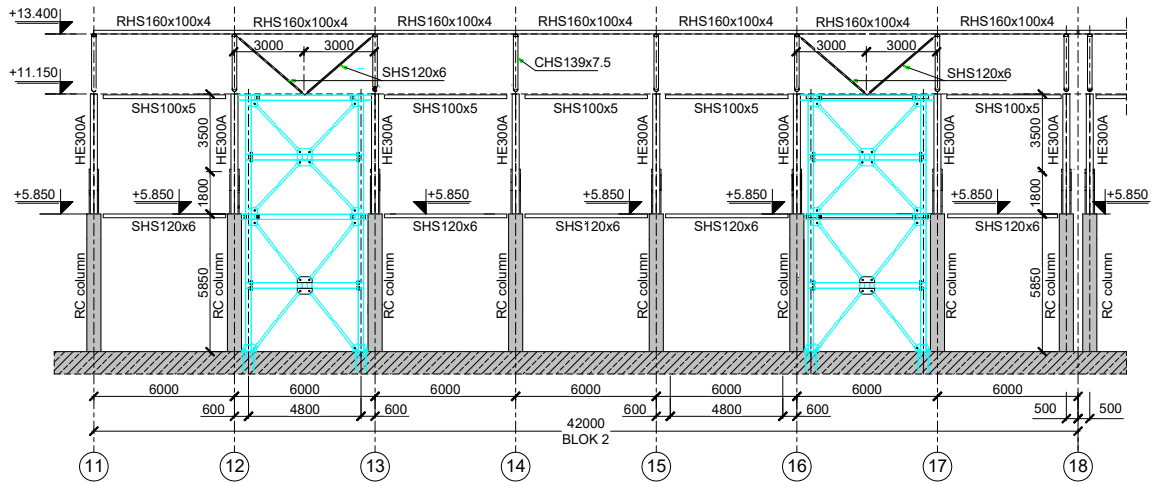
Figure 5.1: The industrial building, subject of renovation and rehabilitation

The design solution for the building case is realized by introducing steel penthouse over the existing reinforced concrete (RC) columns. Steel superstructure is installed into the concrete substructure thus achieving integral dual industrial frame. The frame consists of steel roof truss and compound columns including steel upper pillar and RC down columns. The span of the frame is 28 500 mm and the distance between frames is 6 000 mm. All the gravity and horizontal loads (wind and earthquake) as well as the transverse crane brake forces are carried out by the industrial frame. For that purpose, the RC part of the column is strengthened by concrete jacket and the steel penthouse is designed as per the contemporary code [10] requirements. The longitudinal load resisting system consists of roof and wall bracings, which also ensure the stability of the structure. The wall bracings are realized by a pair of Concentrically Braced Frames with Modified Braces (CBF-MB) connected to the RC columns - Figure 5.2. The overall axial dimensions of the structure, objective of the current case study are 48 000 mm in longitudinal direction and 30 000 mm in transverse direction. The height of the structure to the ridge is 15 000 mm.

CHS profiles are used for the roof truss elements and RHS for the roof purlins. The diagonals of the roof bracing are designed by SHS. The choice of cross section type for all roof members is governed by corrosion protection requirements. The steel columns are designed by hot rolled HEA 300 profile. The crane girder is realized by HEB 450 in a single span solution. The upper beam flange is laterally restrained by continuous steel sheet. Concrete columns are with rectangular cross section 1500/600 mm including the new concrete jacket.



a) View of the industrial frame



b) Side view of the CBFs-MB and gravity frame

Figure 5.2: Structural overview

Each CBF-MB consists of two columns, floor beams, splitting beams and braces. It is integrated between the concrete columns. In this way steel columns of the CBF duplicate with the RC columns. That solution was preferred for the relieved steel connection design and for the easier integration of steel and concrete columns. The braced frame is arranged between axes 23 and 24 and is designed by three panels stacked over the building height - Figure 5.2. The first two panels are with crossed diagonals considered as the dissipative part of the system while the top one is inverted V-type and is considered as non-dissipative.

### 5.1.2.2 Materials

Steel grade S235 is used for the design of modified braces (dissipative elements) The adopted steel grade for CBF columns is S355. CBF-MB floor<sup>1</sup> beams and splitting beams are designed with steel grade S275.

The industrial frame is designed by conventional approach and steel grade S275 is used. Concrete C25/30 and reinforcing steel B500B are used for all RC members. All roof and wall sheeting is realized by corrugated steel sheet, thickness 0.6mm, wave height 55 mm.

### 5.1.2.3 Loads and load combinations

Table 5.1 summarizes the adopted gravity loads and seismic action parameters. The roof is non-occupied one. The altitude of construction site is below 1000 meters and in compliance with the Bulgarian National Annex the snow load is included in the seismic design situation with reduced intensity. Only the self-weight of the crane girder and crane maintenance path were taken into account in the seismic combination.

Table 5.1: Loads and actions

<b>Vertical loads</b>	
Roof sheeting	0.10 kN/m <sup>2</sup>
Roof truss and purling: – top chord, purlins and bracings – bottom chord and bracings	Included in 3D model Included in 3D model
Steel and concrete columns	Included in 3D model
Façade sheeting and girts	0.20 kN/m <sup>2</sup>
Crane girders Crane path	Included in 3D model 1.0 kN/m
Snow	1.16 kN/m <sup>2</sup> / not included into seismic design situation
<b>Seismic action</b>	
Design response spectrum for elastic analysis Reference peak ground acceleration Importance class II (Ordinary building) Ground type Behaviour factor $q$	Type 1 $a_{g,R} = 0.30g$ $\gamma_I = 1.0$ $B (T_B = 0.15 \text{ s}, T_C = 0.50 \text{ s})$ 2.0

<sup>1</sup> To be considered as the inter-stack beams (in order to comply with the CBF-MB system element signature)

Damping ratio	5%
Factors for storey occupancy	NA
Seismic combination coefficient	
Roof (snow)	$\psi_2 = 0.30, \psi_E = 1.00$

The seismic masses are calculated according to Eq. (5.1). Since it is an industrial building with dual structure (RC columns and steel penthouse), the illustration of the mass distribution within the building height is presented in Figure 5.3 and is summarized in Table 5.2.

$$\sum_{j>1} G_{k,j} + \sum_{i>1} \psi_{E,i} \cdot Q_{k,i} \quad \text{Eq. (5.1)}$$

Table 5.2: Seismic masses

Description	Elevation
Roof seismic mass = 102.4 t	Between 13.400 to 15.000
Bottom chord seismic mass = 56.9 t	Elevation 11.150
Crane path seismic mass = 86.3 t	Elevation 7.200
RC columns seismic mass = 397.6 t	Between 0.000 to 5.850

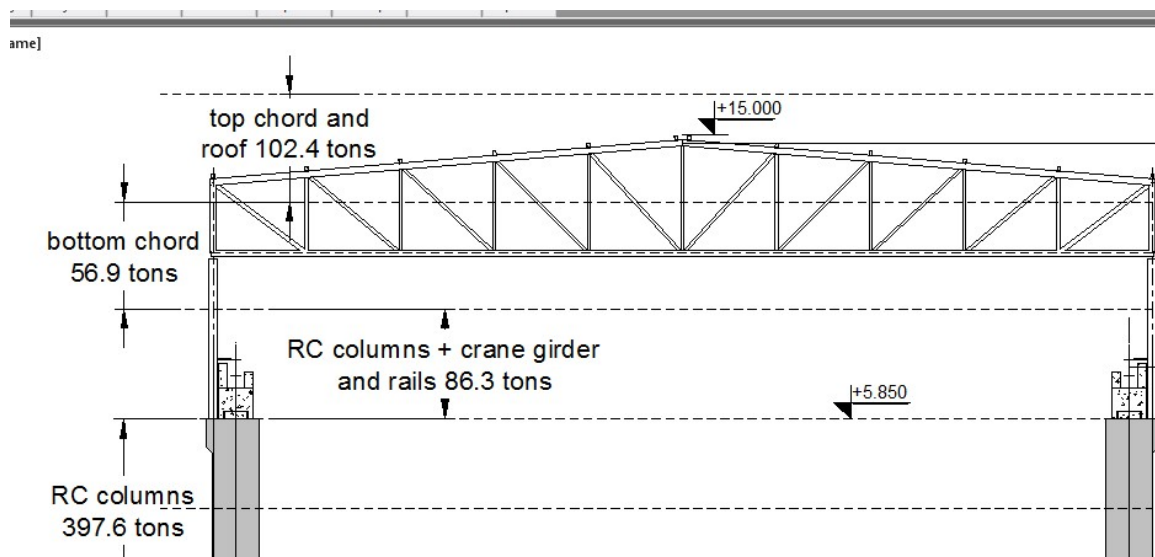


Figure 5.3: Seismic mass distribution and lumped mass model

It was assumed that half of the seismic mass due to the heavy RC columns will be lumped to elevation 5.850 (the top of the RC column) and the rest half will be lumped to the base and therefore will not be included in the lumped mass model.

## 5.2 BASIC ASSUMPTIONS AND DESIGN

### 5.2.1 Basic design assumptions

Since the RC columns were existing ones and having the same original sizes, it was decided that all columns will be strengthened by equal RC jackets. So the jacketed RC columns in cooperation with the upper steel column and the roof truss constitute a Dual Frame that should provide strength and stiffness for all gravity loads and transverse horizontal loads, including the crane as well. The design and analysis of the dual frame will not be elaborated in this case study. The focus will be the implementation of CBFs with Modified Braces (MB) for provision of longitudinal strength and stiffness as well as their seismic design. Two pairs of CBF-MB were designed within the longitudinal facades of the building. In order to avoid the complication of column strengthening and to achieve all RC jacketed columns being equal and in the same stress state it was preferred the system CBF-MB to be inserted between two RC columns. It was also connected and laterally restrained at level 5,850 and 11.150, thus having two independent earthquake resistant systems - the Dual Frame and the CBF-MB.

### 5.2.2 Preliminary selection of modified braces

The modified braces provide the primary source of stiffness and dissipation capacity for the CBF-MB system and their design differs from the ordinary brace design. Initially, brace shape and first-estimation cross sections need to be chosen. The unexperienced user should expect that some iterations would have to be done. The cross-sections to be defined are illustrated in Figure 5.4 and the choice of their recommended lengths is demonstrated in Table 5.3. The recommendations of [5, 6] have been followed.

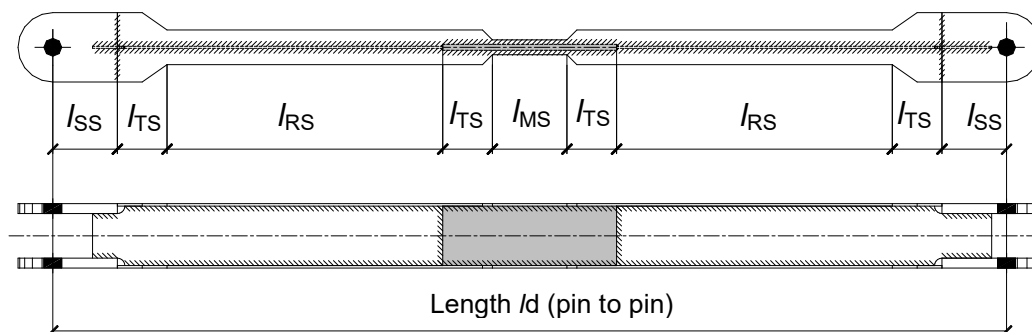


Figure 5.4: Definition of the cross-sections within a modified brace member

Table 5.3: Choice of specific lengths in modified braces

Specific length (mm)	Recommendations according to [5], [6]	The particular value in this example (mm) stack 1 / stack 2 <sup>2</sup>
$l$	NA	7567 / 7150
$l_d$	$(0.375 - 0.40)l$	3000 / 2860
$l_{MS}$	$l_{MS} = (0.067 \div 0.085)l_d$	200 / 200
$l_{TS}$	$\sim 100$	100 / 100
$l_{SS}$	Preference of designer	130 / 130
$l_{RS}$	$l_{RS} \approx (0.3)l_d$	1070 / 1000

Where:

$l$  is the system length of the diagonal in a stack,

$l_d$  is the pin-to-pin length of the brace,

$l_{MS}$  is the length of the modified section,

$l_{TS}$  is the length of the transition section,

$l_{SS}$  is the length of the strong section,

$l_{RS}$  is the length of the reduced section,

MS, RS, SS and TS are abbreviations for modified section, reduced section, strong section and transition section, respectively.

As stated in [5] and [6], some relations between the area and the section modulus of the reduced section and the modified section should be achieved to ensure that yielding in tension and flexural plastic strains due to buckling occur in different zones along the modified brace length. The preliminary adjustment of the brace flange and web geometry is demonstrated in Table 5.4. The MB cross sections will be described by abbreviations for example F110.8W140.6-M200.40-T22 that should be interpreted as explained below:

- For reduced section: F (flange) 110.8 width 110 mm, thickness 8 mm; W (web) 140.6 width 140 mm, thickness 6 mm;
- For modified section: M (modified section) 200.40 length 200 mm, flange width 40 mm – T22 (web thickness of MS) 22 mm.

<sup>2</sup> Stack is the part of the CBF, consisting of four modified braces and one splitting beam, enclosed by columns and floor beams.

Table 5.4: Choice of Area and Section modulus in modified braces

Stack №	Abbreviation of the MB	Recommendations according to [5], [6]	Value, adopted in the particular example
1 <sup>st</sup> stack	F110.8W140.6-M200.40-T22	$A_{MS}/A_{RS} \geq 1.4$	$A_{MS} = 37.2 \text{ cm}^2$
			$A_{RS} = 26.1 \text{ cm}^2$
			$A_{MS}/A_{RS} = 1.43$
		$W_{pl,RS}/W_{pl,MS} \geq 2.0$	$W_{MS} = 23.3 \text{ cm}^3$
			$W_{RS} = 49.7 \text{ cm}^3$
			$W_{pl,RS}/W_{pl,MS} = 2.13$
2 <sup>nd</sup> stack	F90.8W140.4-M200.40-T16	$A_{MS}/A_{RS} \geq 1.4$	$A_{MS} = 28.8 \text{ cm}^2$
			$A_{RS} = 20.1 \text{ cm}^2$
			$A_{MS}/A_{RS} = 1.43$
		$W_{pl,RS}/W_{pl,MS} \geq 2.0$	$W_{MS} = 15.4 \text{ cm}^3$
			$W_{RS} = 32.9 \text{ cm}^3$
			$W_{pl,RS}/W_{pl,MS} = 2.14$

Where:

$A_{MS}$  is the modified section area,  $A_{RS}$  is the reduced section area.

$W_{pl,RS}$  is the reduced section plastic modulus,

$W_{pl,MS}$  is the modified section plastic modulus.

### 5.2.3 Preliminary check of brace slenderness

Since there is modified section inserted in the mid-length, then the real buckling length  $l_{cr} = \mu \cdot l_d$  will be longer than  $l_d$ . The effective length  $l_{cr}$  may be obtained by FE elastic buckling analysis or by Eq. (5.2):

$$\mu = l_{cr} / l_d = 0.88 K_L^{(0.033)} \cdot K_I^{(0.1 \ln(K_L) - 0.36)} \quad \text{Eq. (5.2)}$$

Where:

$K_L = L_{RS} / L_{MS}$  is section length ratio,

$K_I = I_{MS} / I_{RS}$  is inertia moment ratio,

$I_{MS}$  is the moment of inertia of modified section,

$I_{RS}$  is the moment of inertia of reduced section,

$\mu$  is parameter that modifies the geometric brace length  $l_d$  to buckling length  $l_{cr}$ .

Hereafter Eq. (5.2) is used and the results are presented in Table 5.5. According to [1], braces of CBFs with X-configuration must have non-dimensional slenderness in the range of  $1.3 \leq \bar{\lambda}_{\text{eff}} \leq 2.0$ . The effective slenderness is defined by Eq. (5.3).

$$\lambda_{eff} = \mu \cdot l_d / i_{RS} \quad \text{Eq. (5.3)}$$

where  $i_{RS}$  is the minor radius of gyration of the reduced section.

Table 5.5: Modified braces slenderness

Stack No	Modified Brace	$K_L$	$K_I$	$\mu$	$L_{cr}$ (m)	$\lambda_{eff}$	$\bar{\lambda}_{eff}$
1 <sup>st</sup> stack	F110.8W140.6- M200.40-T22	5.35	0.1179	1.403	4.209	161.0	1.714
2 <sup>nd</sup> stack	F90.8W140.4- M200.40-T16	5.00	0.1368	1.379	3.943	178.8	1.904

#### 5.2.4 Simulation

The structural linear elastic model was done by the software SAP 2000 [8]. Common engineering rules and specific rules given in [5, 6] were used. All RC columns are modelled by truss analogy, providing equivalent stiffness and mass. They are considered fixed to the bases in both directions. The elastic flexural and shear stiffness properties of concrete were taken as being 50% from the initial ones in order to simulate the performance of cracked elements.

The upper steel column was simulated as fixed to the RC down column at its strong axis as per the implemented structural detail. In the same time the steel column was simulated as simple connected to the RC column at its weak axis in spite that the structural detail provides some partial fixation. For safe side design, conservative approach for simulation was preferred and implemented, thus the whole lateral stiffness and strength in longitudinal direction will be attributed to the CBF-MB. All joints between bracing struts and columns or trusses are simulated as nominally pinned as they were designed.

CBF-MB members are designed and modelled as follows. CBF-MB columns are continuous. The joints between splitting beams and columns are assumed to be rigid and full strength so they are modelled as continuous while the joints between beams and CBF-MB columns are assumed nominally pinned. The elements, simulating the modified braces are defined through constant H-shape section with characteristics of the reduced section and joined to the frame by simple pin connections. CBF-MB column bases were designed and detailed as pinned which is considered the most practical approach for this case. The elastic analysis requires a tension-only diagonal model [1]. The generated three-dimensional FE model is illustrated on Figure 5.5.

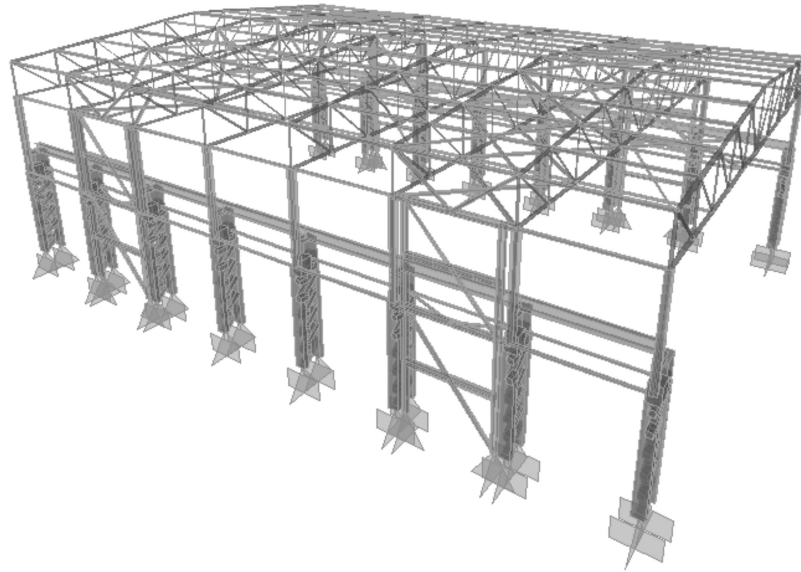


Figure 5.5: FE three-dimensional model

The current case study was developed by centreline-to-centreline (CL-to-CL) model for the CBF-MB. It is quick and easy to be defined, since the axis geometry of the frame is known at the beginning of the design process.

#### 5.2.5 *Design for static combinations*

The conventional design for static loads and combinations will be omitted in this case study.

### 5.3 SEISMIC ANALYSIS

#### 5.3.1 *Seismic design situation*

The building is recognized as regular in plan but irregular in height. Due to its functionality and the case of exploring Dual Frame which combine heavy concrete columns and light weight steel penthouse, mass irregularity in height is established. On the other hand, the building is symmetric in plan in sense of stiffness and masses. The overhead crane stays in special parking position which does not belong to the current building, so the masses due to crane self-weight were not taken into account. Theoretically the centre of masses and the centre of rigidity coincide. In order to account for uncertainties in the location of masses and for the rotational component of the seismic motion, additional accidental mass eccentricities (§4.3.3.3.3 [1]) with value of 1500 mm and 2100 mm (5% of 30 000 mm and 5% of 42 000 mm) were introduced in both transverse and longitudinal directions respectively. For simulating the accidental torsion effects, only the roof masses (top and bottom chord) were used. The mass eccentricity effects were taken into account

by defining two static load cases  $M_x$  and  $M_y$ , simulating rotation. For that analysis, the roof seismic forces in both main directions were approximately but rather reasonably calculated based on the lateral force method (§4.3.3.2 [1]). The torsional effects were simulated by resultant force couples applied at each frame for  $X$  direction and applied at each braced frame for  $Y$  direction. For simulating the load case  $M_x$ , force couple were assumed with linearly variable magnitude while for the load case  $M_y$ , the two couples were assumed with constant magnitude. The final seismic design load case accounting for accidental torsional effects was derived by Eq. (5.4) as recommended by P. Fajfar [7].

$$E = SRSS (E_x \pm M_x, E_y \pm M_y) \quad \text{Eq. (5.4)}$$

where:

$E_x$  and  $E_y$  are the results of analysis without accidental torsion by applying RSA in  $X$  and  $Y$  direction, respectively;

$M_x$  and  $M_y$  are the accidental torsional effects of applied roof seismic force with eccentricity of 5% in  $X$  and  $Y$  direction, respectively;

SRSS is square root of sum of squares combination.

The global torsional effects in  $Y$  direction were estimated as about 9% amplification of the seismic effects (internal forces and displacements) for the top stack of CBF-MB and about 5% for the bottom stack. The global rotational effect in  $X$  direction were estimated as about 12,3% amplification of the seismic effects for the first and last frame. The amplification for the rest of the frames was 8.7%, 7.8% and 2.8%. The closer the dual frames to the centre of the buildings are the less the torsional effects are.

The seismic combination that governs the CBF-MB braces design is calculated according to Eq. (5.5).

$$\sum_{j=1}^4 G_{k,j} + E + 0.3Q_{k,1} \quad \text{Eq. (5.5)}$$

where:

$G_{k,j}$  are the gravity load effects in seismic design situation;

$E$  is the effect of the seismic action including accidental torsional effects;

$Q_{k,1}$  is the snow on the roof in seismic design situation;

### 5.3.2 Response Spectrum Analysis

Modal RSA was performed. The first and the second natural modes of vibrations are presented on Figure 5.6. They are translational and torsional and activate the

masses in X direction. The third mode of vibration is shown on Figure 5.7 and it is translational in Y direction.

According to [1] when  $T_C \leq T$ , the spectrum acceleration has to be greater or equal to the lower bound. In that study it is obvious that the design spectral acceleration of the first mode is much greater than the lower bound. It is proven by Eq. (5.6):

$$S_d(T_1 = 0.647) = 3.544 > \beta \cdot a_g = 0.587, \quad \text{Eq. (5.6)}$$

where  $\beta = 0.2$  is the lower bound factor for the horizontal design spectrum. The check proves that there is no need to increase the base shear.

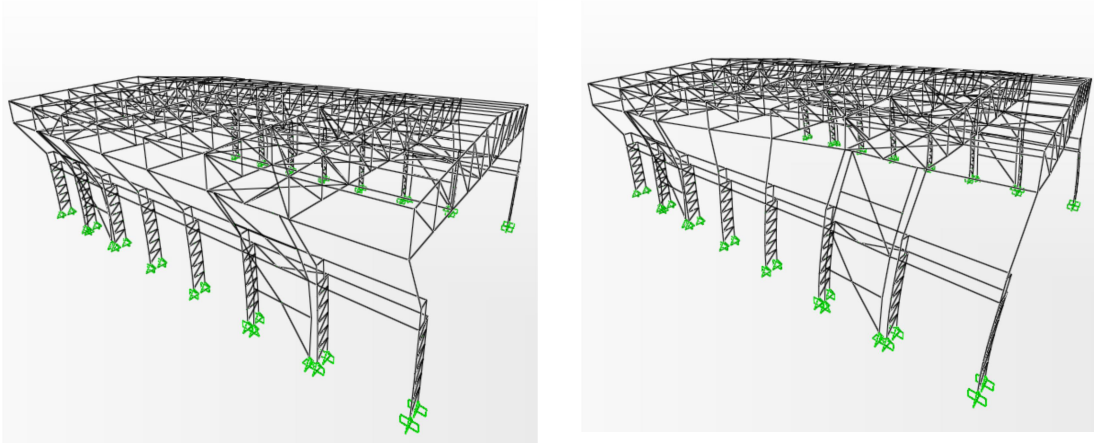


Figure 5.6: First and second mode of free vibrations,  $T_1 = 0.648$  s,  $T_2 = 0.465$  s

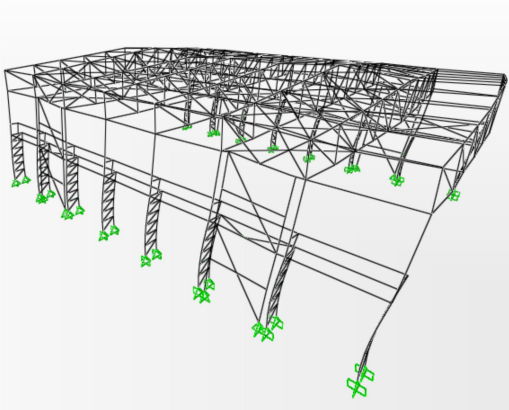


Figure 5.7: Third mode of free vibrations,  $T_3 = 0.449$  s

## 5.4 DETAILED DESIGN

### 5.4.1 Damage limitation – limitation of interstorey drift

Assuming that the building has ductile non-structural elements, the verification is:

$$d_r \cdot \nu \leq 0.0075h = 0.0075 \cdot 5850 = 43.9 \text{ mm},$$

$$d_r \cdot \nu \leq 0.0075h = 0.0075 \cdot 5650 = 42.4 \text{ mm},$$

Eq. (5.7)

Where  $\nu = 0.5$  is the reduction factor according to §4.4.3.2 (1) of [1],  $h$  is the story height and  $d_r$  is the design interstorey drift. For that particular case  $h$  is the height corresponding to the Braced Frame stacks. Table 5.6 includes the results from the analysis for each of the stacks.

Table 5.6: Limitation of interstorey drift

Stack	1 (elevation 5.850)	2 (elevation 11.500)
$d_{e,top}$ (mm)	13.0	25.9
$d_{e,bottom}$ (mm)	0.0	13.0
$d_r = (d_{e,top} - d_{e,bottom}) q$ (mm)	26.0	25.8
$d_r \nu$	26.0 < 30.0	25.8 < 30.0

#### 5.4.2 Second order effects

The sensitivity to second order ( $P-\Delta$ ) effects is estimated by the interstorey drift sensitivity coefficient  $\theta$  given by Eq. (5.8), where  $P_{tot}$  and  $V_{tot}$  are the total gravity load at and above the storey considered in the seismic design situation and the total seismic storey shear, respectively, at the storey under consideration. In this particular case, the first stack of the braced frames was considered as first storey and the second stack - as second storey. The calculated values of  $\theta$  are listed in Table 5.7.

$$\theta = P_{tot} d_r / V_{tot} h$$

Eq. (5.8)

Table 5.7: 2nd order effects

Stack	1	2
$d_r = (d_{e,top} - d_{e,bottom}) q$ (mm)	26.0	25.8
$P_{tot} / V_{tot}$	6310 / 1819	1563 / 995
$h$ (mm)	5850	5650
$\theta$	0.015 < 0.10	0.007 < 0.10

The values of  $\theta$  for both storeys are less than 0.1, therefore second-order effects may be neglected.

### 5.4.3 Final verification of dissipative members

The non-dimensional slenderness of the brace,  $\bar{\lambda}_{eff}$  should be limited to  $1.3 \leq \bar{\lambda}_{eff} \leq 2.0$  as stated in §6.7.3 (1) of [1]. The yield resistance  $N_{pl,Rd}$  of the modified brace should fulfil §6.7.3 (5) of [1] and should be obtained by Eq. (5.9).

According to §6.7.3 (8) of [1] the maximum and minimum overstrength,  $\Omega$  should not differ more than 25% ensuring homogeneous dissipative behaviour of the diagonals. Since the initial brace cross-sections are not changed after the verifications in sections 4.1 and 4.2, the normalized slenderness is not changed and the valid results are shown in Table 5.5. The rest verifications are presented in Table 5.8.

$$N_{pl,Rd} = A_{RS} \cdot f_y / \gamma_{M0} \quad \text{Eq. (5.9)}$$

Table 5.8: Verification of braces and check for homogeneous dissipative behaviour

Stack №	Modified Brace	$A_{RS}$ (cm <sup>2</sup> )	$N_{Ed}$ (kN)	$N_{pl,Rd}$ (kN)	$\Omega = \frac{N_{pl,Rd}}{N_{Ed}}$	$\frac{\max \Omega}{\min \Omega} < 1.25$
1 <sup>st</sup> stack	F110.8W140.6-M200.40-T22	26.0	517.6	581.9	1.124	1.033
2 <sup>nd</sup> stack	F90.8W140.4-M200.40-T16	20.0	385.6	447.6	1.161	

### 5.4.4 Transition stage

The splitting beam should be designed as per the recommendations of [5, 6]. The transition stage (“just before buckling” stage) is introduced because it is proven to cause additional bending moments and axial forces (load case *UNB*) that occur within the storey *H*-frame – Figure 5.8. That internal effect is to be accounted for into design. It is simulated in the model for elastic analysis by introducing unbalanced forces integrally in each of the two stories simultaneously.

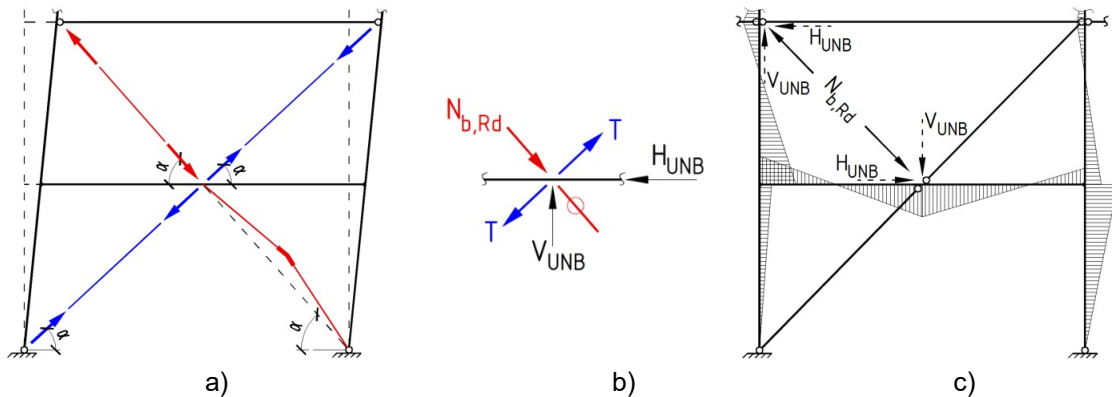


Figure 5.8: a) Transition stage (“just before buckling”); b) Unbalanced forces; c) Internal moments ( $M_{UNB}$ ) resulting from the unbalanced forces (load case UNB)

The unbalanced forces are calculated based on Eq. (5.10), Eq. (5.11), Eq. (5.12) and the results are presented in Table 5.9.

$$V_{UNB} = N_{b,Rd} \cdot \sin \alpha \quad \text{Eq. (5.10)}$$

$$H_{UNB} = N_{b,Rd} \cdot \cos \alpha \quad \text{Eq. (5.11)}$$

$$N_{b,Rd} = \chi \cdot A_{RS} \cdot f_y / \gamma_{M1} \quad \text{Eq. (5.12)}$$

Table 5.9: Unbalanced forces in splitting beams

Stack №	Modified Brace	$A_{RS}$ (cm <sup>2</sup> )	Buckling curve	$\chi$	$N_{b,Rd}$ (kN)	$V_{UNB}$ (kN)	$H_{UNB}$ (kN)
1 <sup>st</sup> stack	F110.8W140.6- M200.40-T22	26.0	“c”	0.255	148.4	114.7	94.1
2 <sup>nd</sup> stack	F90.8W140.4- M200.40-T16	20.0	“c”	0.213	95.3	72.7	61.7

#### 5.4.5 Capacity design of non-dissipative members

CBF-MB columns shall be verified to resist design forces obtained from Eq. (5.13) to Eq. (5.15). The results for column verifications are presented in Table 5.10.

$$N_{col,Ed} = N_{Ed,G} + 1.1\gamma_{OV}\Omega_{min}\rho(N_E + N_{UNB}) \quad \text{Eq. (5.13)}$$

$$M_{col,Ed} = M_{Ed,G} + 1.1\gamma_{OV}\Omega_{min}\rho(M_E + M_{UNB}) \quad \text{Eq. (5.14)}$$

$$V_{col,Ed} = V_{Ed,G} + 1.1\gamma_{OV}\Omega_{min}\rho(V_E + V_{UNB}) \quad \text{Eq. (5.15)}$$

Where:

$\gamma_{OV}=1.25$  is the material overstrength factor according to §6.2 (3) of [1],

$\Omega_{MIN} = 1.124$  as per Table 5.8,

$\rho = 1.00$  is factor accounting for the available overstrength of the system, when DCM or lower is adopted (see [6]).

Table 5.10: CBF columns verification

Stack №	Column cross-section / Material	$N_{col,Ed}$	$M_{col,Ed}$	Utilization factor
1 <sup>st</sup> stack	HEB 260 / S355	-1016	151.2	0.946
2 <sup>nd</sup> stack	HEB 260 / S355	-352.5	91.2	0.493

Splitting beams shall be verified to resist design forces obtained from Eq. (5.16) to Eq. (5.18). The results for splitting beams verifications are presented in Table 5.11.

$$N_{sb,Ed} = N_{Ed,G} + 1.1\gamma_{OV}\Omega_{min}\rho(N_E + N_{UNB}) \quad \text{Eq. (5.16)}$$

$$M_{sb,Ed} = M_{Ed,G} + 1.1\gamma_{OV}\Omega_{min}\rho(M_E + M_{UNB}) \quad \text{Eq. (5.17)}$$

$$V_{sb,Ed} = V_{Ed,G} + 1.1\gamma_{OV}\Omega_{min}\rho(V_E + V_{UNB}) \quad \text{Eq. (5.18)}$$

Table 5.11: Splitting beam verification

Stack No	Splitting beam cross-section / Material	$N_{sb,Ed}$	$M_{sb,Ed}$	Utilization factor	$\bar{\lambda}_{LT}$
1 <sup>st</sup> stack	HEA 260 / S275	-105.0	140.0	0.685	0.45
2 <sup>nd</sup> stack	HEA 260 / S275	-72.7	93.0	0.457	0.45

Floor beams shall be verified to resist design forces obtained from Eq. (5.19) to Eq. (5.21). The results are presented in Table 5.12.

$$N_{b,Ed} = N_{Ed,G} + 1.1\gamma_{OV}\Omega_{min}\rho(N_E + N_{UNB}) \quad \text{Eq. (5.19)}$$

$$M_{b,Ed} = M_{Ed,G} + 1.1\gamma_{OV}\Omega_{min}\rho(M_E + M_{UNB}) \quad \text{Eq. (5.20)}$$

$$V_{b,Ed} = V_{Ed,G} + 1.1\gamma_{OV}\Omega_{min}\rho(V_E + V_{UNB}) \quad \text{Eq. (5.21)}$$

Table 5.12: Floor beam verification

Stack No	Floor beam cross-section / Material	$N_{b,Ed}$	$M_{b,Ed}$	Utilization factor
1 <sup>st</sup> stack	HEA 240 / S275	-517.5	2.4	0.286
2 <sup>nd</sup> stack	HEA 240 / S275	-392	54	0.506

The splitting beam shall be designed so that avoiding lateral-torsional buckling by satisfying Eq. (5.22). Results are presented in Table 5.11. It is worth noting that through keeping splitting beam almost elastic the self-centering capacity of the system is provided. However, in the current rehabilitation case study, the self-centering capacity should be addressed to the concrete columns rather than to the CBF-MB. That is why the checks according to Eq. (5.22) are not strictly fulfilled. Satisfying Eq. (5.22) requires selection of a larger profile or a RHS profile ensuring high lateral-torsional stiffness of the splitting beam.

$$\bar{\lambda}_{LT} \leq 0.40 \quad \text{Eq. (5.22)}$$

The cross sections of splitting beam and columns shall be chosen to satisfy Eq. (5.23) in accordance with §4.4.2.3 (4) of [1].

$$2.M_{RC} \geq 1.3M_{Rb}, \quad \text{Eq. (5.23)}$$

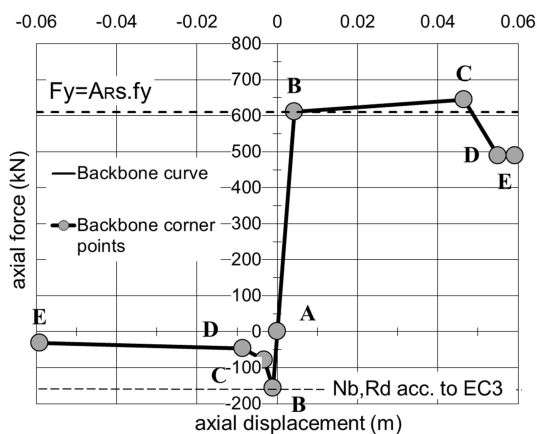
In that particular case it is obvious that Eq. (5.23) is fulfilled.

## 5.5 STATIC NONLINEAR ANALYSIS

In spite that q-factor approach is applicable according to [10], the reliability of the analysis fully relies on the proper choice of the behavior factor. The structure, object of the current study is combined one for which lateral forces in longitudinal direction should be carried by CBF-MB in cooperation with strengthened RC columns. Therefore, in order to investigate the plastic mechanism and the sequence of plastic hinges development and to prove the applicability of the selected q-factor, Static Nonlinear Analysis (SNA) was performed as well.

### 5.5.1 Model for Static Nonlinear Analysis

2-D nonlinear model based on SAP 2000 [8] is developed. The nonlinear behavior of the CBF-MB is simulated by introducing P-hinges in the middle of the braces and P-M3 hinges at the ends of columns and splitting beams. Detailed recommendations for non-linear hinge modelling strategy are presented in [5, 6]. The characteristic points of the backbone curves for the modified braces are illustrated on Figure 5.9 and Table 5.13. Data for the boundary relative displacements of the MB model in compression and tension, corresponding to each of the assumed limit states is given in Table 5.14. Eq. (5.24) to Eq. (5.28) shall be used for calculation of the forces and corresponding displacements.



$$\Delta_y = f_y \cdot L / E \quad \text{Eq. (5.24)}$$

$$F_y = A_{RS} \cdot f_y \quad \text{Eq. (5.25)}$$

$$F_{SH} = F_y + (F_y / \Delta_y \cdot 0.005) \cdot (11 \Delta_y) \quad \text{Eq. (5.26)}$$

$$N_{b,Rd} = \chi A_{RS} \cdot f_y \quad \text{Eq. (5.27)}$$

$$\Delta_C = N_{b,Rd} \cdot \Delta_y / F_y \quad \text{Eq. (5.28)}$$

Figure 5.9: Backbone curve of modified braces

Table 5.13: Characteristic backbone curve points of MB in the first stack

Point	Tension		Point	Compression	
	Axial force, [kN]	Axial displ. [m]		Axial force, [kN]	Axial displ. [m]
A	0	0	A	0	0
B	$F_y=611$	$\Delta y=0.00423$	B	$N_{b,Rd} = 155.8$	$\Delta c=0.00108$
C	$F_{SH}=644.6$	$11\Delta y=0.0465$	C	$0.5N_{b,Rd}=77.9$	$3\Delta c=0.00324$
D	$0.8F_y=488.8$	$13\Delta y=0.0550$	D	$0.3N_{b,Rd}=46.7$	$8\Delta c=0.00864$
E	$0.8F_y=488.8$	$14\Delta y=0.0592$	E	$0.2N_{b,Rd}=31.2$	$14\Delta y=0.0151$

Table 5.14: Limit states for modified braces

Limit State in SAP 2000 model	Tension	Compression	Limit State acc. to EN 1998-3 [10]
IO	$2\Delta y$	$-8\Delta c$	Damage Limitation (DL)
LS	$6\Delta y$	$-24\Delta c$	Significant Damage (SD)
CP	$10.5\Delta y$	$-42\Delta c$	Near Collapse (NC)

The backbone curves for the columns of the CBF are illustrated on Figure 5.10 and relevant data for their constriction is presented in Table 5.15 and Table 5.16. The yield rotation  $\theta_y$ , should be calculated according to the recommendations of FEMA 356 [11] while the M-N interaction curve (Figure 5.10 b) may be constructed according to [3] or [11].

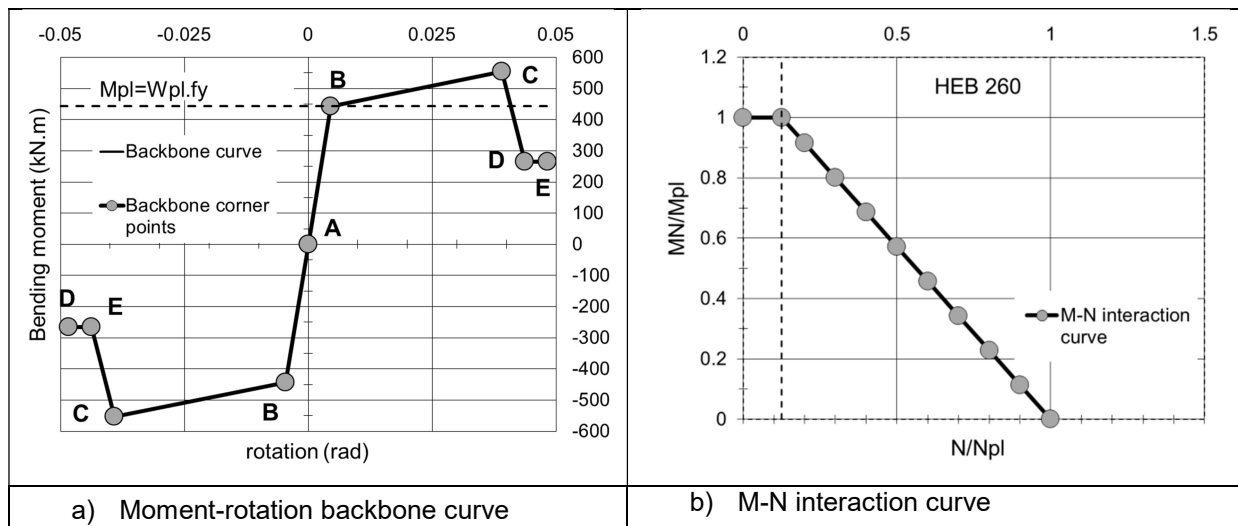


Figure 5.10: Backbone curve and interaction curve of the CBF columns

Table 5.15: Characteristic backbone curve points of CBF columns

Point	Rotation	Moment M/Mpl
A	0	0
B	$1.0 \theta_y$	1.0
C	$8.5 \theta_y$	1.25

D	$9.5 \theta_y$	0.6
E	$10.5 \theta_y$	0.6

Table 5.16: Limit states for CBF columns

Limit State in SAP 2000 model	Rotation	Limit State acc. to EN 1998-3 [10]
IO	$1.0 \theta_y$	Damage Limitation (DL)
LS	$6.0 \theta_y$	Significant Damage (SD)
CP	$8.0 \theta_y$	Near Collapse (NC)

The P-M3 hinges assigned in the splitting beams are defined following the rules used in the definition of CBF columns hinges. Additionally, since the main RC columns are fixed in the foundation and they should follow the overall lateral displacements of the structure, plastic hinges are also assigned in the column base. For that reason, the RC column and its reinforcement were modeled by nonlinear fiber elements in Seismostruct [12] and the backbone curve was calibrated to the detailed FE-model results taking into account the recommendations of [11] as well. Illustration of the backbone curve and data for the characteristic points is presented in Figure 5.11 and Table 5.17 and Table 5.18.

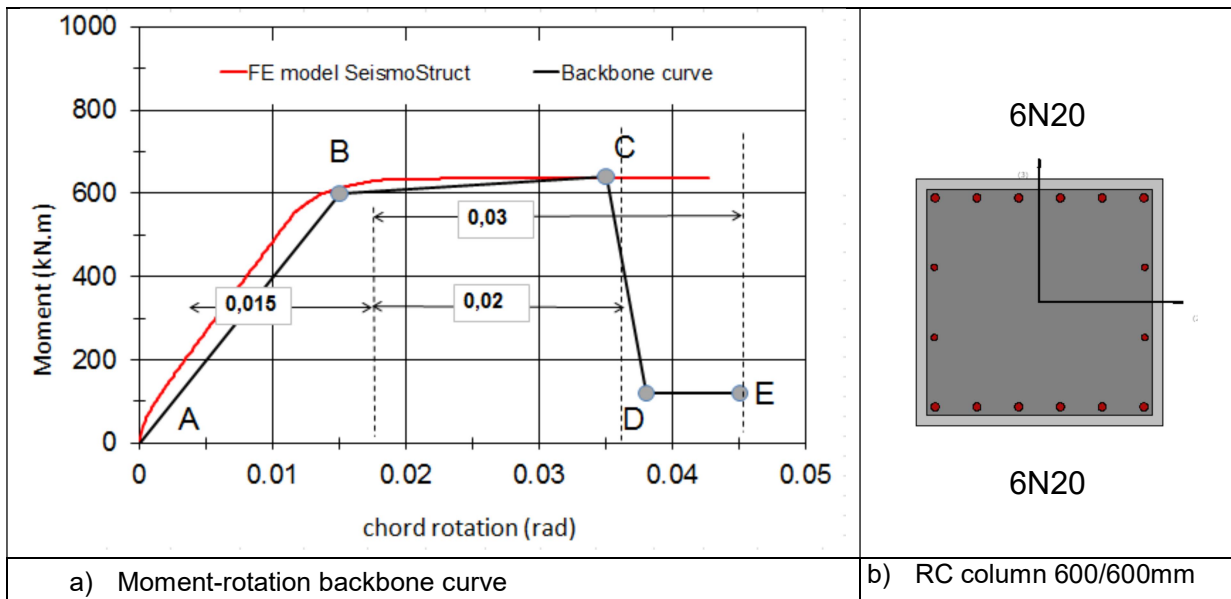


Figure 5.11: Backbone curve for RC columns

Table 5.17: Characteristic backbone curve points of RC columns

Point	Rotation	Moment $M/Mpl$
A	0	0
B	$1.0 \theta_y = 0.015$	1.0; $Mpl=600\text{kN.m}$
C	$2.33 \theta_y = 0.035$	1.05
D	$2.54 \theta_y$	0.2

E	$3.00 \theta_y = 0.030$	0.2
---	-------------------------	-----

Table 5.18: Limit states for RC columns

Limit State in SAP 2000 model	Rotation	Limit State acc. to EN 1998-3 [10]
IO	$0.333 \theta_y$	Damage Limitation (DL)
LS	$1.0 \theta_y = 0.015$	Significant Damage (SD)
CP	$1.33 \theta_y = 0.02$	Near Collapse (NC)

The final model for SNA is presented in Figure 5.12. It includes a leaning column that simulates the  $P-\Delta$  effects and initial geometrical non-verticality of the columns. The CBF-MB is modelled by joint offset model as recommended in [5, 6]. Four RC columns are included into the model since the half of the structure is modelled, taking advantage of the available symmetry.

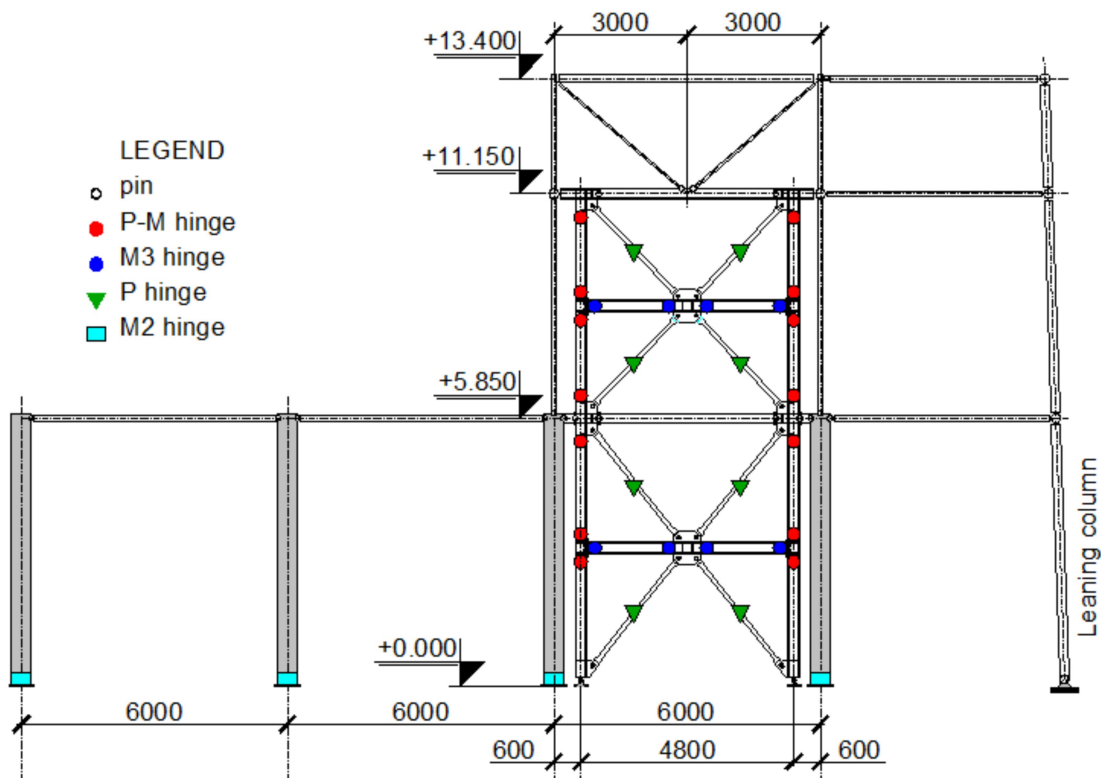


Figure 5.12: Model for Static Nonlinear Analysis

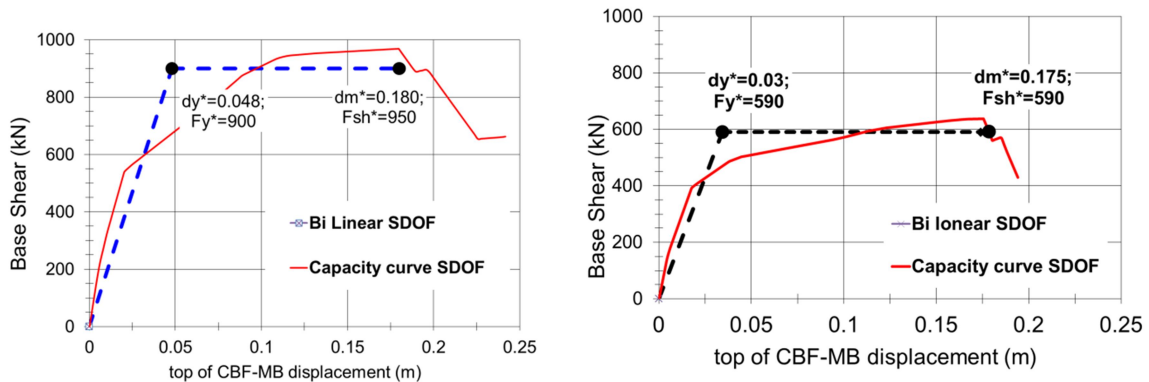
### 5.5.2 Application of N-2 method

Nonlinear static analysis was performed under constant gravity loads and monotonically increasing horizontal forces. Since the building complies with the criteria of [1] for regularity in plan, the analysis was performed using 2-D model for the horizontal direction aligned with the CBF-MB plane. Two patterns of lateral load

distribution were assigned - “uniform”, based on lateral forces that are proportional to the mass and “modal” pattern, proportional to the lateral displacements corresponding to the first mode of free vibrations through elastic modal analysis.

The lateral displacement of the top of the CBF-MB was used as control displacement. The relation between base-shear force and the control displacement (the capacity curve) was determined for the both load patterns and are shown on Figure 5.13. The target displacement and supplementary parameters were calculated according to [1] and [13].

The method is based on the determination of the performance point of the structure, being the intersection between the capacity spectrum of the system (outcome by the SNA) and the seismic demand represented by Inelastic Demand Spectrum [13]. Despite that Eurocode 8 [1] does not mandatory requires the acceleration-displacement format (acceleration displacement response spectra - ADRS), it was used and presented in Figure 5.14 for both load configurations. The performance point illustrates the condition in which the structural capacity equals the seismic demand due to the design earthquake. The horizontal coordinate of the Performance Point is the target displacement. The results from the application of N-2 method represented by basic parameters for both load patterns are presented in Table 5.19.



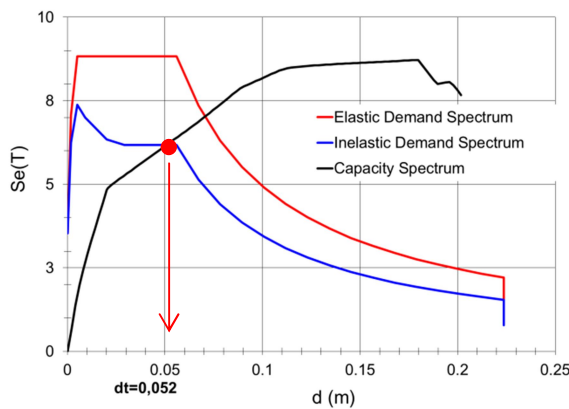
a) Uniform load pattern configuration

b) Modal load pattern configuration

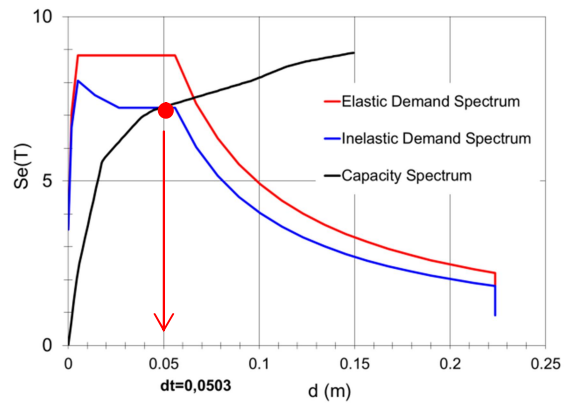
Figure 5.13: Capacity curves of equivalent SDOF and bi-linear approximation

Table 5.19: Basic parameters after application of N-2 method [1, 13]

Parameter	Symbol	Uniform pattern	Modal pattern
transformation factor	$\Gamma$	1.0	1.375
mass of an equivalent SDOF	$m^*$	111.1	70.2
yield displacement of the idealized SDOF system	$d_y^*$	0.048	0.0344
maximum displacement of the idealized SDOF system	$d_m^*$	0.180	0.175
yield force of the idealized SDOF system	$F_y^*$	900	590
maximum force of the idealized SDOF system	$F_{sh}^*$	900	590
period of the idealized equivalent SDOF system	$T^*$	0.483	0.402
target displacement of the structure with period $T^*$ and unlimited elastic behaviour	$d_{et}^*$	0.052	0.0361
elastic acceleration response spectrum at the period $T^*$	$Se(T^*)$	8.829	8.829
ratio between the acceleration of the structure with unlimited elastic behaviour $Se(T^*)$ and of the structure with limited strength $F_y^* / m^*$	$q_u$	1.09	1.05
target displacement of the MDOF system	$d_t$	0.0523	0.0503



a) Uniform load pattern configuration



b) Modal load pattern configuration

Figure 5.14: Elastic and inelastic demand spectrum vs capacity spectrum

### 5.5.3 Comparison of results after SNA

After application of the both analysis approaches, q-factor based RSA and N-2 method, it is a matter of interest to compare the internal forces in the basic members of the system. The comparison is presented in Table 5.20.

Table 5.20: Comparison of internal forces calculated by different methods

Structural member	RSA, q=2.0		N-2 method, Uniform load pattern		N-2 method, Modal load pattern	
	$M_y$ (Mz) [kN.m]	$N$ [kN]	$M_y$ (Mz) [kN.m]	$N$ [kN]	$M_y$ (Mz) [kN.m]	$N$ [kN]
CBF column	150	-1110	123.4	-846.3	97.4	-949.2
Splitting beam 1	140	-90	149	-17.4	125.5	-14.5
Floor beam 1	2.2	-515	0	-495.5	0	-464.8
Floor beam 2	32.3	-392	1.3	-188	3.6	-296.7
Diagonal in top "V" stack	-	-206	-	-102	-	-154.8
RC column (Mz)	309	NA <sup>3</sup>	295.9	NA	254.8	NA

According to the results from Table 5.20 it may be concluded that the design of the system CBF-MB based on RSA with  $q=2.0$  and application of the design methodology presented in [5, 6] leads to conservative and reliable design forces. The difference in the internal forces varies from 4% to 32%. The proposed  $q$ -factor is verified to be an appropriate estimation for the current case study. Another matter of interest is the plastic mechanism and the pattern of the hinges, developed in the system at lateral displacement equal to the target displacement and 150% of target displacement. The results are illustrated in Figure 5.15 and Figure 5.16.

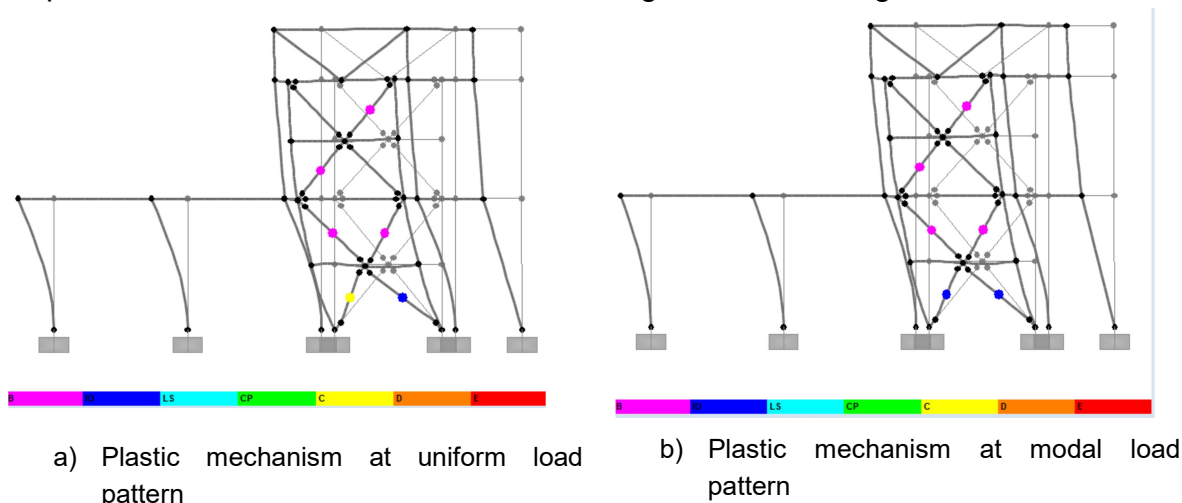


Figure 5.15: Plastic mechanism at target displacement

<sup>3</sup> The axial forces in the RC columns are due to gravity loads, not the seismic action. That is why they are not included in the table.

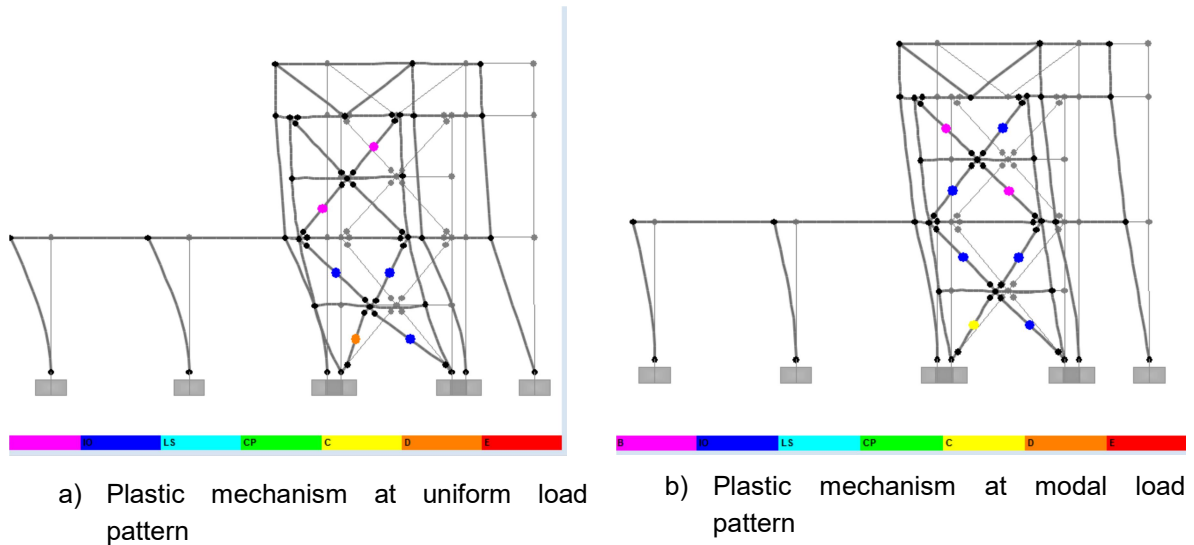


Figure 5.16: Plastic mechanism at 150% target displacement

The analysis of the plastic mechanisms shows that the plastic deformations are spread within the diagonals only in both load patterns. The behavior of the non-dissipative elements and the RC columns remains elastic. The “uniform” load pattern leads to more concentration of plastic hinges in the lower stack while the “modal” load pattern engages the second stack more. The proposed design procedure and the recommended behavior factor  $q=2.0$  result in predictable seismic performance of the structure.

## 5.6 BRACE SECTION DETAILING AND CONNECTION DESIGN

After fulfilment of all checks in §4 the modified diagonals may be detailed. Their final design is presented in Figure 5.17 and Figure 5.18.

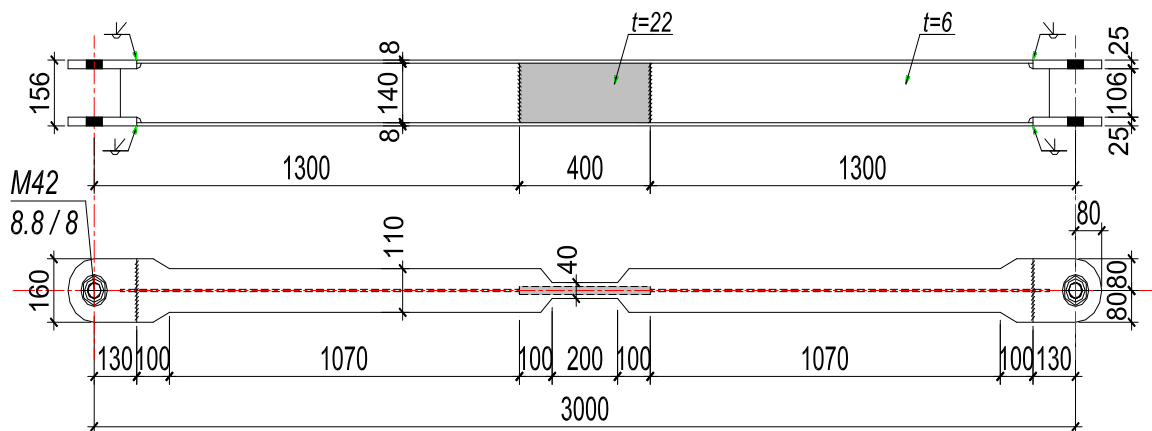


Figure 5.17: Overview of modified brace member at the first stack in CBF-MB

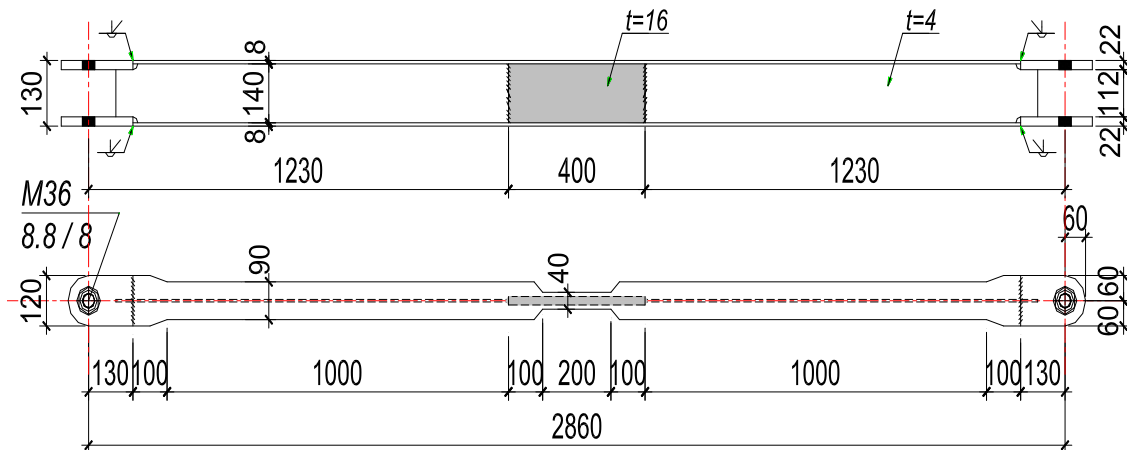


Figure 5.18: Overview of modified brace member at the second stack in CBF-MB

The connection between modified braces and the gusset plate should be designed by bolts. The tests carried out [9] have proven that bolted connections in shear and bearing (category A), realized by fit bolts, exhibit satisfactory fatigue behaviour and provide enough overstrength, therefore, in the context of §6.5.5 (6) of [1], are recommended to be used for CBF-MBs. Their dimensioning should fulfil §6.5.5 (3) and (5) of [1]. Table 5.21 summarizes the results from verification checks. It is worth noting that the design force for bolted connection should be obtained by Eq. (5.29). The factor  $\rho$  that accounts for the available overstrength of the system is not included since the mentioned overstrength is generated apart from the brace and it will not affect the connection.

Table 5.21: Bolted connection design

Stack No	$N_{pl,Rd}$ (kN)	$N_{con,Ed}$ (kN)	Bolt diameter / grade	Plate thickness (mm) / steel grade	Bolt shear resistance (kN)	Plate bearing resistance (kN)	Utilization factor
1 <sup>st</sup> stack	581.9	800.1	M42 / 8.8	24 / S235	1064	871	0.919
2 <sup>nd</sup> stack	447.6	615.5	M36 / 8.8	20 / S235	781,7	622	0.989

$$N_{con,Ed} = 1.1\gamma_{OV}N_{pl,Rd} = 1.375N_{pl,Rd} \quad \text{Eq. (5.29)}$$

## 5.7 STRUCTURAL DETAILING

The configurations of some specific structural joints are illustrated in Figure 5.19. They present the connection between the CBF-MB and the industrial frame at elevation +0.000 and elevation +11.150. Appropriate structural detailing of other

typical joints as the joints between the modified braces and the column and the joint at the intersection between the modified braces and the splitting beam may be seen in [14, 15].

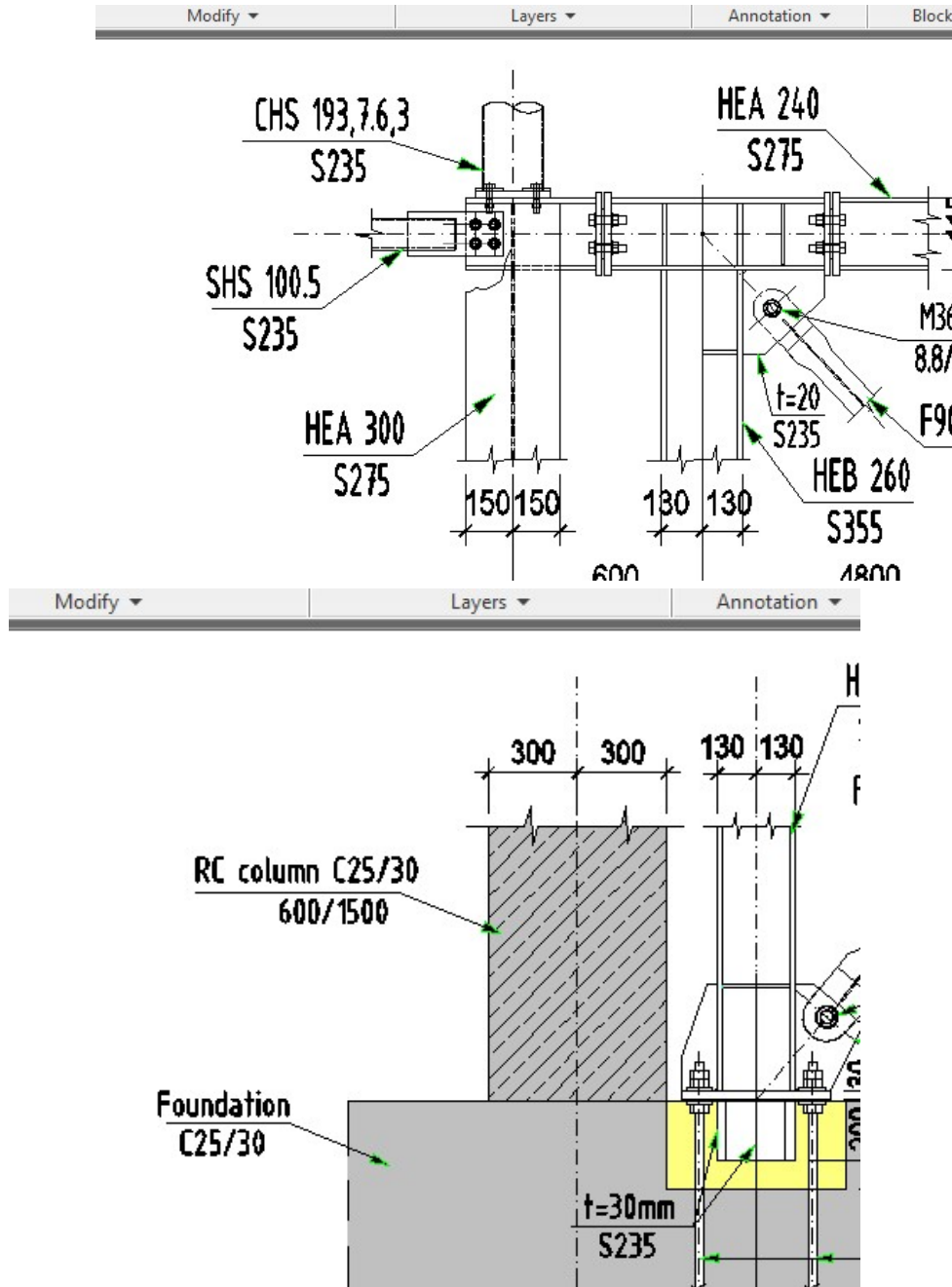


Figure 5.19: Structural detailing at level +0.000 and +11.150

## 5.8 REFERENCES

- [1] Eurocode 8: Design of structures for earthquake resistance - Part 1: General rules, seismic actions and rules for buildings; EN 1998-1:2004.
- [2] Hot rolled products of structural steels – Part 2: Technical delivery conditions for non-alloy structural steels; EN 10025-2:2001.

- [3] EN1993-1-1, Eurocode 3: Design of steel structures - Part 1-1: General rules and rules for buildings. Brussels: Comité Européen de Normalisation (CEN); 2005.
- [4] EN1993-1-8, Eurocode 3: Design of steel structures - Part 1-8: Design of Joints. Brussels: Comité Européen de Normalisation (CEN); 2005.
- [5] Georgiev Tzv., Zhelev D., Raycheva L., Rangelov N., "INNOSEIS - Valorization of innovative anti-seismic devices", WORK PACKAGE 1 – DELIVERABLE 1.1, Volume with information brochures for 12 innovative devices in English, European Commission Research Programme of the Research Fund for Coal and Steel.
- [6] Georgiev Tzv., Rangelov N., Raycheva L., Raykov St., INNOSEIS - Valorization of innovative anti-seismic devices", WORK PACKAGE 3 – DELIVERABLE 3.2, Volume with pre-normative design guidelines for innovative devices, European Commission Research Programme of the Research Fund for Coal and Steel, (Article in Press).
- [7] Fajfar P., Kreslin M., "Modelling and Analysis, Chapter 4 of EC8-1", EUROCODE 8 Background and Applications, Dissemination of information for training – Lisbon, 10-11 February 2011.
- [8] SAP2000, CSI, Computers and Structures Inc., [www.csiberkeley.com](http://www.csiberkeley.com).
- [9] Tzvetan Georgiev, „Improvement of X-CBF hysteresis behaviour by introduction of MCS”, 8th Hellenic National Conference on Steel Structures, Tripoli, Greece, 2-4 October 2014, page 75.
- [10] Eurocode 8: Design of structures for earthquake resistance - Part 3: Assessment and retrofitting of buildings, EN 1998-3 :2005.
- [11] FEMA – 356: Prestandard and Commentary for the seismic rehabilitation of Buildings. Washington; 2000.
- [12] Seismosoft [2014] "SeismoStruct v7.0 – A computer program for static and dynamic nonlinear analysis of framed structures," available from <http://www.seismosoft.com>.
- [13] Peter Fajfar, "Capacity spectrum method based on inelastic demand spectra", Earthquake Engineering & Structural Dynamics, 28(9):979 - 993, September 1999.
- [14] Georgiev Tzv., Zhelev D., Raycheva L., Rangelov N., "INNOSEIS - Valorization of innovative anti-seismic devices", WORK PACKAGE 4 – DELIVERABLE 4.1, Volume on case studies for low-rise buildings, European Commission Research Programme of the Research Fund for Coal and Steel.
- [15] Georgiev Tzv., Zhelev D., Raycheva L., Rangelov N., "INNOSEIS - Valorization of innovative anti-seismic devices", WORK PACKAGE 4 – DELIVERABLE 4.2, Volume on case studies for middle-rise buildings, European Commission Research Programme of the Research Fund for Coal and Steel.

## 6 SEISMIC UPGRADING OF AN EXISTING R.C. INDUSTRIAL BUILDING IN ITALY THOROUGH STEEL-SELF CENTERING DEVICES

### 6.1 GENERAL

#### 6.1.1 Introduction

This case study refers to the seismic rehabilitation of an existing precast concrete industrial building, interested by the 2012 Emilia (Italy) earthquake. The rehabilitation is carried out introducing through the inclusion of the Steel Self-Centering Devices (SSCDs) [1] in order to guarantee also the re-centering capability of the structure. Given the strong nonlinear behavior of such system, nonlinear analyses are used to design them.

#### 6.1.2 Description of case study building

The considered existing case study is an industrial one storey r.c. precast building located in Correggio (Emilia-Romagna, Italy), of global dimensions equal to about 510 m<sup>2</sup> (**Error! Reference source not found.**).

The building presents a simple structure characterized by squared columns (40x40 cm) with specific slots introduced for the placement of infill panels, directly loading on isolated foundations and positioned at a relative distance of about 6.0 m.

The foundations have different dimensions in relation to the position of structural elements (i.e. 1,02x1,02 m along the short side of the building and 1,20x1,40 m along the long side of the building).

Inclined beams (inclination up to 10%) cover a length equal to 16.40 m; light infill panels with thickness equal to 15 cm are also present. Several information regarding structural details (global dimension, number, disposition and typology of longitudinal and transversal reinforcements) have been derived from the documents provided by Regional Technical Offices (**Error! Reference source not found.**).

According to the prescriptions of the actual Italian standard for Constructions, experimental tests shall be executed on r.c. elements in order to determine the strength of concrete and steel reinforcements. The obtained average values shall be moreover divided by the Confidence Factor (FC), depending on the Knowledge Level (KL) reached for the building, for taking into consideration all the uncertainties due to the existence and remote construction of the case study. For the case study industrial building, considering KL 1, associated to a FC equal to 1.35 due to the absence of experimental recent data, the values of Table 6.1 were then adopted on

the bases of the original documents provided by technical offices. Different values of the mechanical properties of concrete and steel reinforcements were considered in the case of ductile or brittle mechanisms (i.e. bending or shear).



Figure 6.1: General external view of the case study building.



Figure 6.2: Details of connections between structural elements and structural/non-structural elements.

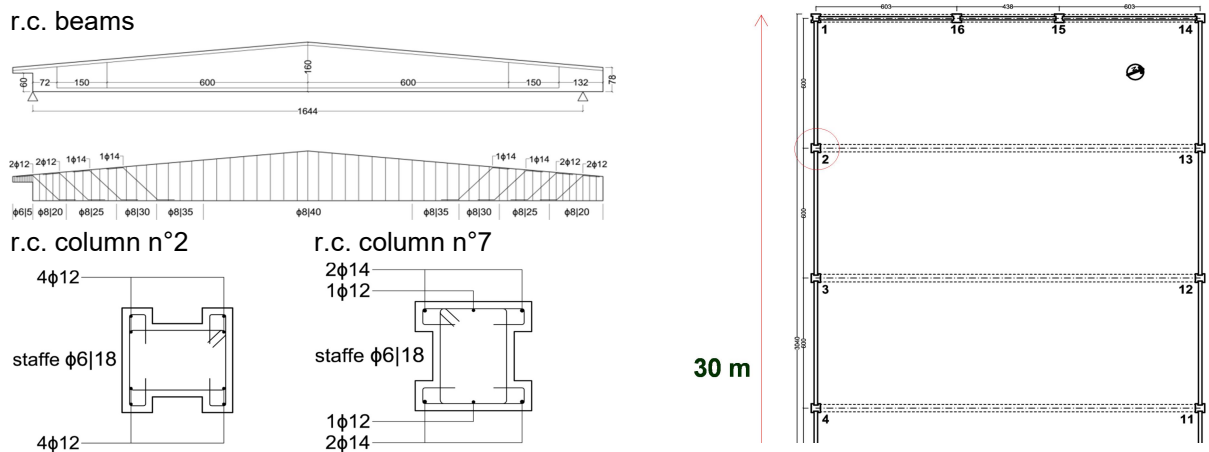


Figure 6.3: General presentation of the case study building with indications of executive structural details for r.c. elements.

Table 6.1: Mechanical properties adopted for concrete and steel reinforcing bars.

concrete			reinforcing steel		
$R_{cm}$	53,6	MPa	$f_{tm}$	619.5	MPa
$f_{cm}$	44,6	MPa	$f_{ym}$	486.6	MPa
$E_c$	32808	MPa	$E_s$	210000	MPa
$f_{cd, DUCTILE}$	28,07	MPa	$f_{yd, DUCTILE}$	360.5	MPa
$f_{cd, BRITTLE}$	18,71	MPa	$f_{yd, BRITTLE}$	313.4	MPa
$f_{ctm}$	3,77	MPa			
$f_{cfm}$	4,53	MPa			

## 6.2 ANALYSIS OF THE CASE OF STUDY

### 6.2.1 Linear modelling, analysis and safety checks

Due to the effective configuration of the one storey building and to the execution of preliminary local retrofit intervention in the period immediately after the Emilia-Romagna earthquake (2012) [2] [3] able to restore the pre-damaged condition, the simple schematization presented in Figure 6.4 was assumed. A three dimensional model was elaborated using SAP2000 software and used for the preliminary safety checks of the building according to what foreseen by the actual Italian standard for constructions (D.M. 14/01/2008 [4]) for r.c. structures (bending and shear checks for r.c. beams and columns).

In order to directly include in the model cracking phenomena of r.c. elements, a reduced stiffness was considered (equal to the 55% of the initial one, both in the case of beams and columns).

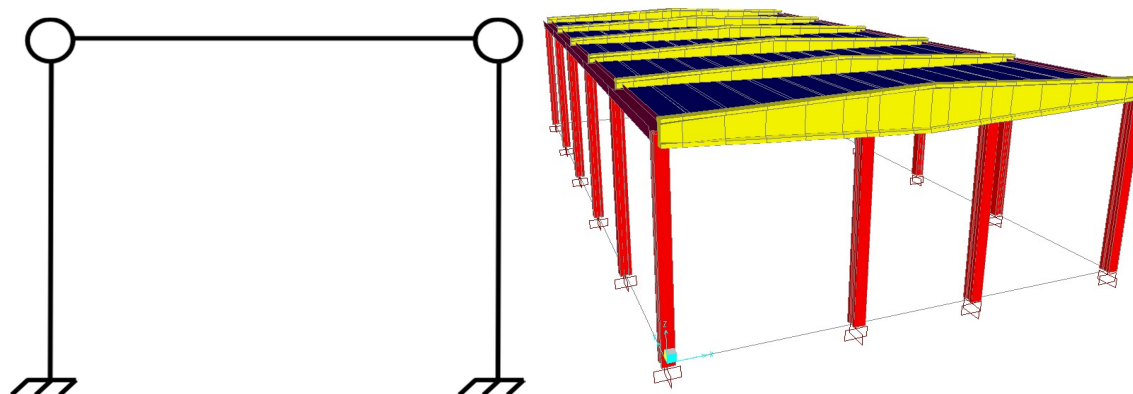


Figure 6.4: **Error! Use the Home tab to apply Titolo 1;RFCS TITLE 1;RFCS Title1;Title1;ChapterTitle 1 to the text that you want to appear here.** Simplified schematization of the building for the modelling.

The following permanent, live and external loads, in relation to the specific location of the building, were considered:

- Permanent - roof storey: 0.10 kN/m<sup>2</sup> (corrugated sheet)
- Permanent – infill panels: 2.50 kN/m<sup>2</sup>
- Live load (H1): 0.50 kN/m<sup>2</sup>
- Wind load: 0.638 c<sub>p</sub> kN/m<sup>2</sup>
- Snow load: 1.20 kN/m<sup>2</sup>

Seismic action was defined according to D.M.14/01/2008 considering nominal life  $V_N$  equal to 50 years, unitary use coefficient  $C_u$  and soil category C according to the owned geological information. The response spectrum evaluated for Life Safety limit state (i.e. return period  $T_R=475$  years, peak ground acceleration  $PGA=0.153$  g, amplification factor  $F_0=2.540$  and  $T_c^*=0.274$  sec) is presented in Figure 6.5, as well as the one for Damage Limitation (DL) limit state. For LS a behaviour factor equal to 1.50 was assumed. A linear dynamic analysis was then executed on the model as well as safety checks of structural elements, including r.c. beams, r.c. columns, r.c. foundation, roof elements, foundation soil pressure).

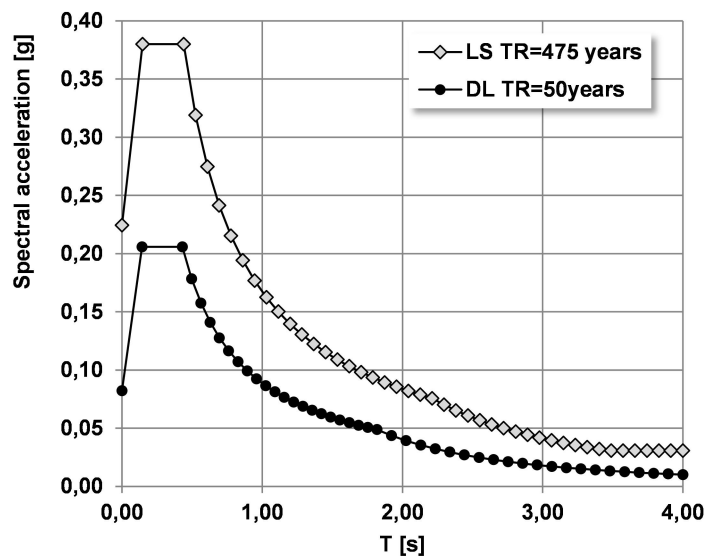


Figure 6.5: Response spectrum evaluated for LS and DL for the considered case ( $q=1.50$  for LS).

Trying to summarize the results of safety assessment through dynamic modal analysis with design response spectrum, the following considerations can be done:

- Standards' requirements for both flexural and shear mechanisms were satisfied for all r.c. beams, considering both the gravitational (static) load combination and the seismic one.
- Several r.c. columns (the ones in correspondence of the bottom and of the top portions of the building) were not able to satisfy the actual safety requirements for what concerns the flexural behaviour (seismic combination).
- Standards' requirements were satisfied for roof elements and for all the typical connections between structural and non-structural elements.

- Structural problems in correspondence were evidenced of the *totality* of foundation elements and for what concerns the resulting stresses due to the building on the ground soil (seismic combination), whose characteristic were determined in relation to the information provided by the geological documentation.

### 6.2.2 Nonlinear modelling and analysis of the building

The structural assessment of the building was moreover executed through nonlinear static (pushover) analysis, determining the capacity curve of the building (base shear/displacement); the structural capacity was compared to the effective seismic demand, determining the effective performance of the structure and evidencing the eventual need of retrofit interventions.

A nonlinear lumped plasticity model of the building was elaborated, defining the moment/rotation relationships of plastic hinges in correspondence of significant structural elements. The rotational capacity of plastic hinges was determined according to EN1998-3:2005 [5] for existing r.c. elements; two different approaches (i.e. theoretical and empirical) can be adopted.

According to the *theoretical approach* the curvature of the section (and consequently the rotation of the element) is defined by two different components: the elastic part  $\phi_y$  and the plastic part  $\phi_{pl}$  (this last is constant along the plastic hinge length  $L_{pl}$ ). The elastic part of the rotation is then defined as:

$$\theta_y = \phi_y \frac{L_s}{3} + 0.0013 \left( 1 + 1.5 \frac{h}{L_s} \right) + 0.13 \phi_y \frac{d_b f_{ylm} / FC}{\sqrt{f_{cm} / FC}} \quad \text{Eq. ( 6.1)}$$

The plastic part is defined according to the following expression (in which the shear length  $L_v$  can be here assumed equal to  $L$ ):

$$\theta_{pl} = (\phi_u - \phi_y) L_{pl} \left( 1 - \frac{L_{pl}}{2L_v} \right) \quad \text{Eq. ( 6.2)}$$

The yielding curvature  $\phi_y$  can be determined as:

$$\phi_y = \frac{f_{ylm}}{E_s \cdot (d - x_y) \cdot FC} \quad \text{or} \quad \phi_y = \frac{0.8 f_{cm}}{E_c \cdot x_y \cdot FC} \quad \text{Eq. ( 6.3)}$$

In which  $x_y$  is the distance from the compressed side of the section,  $E_c$  and  $E_s$  the elastic moduli of steel and concrete,  $f_{ylm}$  and  $f_{cm}$  the mechanical properties of steel reinforcement and concrete and  $FC$  the confidence factor assumed.

The plastic hinge length  $L_{pl}$  can be defined as:

$$L_{pl} = 0.1L_s + 0.17h + 0.24 \frac{d_{bl} f_{ytm} / FC}{\sqrt{f_{cm} / FC}} \quad \text{Eq. ( 6.4)}$$

The ultimate curvature  $\phi_u$  is evaluated considering  $\varepsilon_{su}=0.04$  and  $\varepsilon_{cu}=0.004$  (ultimate deformation of steel reinforcements and concrete). If the collapse happens due to steel or due to concrete, the ultimate curvature can be determined respectively as:

$$\phi_u = \frac{\varepsilon_{su}}{d - x_y} \quad \text{or} \quad \phi_u = \frac{\varepsilon_{cu}}{x_y} \quad \text{Eq. ( 6.5)}$$

Leading to an ultimate rotational capacity of the section equal to:

$$\theta_u = \frac{1}{\gamma_{el}} \left[ \theta_y + (\phi_u - \phi_y) L_{pl} \cdot \left( 1 - \frac{L_{pl}}{2L_s} \right) \right] \quad \text{Eq. ( 6.6)}$$

Being  $\gamma_{el}$  equal to 1.50 for primary structural elements.

The value of ultimate rotation for LS, according to current standard, is equal to 0.75  $\theta_u$ .

If the empirical approach is adopted, the following expression shall be used for the ultimate rotation (for the meaning of the different coefficient both Eurocode 8 and Italian standard can be followed):

$$\theta_u = \frac{1}{\gamma_{el}} 0.016 \cdot (0.3^v) \cdot \left[ \frac{\max(0.01; \omega')}{\max(0.01; \omega')} \cdot \frac{f_{cm}}{FC} \right]^{0.225} \cdot \left( \frac{L_v}{h} \right)^{0.35} \cdot 25^{\left( \alpha \rho_{sx} \frac{f_{ytm}}{f_{cm}} \right)} \cdot (1.25^{100 \rho_d}) \gamma_{det} \quad \text{Eq. ( 6.7)}$$

The modelling of plastic hinges also requires the evaluation of yielding and ultimate bending moment of considered sections, according to the values of axial force effectively present and to the two main directions considered. Table 6.2 shows the values of the ultimate rotations for r.c. columns evaluated using the two different theoretical and empirical approach.

Table 6.2: Ultimate rotations for columns with theoretical and empirical formulations.

r.c. columns	dir.	$\theta_{u,th}$ [mrad]	$\theta_{LS}$ [mrad]	$\theta_{u,em}$ [mrad]	$\theta_{LS}$ [mrad]
lateral	x	43.41	32.48	51.88	38.91
	y	75.28	56.46	49.06	36.79
front	x	92.35	69.26	50.86	38.15
	y	65.78	49.33	53.79	40.34
angular (S)	x	69.03	51.77	51.90	38.93
	y	69.03	51.77	55.49	41.62
angular (N)	x	68.7	51.52	52.27	39.20
	y	68.7	51.52	52.27	39.20

The determination of the moment/rotation relationships for plastic hinges allowed the calibration of the model for the execution of static pushover analysis in the two main directions.

The Capacity Spectrum Method (CSM) was then applied (ATC-40 [6]). The method is based on the determination of the performance point of the building, representing the intersection between the capacity spectrum of the system (elaborated through the execution of pushover analysis) and the seismic demand represented in an acceleration/displacement plane (acceleration displacement response spectra - ADRS) and opportunely reduced to take into consideration nonlinear effects. The performance point represents the condition in which the seismic capacity of the building is exactly equivalent to the seismic demand due to a specific earthquake input.

In order to shift the traditional response spectrum (in terms of spectral acceleration  $S_a$  vs. period  $T$ ) into the ADRS plane and to evaluate the spectral displacement  $S_{di}$  (being  $T_i$  the period of the building) the following relationship can be used:

$$S_{di} = \frac{T_i^2}{4\pi^2} \cdot S_{ai} g \quad \text{Eq. ( 6.8)}$$

In order to convert the capacity curve of the system in the capacity spectrum, a punctual transformation is needed. Each single point ( $F_b$  – base shear vs.  $d_c$  – displacement of the control point) is translated into a ( $S_{di}$ ,  $S_{ai}$ ) point through the following equations:

$$S_{di} = \frac{d_c}{FP_1 \times \phi_{1,c}} \quad \text{and} \quad S_{ai} = \frac{F_b}{W} \cdot \frac{1}{\alpha_1} \quad \text{Eq. ( 6.9)}$$

Being  $\alpha_1$  and  $FP_1$  the modal mass coefficient and the participating factor for the first vibration mode, while  $\phi_{1,c}$  is the amplitude of the control point for the first vibration mode. After the representation of the two diagrams in the same ADRS plane, a preliminary performance point ( $d_{pi}$ ,  $a_{pi}$ ) is selected on the base of the equivalent displacement approach.

A bilinear representation of the capacity curve can be used, with the first branch characterized by the same slope of the elastic branch of the capacity curve and the second branch defined in order to have the energy dissipation equivalence (Figure 6.6,a).

The Spectral Reduction (SR) factors shall be then evaluated (Figure 6.6,b): the dissipation of seismic energy of the structure in the post-elastic field can be considered as the combination of two parts, a viscous part and an hysteretic part. The hysteretic part is related to the internal area of executed cycles when the maximum base shear is obtained as a function of the displacement  $d_c$ .

The hysteretic dissipation can be represented with its equivalent viscous dissipation through the adoption of literature expressions. The equivalent viscous dissipation  $\beta_{eq}$  associated to the maximum displacement  $d_{pi}$  can be evaluated according to:

$$\beta_{eq} = \beta_0 + 0.05 \quad \text{where} \quad \beta_0 = \frac{1}{4\pi} \frac{E_D}{E_{S0}} \quad \text{Eq. ( 6.10)}$$

In which  $\beta_0$  is the hysteretic dissipation represented as viscous and 0.05 represents the 5% intrinsic viscous dissipation of the structure (constant),  $E_D$  is the dissipated energy per cycle and  $E_{S0}$  is the maximum energy deformation associated to the same cycle.

The values of  $E_D$  and  $E_{S0}$  can be evaluated according to:

$$E_D = 4(a_y d_{pi} - d_y a_{pi}) \quad \text{and} \quad E_{S0} = \frac{a_{pi} d_{pi}}{2} \quad \text{Eq. ( 6.11)}$$

If  $\beta_0$  is expressed through percentage, according to:

$$\beta_0 = \frac{63.7(a_y d_{pi} - a_{pi} d_y)}{a_{pi} d_{pi}} \quad \text{Eq. ( 6.12)}$$

If  $k$  coefficient, that is a reduction factor depending on the quality of the structural system and the duration of the earthquake (Table 6.3, Table 6.4) is introduced,  $\beta_{eq}$  shifts into the following equation:

$$\beta_{eq} = k\beta_0 + 5 = k \frac{63.7(a_y d_{pi} - a_{pi} d_y)}{a_{pi} d_{pi}} + 5 \quad \text{Eq. ( 6.13)}$$

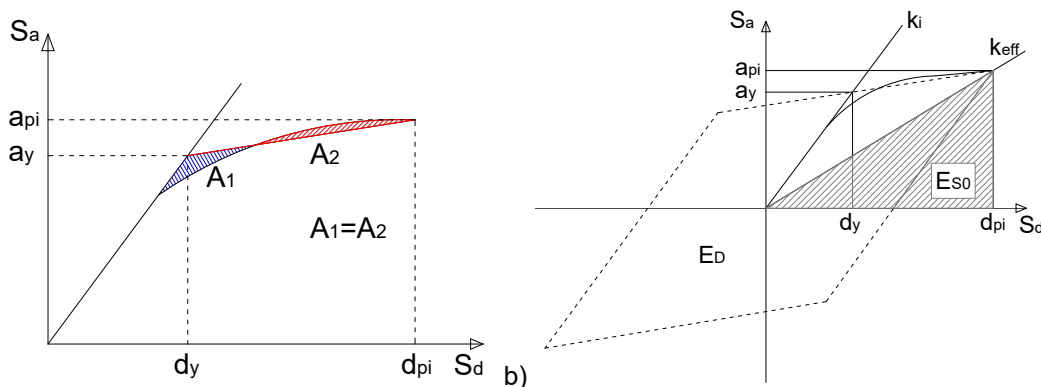


Figure 6.6: a) Bilinear representation for CSM, b) scheme for the evaluation of the spectral reduction factor.

The spectral reduction factors, necessary to evaluate the 5% reduced factor, can be then evaluated according to the following expressions, respectively for the reduction of the acceleration and velocity spectra. The control of the intersection between the demand and the capacity spectra present in correspondence of point  $(d_{pi}; a_{pi})$  shall be executed (at least controlling if the intersection displacement  $d_i$  is within the

confidence range  $0.95 \cdot d_{pi} \leq d_i \leq 1.05 \cdot d_{pi}$ ). If there is not intersection between demand and capacity spectra in the confidence interval, a new point  $(d_{pi}; a_{pi})$  shall be selected and the procedure executed again. If the intersection is allowable, the point  $(d_{pi}; a_{pi})$  represents the effective “performance point”  $(d_p; a_p)$  where  $d_p$  represents the maximum displacement demand attainable.

$$SR_A = \frac{3.21 - 0.68 \ln(\beta_{eff})}{2.12} \quad \text{and} \quad SR_V = \frac{3.21 - 0.41 \ln(\beta_{eff})}{1.65} \quad \text{Eq. ( 6.14)}$$

Table 6.3: Different quality and behaviour of building (for k determination).

Shaking duration	New building	Average existing building	Poor existing building
Short	Type A	Type B	Type C
Long	Type B	Type C	Type C

Table 6.4: Value of k coefficient.

Structural behaviour type	$\beta_0$ [%]	k
Type A	$\leq 16.25$	1.0
	$\geq 16.25$	$1.13 - \frac{0.51(a_y d_{pl} - a_{pl} d_y)}{a_{pl} d_{pl}}$
Type B	$\leq 25$	0.67
	$\geq 25$	$0.845 - \frac{0.446(a_y d_{pl} - a_{pl} d_y)}{a_{pl} d_{pl}}$
Type C	Any value	0.33

For the considered building, for the evaluation of  $k$  factor the behaviours “B” and “C” respectively for short and long duration earthquake were considered.

The execution of pushover analyses for each one of the two main directions of the building and the application of the Capacity Spectrum Method (CSM) allowed the determination of the performance points. Figure 6.7 shows the demand spectra both for the 100% of actual standard seismic action and for the corresponding reduction of 40% (i.e. 60% of the seismic demand).

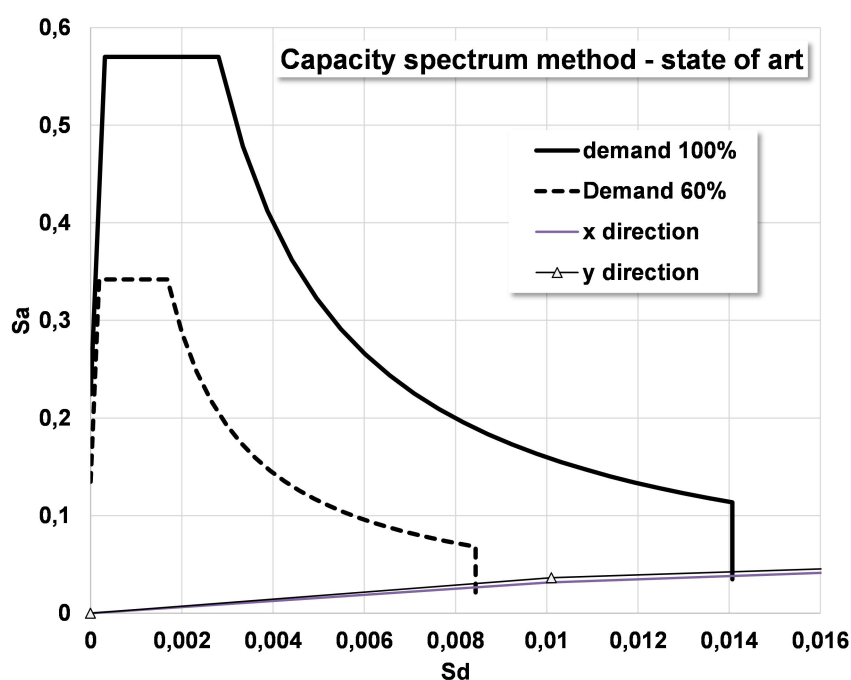


Figure 6.7: Capacity spectrum method applied for the state of art condition (x and y direction).

The analysis of the condition of structural elements evidenced structural problems of foundation and ground soil in correspondence of the second step of pushover analysis, highlighting the inadequacy of the system and the need of retrofit intervention.

### 6.3 RETROFIT OF THE EXISTING CASE STUDY BUILDING

The main problems affecting the building were related, as evidenced, to the safety checks on foundation and ground soil, not able to satisfy the actual standards requirements in the totality of the elements. A first preliminary retrofit proposal was the “*local intervention*” on single structural elements; this kind of retrofit, on the other hand, did not represent the better possibility for a building such as the considered one in which activities shall be preserved in order to limit the economic losses.

The application of different possible configurations of the SSCD systems was then analyzed, according to what simply represented in Figure 6.8. The SSCD system was applied to the existing building as “bracing system”, globally modifying the structural behaviour of the case study.

In the first solution (called “A”) one SSCD brace was applied for each side of the building, while two braces were used for each side in the second solution (“B”).

Different dissipative devices were also adopted; the main parameters describing the dissipative re-centering systems are summarized in Table 6.5, according to the meaning of terms previously determined.

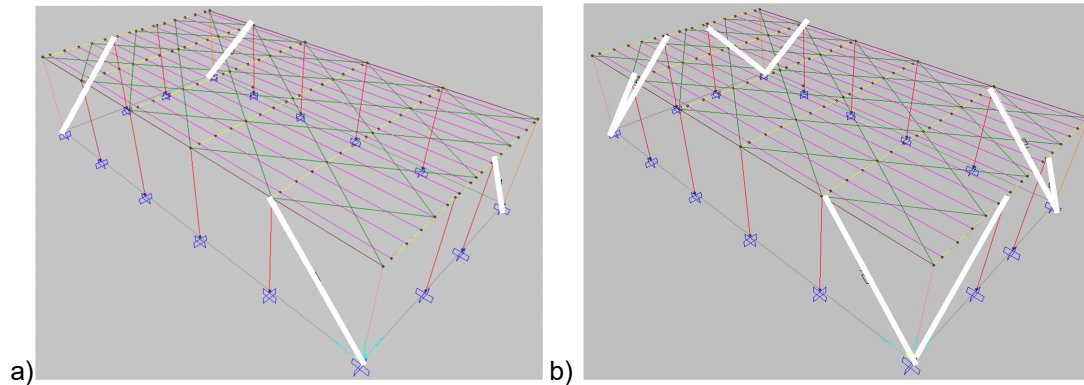


Figure 6.8: Different configurations of SSCD studied for the analyzed building: a) solution A, b) solution B.

Table 6.5: Main characteristics of the proposed systems for retrofit solutions A and B.

Solution "A"				Solution "B"							
$k_{el}$	48,24	kN/mm	$d_{pl}$	17,89	mm	$k_{el}$	34,25	kN/mm	$d_{pl}$	20,45	mm
$k_{pe}$	5,04	kN/mm	$d_y$	3,13	mm	$k_{pe}$	6,08	kN/mm	$d_y$	3,06	mm
$\alpha$	0,24	-	$a_{pl}$	318,42	mm	$\alpha$	0,18	-	$a_{pl}$	210,55	mm
$\beta$	0,61	-	$a_y$	151,10	mm	$\beta$	0,73	-	$a_y$	104,88	mm
$F_y$	151,10	kN	$\delta$	2,57		$F_y$	104,88	kN	$\delta$	1,65	
$d_y$	3,13	mm	$d_a$	15,32	mm	$d_y$	3,06	mm	$d_a$	18,80	mm
$F_u$	318,42	kN	$d_b$	0,56	mm	$F_u$	210,55	kN	$d_b$	1,41	mm
$d_u$	17,89	mm				$d_u$	20,45	mm			

The dissipative system "A" was realized considering pre-tensioned cables of diameter equal to 10 mm, considering a pre-tension percentage  $\rho_{PTE}=0,40$  and with 8 dissipative elements with transversal area equal to  $40 \text{ mm}^2$ . The dissipative system "B" was realized considering pre-tensioned cables of diameter equal to 120 mm, considering a pre-tension percentage  $\rho_{PTE}=0,50$  and with 8 dissipative elements with transversal area equal to  $60 \text{ mm}^2$ . For all the other components of the SSCD system, the parameters presented in Table 6.6 were assumed (constant).

Table 6.6: Dimensional data of the elements constituting the SSCD system.

Element	$A_i$ [ $\text{mm}^2$ ]	$L_i$ [mm]	$k_i$ [kN/mm]
Carter 1	11088	4200	$k_c = 554.4$
Carter 2	-	690	$k_{c2} = \infty$
Sliding Frame	1538.72	4000	$k_{TM} = 80.80$
Piston	861.55	5000	$k_P = 36.20$
Endplates	66538	50	$k_{cT} = \infty$
Pre-tensioned cables	157	4000	$k_{PT} = 7.69$
Dissipative elements (right)	320	170	$k_{DE} = 395.29$
Dissipative elements (left)	320	170	$k_{DE} = 395.29$

For the determination of  $\beta_{eq}$  in the proposed solutions with dissipative systems, the dissipative capacity of the introduced SSCD is considered, directly corresponding to the area of the flag-shaped curved. In such cases, no difference existed between short and long duration earthquakes since not influencing the behaviour of the dissipative device.

Figure 6.9: Capacity curve before and after retrofit with dissipative system according to solution A.

and Figure 6.10 show the comparison between the capacity curves evaluated through the execution of pushover analyses on the considered building before and after the application of dissipative braces according to the solutions A and B as previously presented. As visible, the introduction of bracing system strongly influences the global behaviour of the existing building, with evident increase of the stiffness both in x and y directions.

Figure 6.11 and Figure 6.12 show the application of the capacity spectrum method (ADSR plane) for the considered solutions A and B for the location of dissipative devices. The demand spectra are evaluated considering both the 100% of standard seismic action and the 60% of it, due to the high structural problems encountered during the analysis and design.

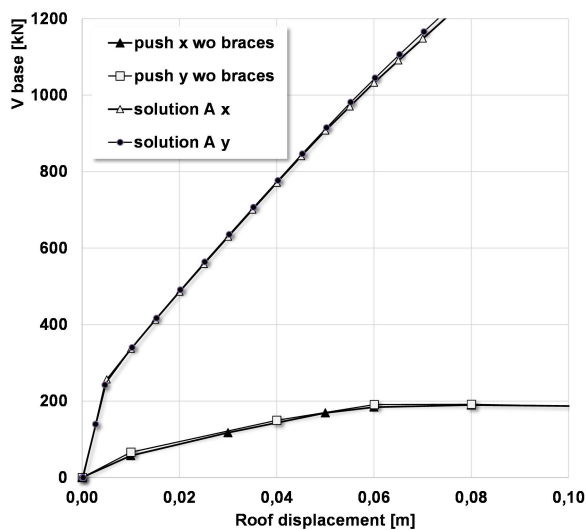


Figure 6.9: Capacity curve before and after retrofit with dissipative system according to solution A.

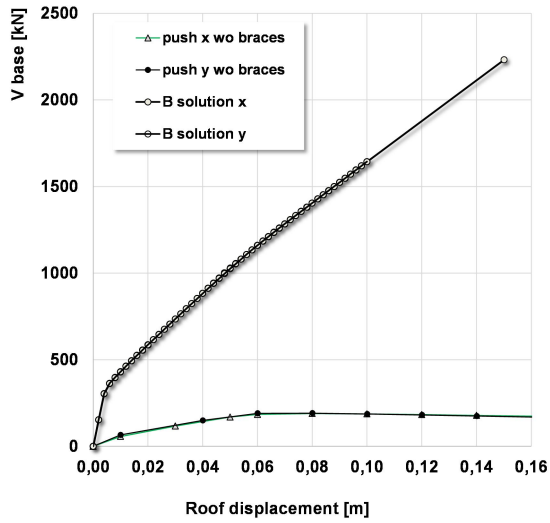


Figure 6.10: Capacity curve before and after retrofit with dissipative system according to solution B.

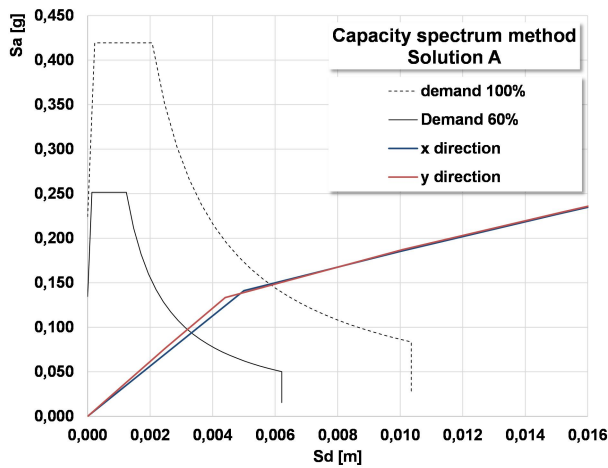


Figure 6.11: Capacity Spectrum Method for solution A.

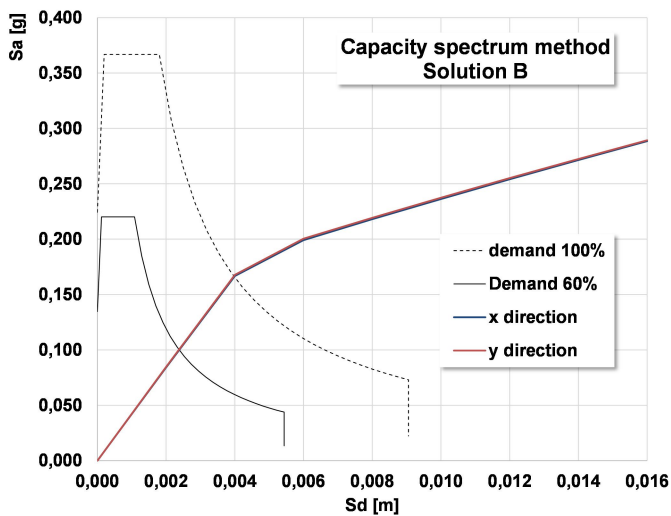


Figure 6.12: Capacity Spectrum Method for solution B.

The application of the dissipative devices strongly conditions the structural behaviour of the existing building. Safety checks according to the prescriptions of actual standards were executed on the updated model of the building, evidencing the higher capability of structural systems, with satisfaction of standards' requirements for columns and, globally, also for isolated foundations and ground soil. Localized problems still remain in correspondence of few foundations, for which a specific intervention shall be adopted.

What is evident, moreover, in the application of considered retrofit intervention is the necessity to locally executed strengthening of the elements characterized by the introduction of SSCD: the connections between the re-centering system and the structural elements shall be deeply analyzed as well as the joint at foundation level.

#### **6.4 CONCLUSIONS**

The vulnerability analysis of the existing case study building, preliminarily executed with linear dynamic analysis with design response spectrum characterized by behaviour factor equal to 1.50 evidenced significant structural problems in correspondence of the isolated foundations (probably not opportunely designed since not required by old standards) and of the ground soil. Several problems were also encountered for some r.c. columns under flexural condition.

A further static pushover analysis, executed on a nonlinear model with concentrated plasticity globally confirmed the results of linear analysis, except in the case of columns that were, in this case, able to satisfy the safety checks.

The design of retrofit interventions was then concentrated in correspondence of the ground soil and of foundations. Several "traditional" solutions were initially proposed but neglected since too much requiring from an economical point of view and in relation to the need to temporarily stop the industrial activities developed inside the building.

The application of the dissipative SSCD (Steel Self Centering Device) developed by University of Pisa was then deeply analyzed to evaluate the influence on the global structural behaviour of the building. Different solutions were considered, corresponding to two different SSCD with specific mechanical properties and located in different configurations (respectively called A and B).

The introduction of the dissipative devices allowed the decrease of the solicitations in correspondence of foundations, limiting the residual punctual interventions to few elements that needed, in any case, to be strengthened adopting traditional techniques, regarding both isolated foundation and ground soil.

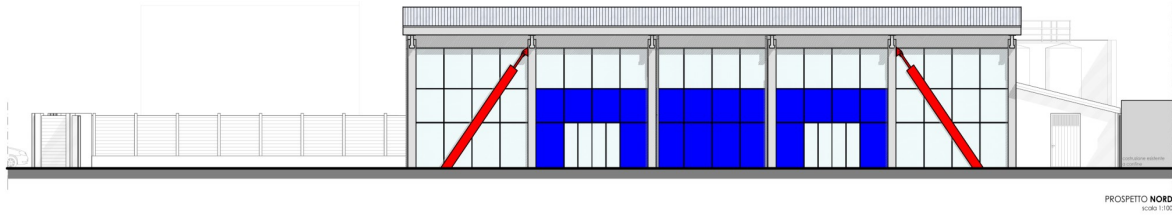


Figure 6.13: Front view of the building after the retrofit intervention

## 6.5 REFERENCES

- [1] Braconi A., Morelli F., Salvatore W. *Development, design and experimental validation of a steel self centering device (SSCD) for seismic protection of buildings*. Bulletin of Earthquake Engineering 10 (6), 1915-1941, 2012.
- [2] Braga, F., Gigliotti, R., Monti, G., Morelli F., Nuti, C., Vanzi, I., Salvatore, W., (2015). "Post-seismic assessment of existing constructions: evaluation of the shakemaps for identifying exclusion zones in Emilia". Earthquakes and Structures, Vol. 8, No. 1 DOI: <http://dx.doi.org/10.12989/eas.2015.8.1.895>.
- [3] Braga, F., Gigliotti, R., Monti, G., Morelli F., Nuti, C., Vanzi, I., Salvatore, W., (2014). "Speedup of post earthquake community recovery. The case of precast industrial buildings after the Emilia 2012 earthquake". Bulletin of Earthquake Engineering 10/2014; 12(5). DOI: 10.1007/s10518-014-9583-3
- [4] NTC (2008) Norme tecniche per le Costruzioni. Gazzetta Ufficiale n. 29, February 4, 2008, Suppl. Ordinario n.30, Italy. (in Italian)
- [5] EN1998-3:2005 - *Eurocode 8 –Design of structures for earthquake resistance, Part 1: Assessment and retrofitting of buildings*.
- [6] ATC-40, 1996 Applied Technology Council 1996, ATC40, Seismic evaluation and retrofit of concrete buildings, California Seismic Safety Commission, Proposition 122, Seismic Retrofit Practices Improvement Program, Report SSC 96

## 7 SEISMIC REHABILITATION OF AN EXISTING R.C. BUILDING USING TRIANGULAR SHAPED HYSTERETIC DEVICES

### 7.1 GENERAL

#### 7.1.1 Introduction

This case study refers to the seismic rehabilitation of an existing reinforced concrete building, located in Napoli (Italy). The building under study can be considered as representative of a large number of existing RC buildings in the South of Italy, built during the 60s and 70s when Naples was considered a non-seismic area. The seismic rehabilitation is carried out introducing TRIangular Shaped Hysteretic (TRSH) devices with “V-bracing” systems [1]. Due to the significant nonlinear behavior of such system, nonlinear analyses are used to design the retrofiting system.

#### 7.1.2 Description of case study building

The RC structure was built at the beginning of ‘80s within the steel mill ILVA in Bagnoli (Naples, Italy). Figure 7.1 shows the investigated building.

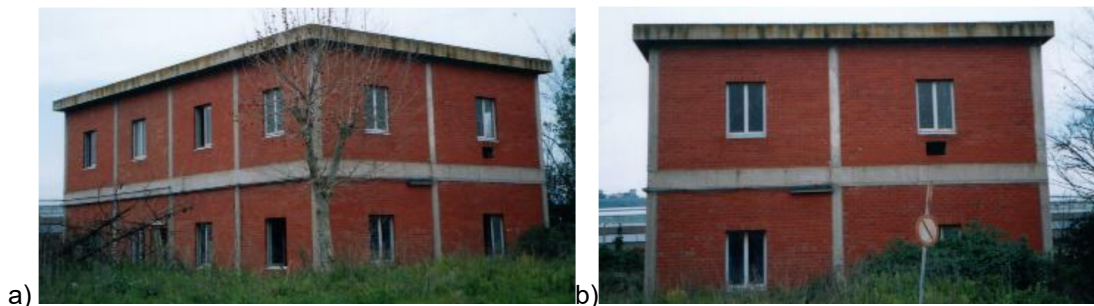
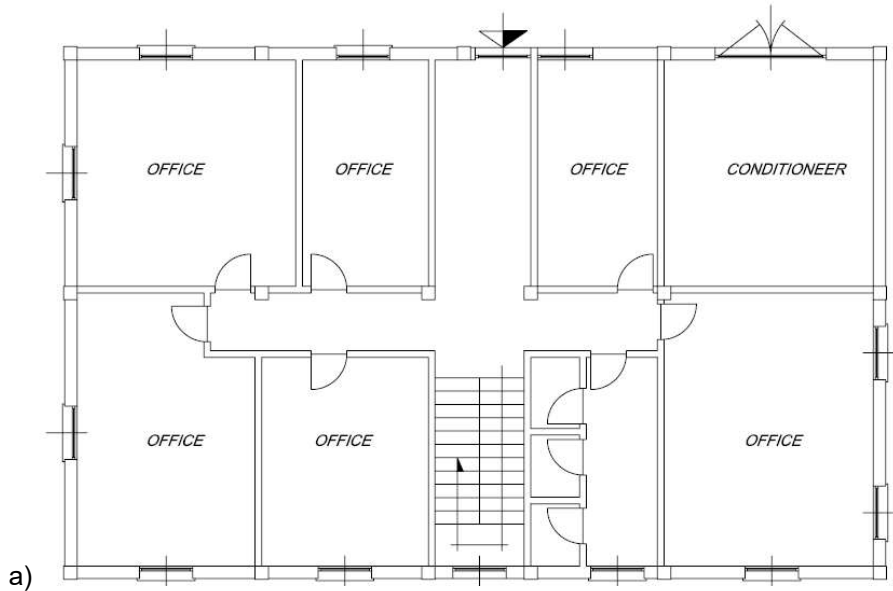


Figure 7.1: The building under investigation.

The geometrical survey and the constructional details in the original design drawings clearly show that the structure has been designed to resist vertical loads only. Figure 7.2 shows two drawings representing the architectural plans, while in Figure 7.3 the structural plans show the essential characteristics of the RC frame structure at first and second floor, respectively. At first floor, all beams have rectangular 20cmx60cm cross-section except the transverse beam in X direction that is 25cmx60cm. At second floor, all beams are rectangular 15cmx60cm cross-section, except for the transverse beam in X direction which is 25cmx60cm. All columns have square

30cmx30cm cross-section, with twelve longitudinal ribbed bars (12 mm in diameter) as reinforcement uniformly distributed along the perimeter of the cross-section.

FIRST FLOOR PLAN



SECOND FLOOR PLAN

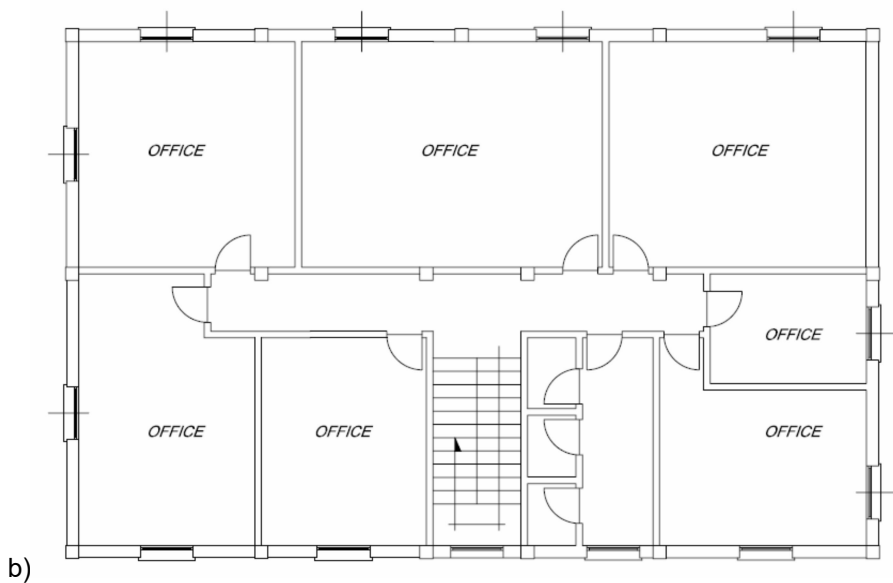


Figure 7.2: The building under investigation- architectural plans: first floor plan (a); second floor plan (b).

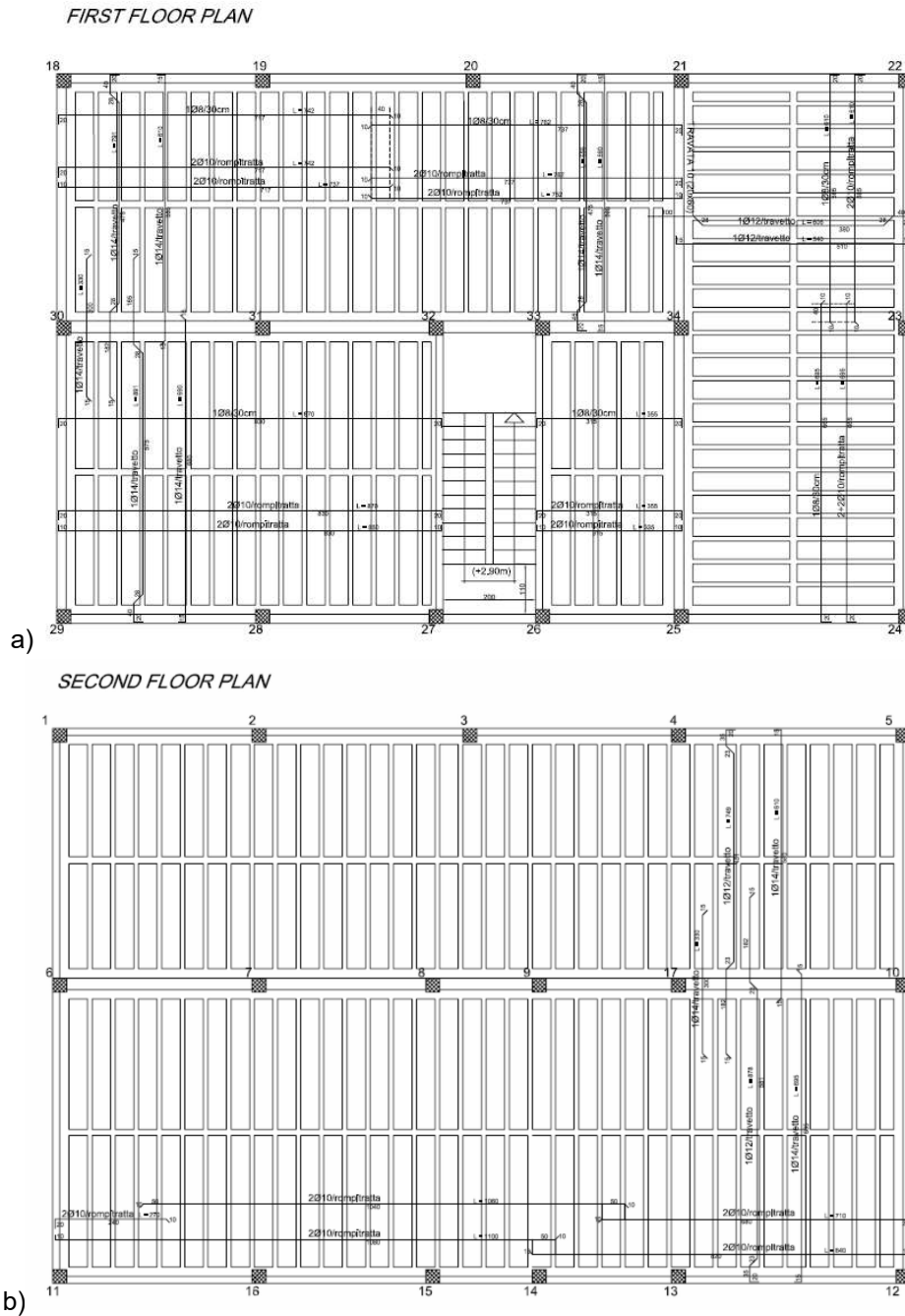


Figure 7.3: The building under investigation- structural plans: first floor plan a); second floor plan (b).

The extrados floor heights, measured from foundations, are respectively 4.60 m at first floor and 8.95 m at second floor. Structural details are in accordance with the past Italian non-seismic code. For example, transverse stirrups in beams and columns are discontinuous, largely spaced and not well bent inside the cross section. Also insufficient anchorage and incorrect overlaps of the longitudinal steel rebars can be observed, together with the absence of suitable confinement of joints,

eccentricities in beam to column joints, scarce care of the resumptions of concrete casting of columns.

The main mechanical properties of both concrete and steel have been measured in the laboratory on the coupon sampled from the existing structure. Moreover, a number of Non-Destructive Tests (NDT) have been carried out on site. Table 7.1 summarizes the average measured values of Young modulus, the axial compression strength of concrete and the tensile yield resistance of steel rebars.

Table 7.1: Average measured mechanical properties of concrete and steel rebars

material	$E$ (MPa)	$f_{cm}$ (MPa)	$f_{ym}$ (MPa)
Concrete	30500	28.5	
Steel rebars	207000		480

## 7.2 ANALYSIS OF THE CASE STUDY

### 7.2.1 Non-Linear modelling, analysis and safety checks of the original building

A three dimensional model was elaborated using SAP2000 software. The geometrical and mechanical features of the RC frame are consistent with those reported in the previous section.

Beams and columns have been modelled as frame elements. A fixed restrained at columns' bases was assumed. The first and second floors were modelled considering all floor joists. The geometry of the model is shown in Figure 7.4.

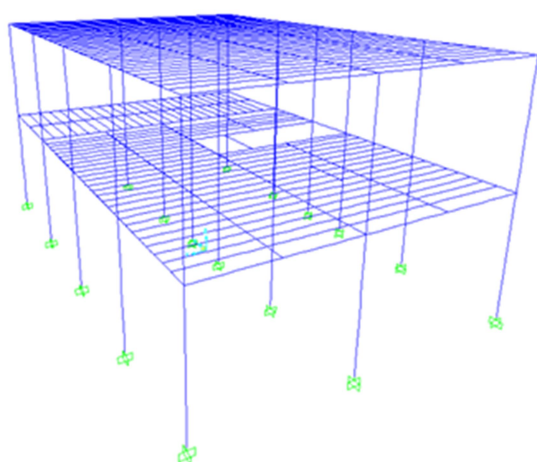


Figure 7.4: Simplified schematization of the building for the modelling.

The elastic properties of RC members were properly reduced to account for cracking due to bending effects. The reduction factors of cross sectional properties of RC

members of FEMA 356 [2] were used, namely 0.5 times the second moment of area and 0.4 times the shear area of RC members.

The inelastic behaviour of RC unit has been schematized by means of a lumped-plasticity modelling approach according to the multi-linear response curves provided by FEMA 356 [2]. The criteria and the modelling parameters differ for primary and secondary components, as well as for ductile and brittle elements. With this regard, both EC8-3 [3] and FEMA356 [2] define ductile elements as “deformation-controlled”, while brittle elements are “force-controlled”. In the first case, the plastic behaviour includes strain hardening and a strength-degradation with residual strength capacity. In the second case, the behaviour is characterized by an elastic range followed by loss of strength.

According to this definition, FEMA 356 [3] provides a generalized force - deformation response curve for the plastic hinges (see Figure 7.5,a), which allows covering all non-linear response curves by particularizing the proper modelling parameters.

Both FEMA 356 (Chapter 5) and EN1998-3 (Annex B) define criteria for the acceptable damage state condition of the plastic hinges associated to three limit states that are similar in both codes, see the three points on generalized force-displacement curve in Figure 7.5,b. In particular, it can be roughly assumed that Immediate Occupancy (IO) corresponds to Damage Limitation (DL), Life Safety (LS) stands for Significant Damage (SD), while Collapse Prevention (CP) relates to Near Collapse (NC).

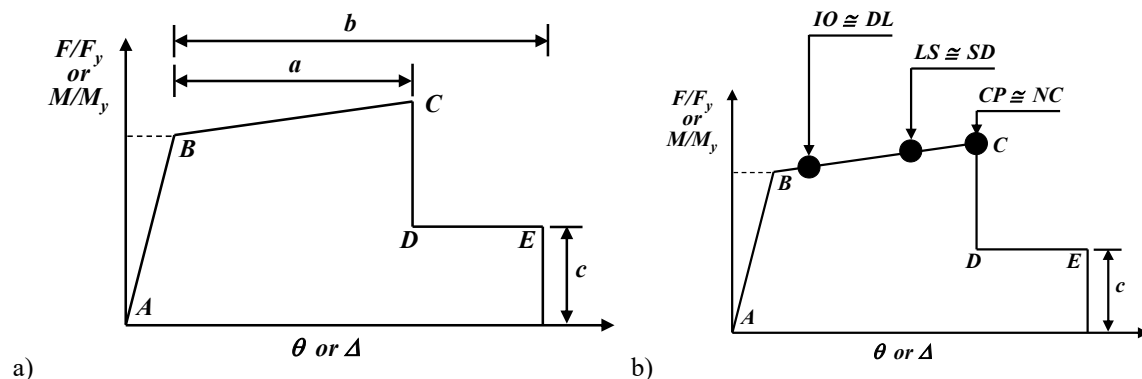


Figure 7.5: Generalized force-deformation relationship of plastic hinge (a) and relevant acceptance criteria (b).

In the examined case the inelastic response parameters (i.e. plastic hinges properties) for the bare RC structure numerical model were deduced from average material properties coming from laboratory tests.

The following permanent, live and external loads, in relation to the specific location of the building, were considered:

- Permanent – storey load: 8.20 kN/m<sup>2</sup>

- Permanent – infill panels: 1.50 kN/m<sup>2</sup>
- Live load: 2.00 kN/m<sup>2</sup>
- Snow load: 0.50 kN/m<sup>2</sup>

Seismic action was defined according to D.M.14/01/2008 [4] considering nominal life  $V_N$  equal to 50 years, unitary use coefficient  $C_u$  and soil category C according to the owned geological information. The response spectrum evaluated for Significant Damage (SD) limit state (which corresponds to the Life Safety limit state of Italian code D.M.14/01/2008 with return period  $T_R=475$  years) is characterized by peak ground acceleration  $PGA=0.17$  g. The corresponding spectra at Damage limitation state (which is representative of return period  $T_R=225$  years) has a  $PGA = 0.10$ g, while at Near Collapse (which is representative of return period  $T_R=2475$  years) the  $PGA$  is equal to 0.29g. The spectra are depicted in Figure 7.6.

A non-linear static or pushover analysis was then executed on the model. Thanks to the detailed knowledge of the structure, the non-linear analysis incorporates the safety checks of structural RC elements.

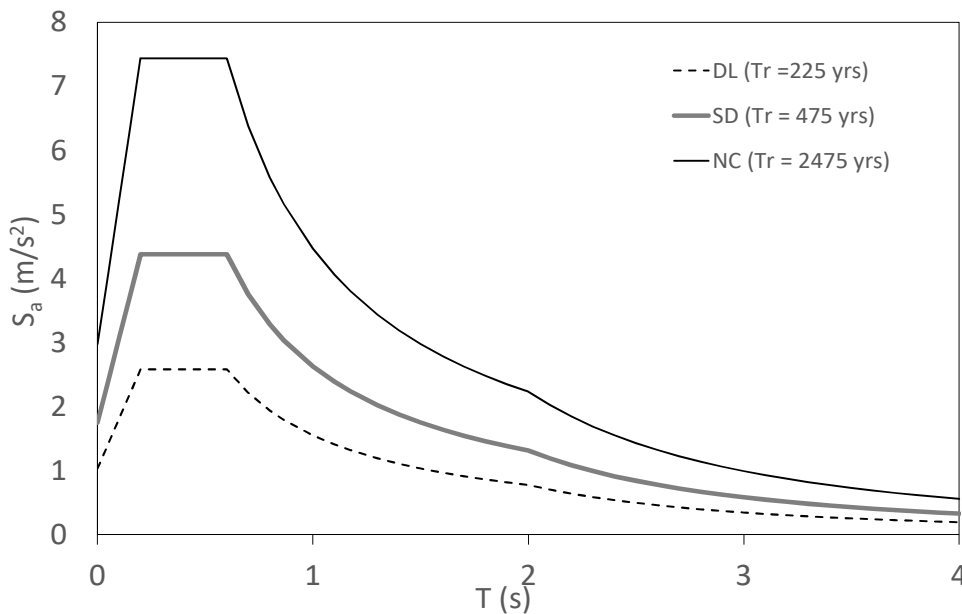


Figure 7.6: Elastic response spectra evaluated for DL, SD and NC limit states.

The structural assessment of the building was performed through nonlinear static (pushover) analysis, determining the capacity curve of the building (base shear/displacement); the structural capacity was compared to the effective seismic demand, determining the effective performance of the structure and evidencing the eventual need of retrofit interventions.

The N2 method recommended by EN1998 was used to assess the performance of the building. The method is based on the determination of the performance point of the building, representing the demand of an equivalent SDOF according to the equal displacement rule for effective period larger than TC or equal area rule for period smaller than TC.

The capacity curve of the equivalent SDOF and the seismic demand can be directly compared in an acceleration/displacement plane (acceleration displacement response spectra - ADRS). The performance point represents the condition in which the seismic capacity of the building is exactly equivalent to the seismic demand due to a specific earthquake input.

In order to shift the traditional response spectrum (in terms of spectral acceleration  $S_a$  vs. period  $T$ ) into the ADRS plane and to evaluate the spectral displacement  $S_{di}$  (being  $T_i$  the period of the building) the following relationship can be used:

$$S_{di} = \frac{T_i^2}{4\pi^2} \cdot S_{ai} g \quad \text{Eq. ( 7.1)}$$

In order to convert the capacity curve of the system in the capacity spectrum, a punctual transformation is needed. Each single point ( $F_b$  – base shear vs.  $d_c$  – displacement of the control point) is translated into a ( $S_{di}$ ,  $S_{ai}$ ) point through the following equations:

$$S_{di} = \frac{d_c}{FP_1 \times \phi_{1,c}} \quad \text{and} \quad S_{ai} = \frac{F_b}{W} \cdot \frac{1}{\alpha_1} \quad \text{Eq. ( 7.2)}$$

Being  $\alpha_1$  and  $FP_1$  the modal mass coefficient and the participating factor for the first vibration mode, while  $\phi_{1,c}$  is the amplitude of the control point for the first vibration mode. After the representation of the two diagrams in the same ADRS plane, a preliminary performance point ( $d_{pi}$ ,  $a_{pi}$ ) is selected on the base of the equivalent displacement approach.

A bilinear representation of the capacity curve can be used, with the yield displacement selected to guarantee the so-called equal area rule.

For the sake of example, the performance of the structure is focused in the transverse direction of the building (the short side). Figure 7.7 shows the capacity curve in transverse direction and the corresponding bi-linearization.

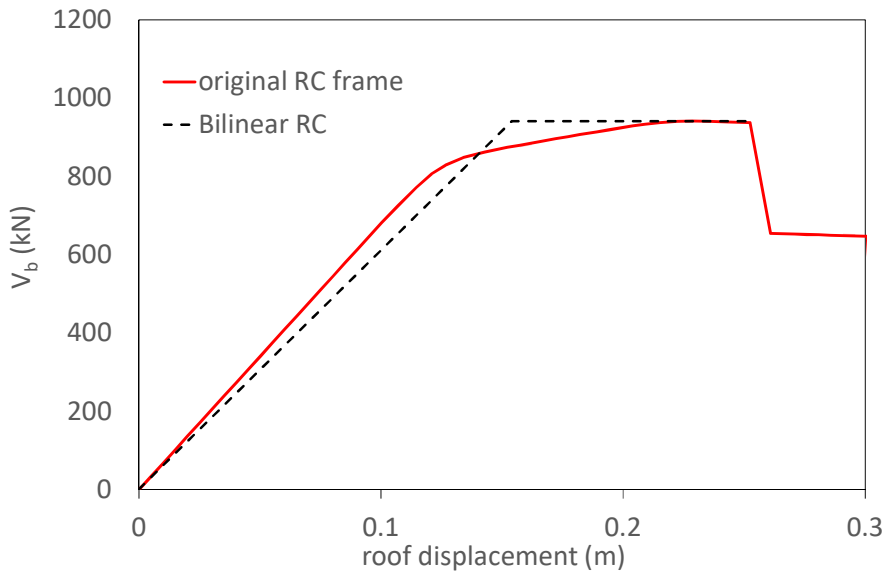


Figure 7.7: a) Bilinear representation for CSM, b) scheme for the evaluation of the spectral reduction factor.

Figure 7.8 shows the demand spectra both for the SD limit state (i.e. 100% of code spectrum) and for the NC limit state (i.e. 172% of the code spectrum). The analysis of the condition of structural elements evidenced the formation of soft storey mechanism at the first level with brittle behavior of the column. The RC building shows moderate plastic deformations at DL limit state (see Figure 7.9,a) is highly prone to severe damage at SD limit state (see Figure 7.9,b) and unacceptable performance at NC (see Figure 7.9,c).

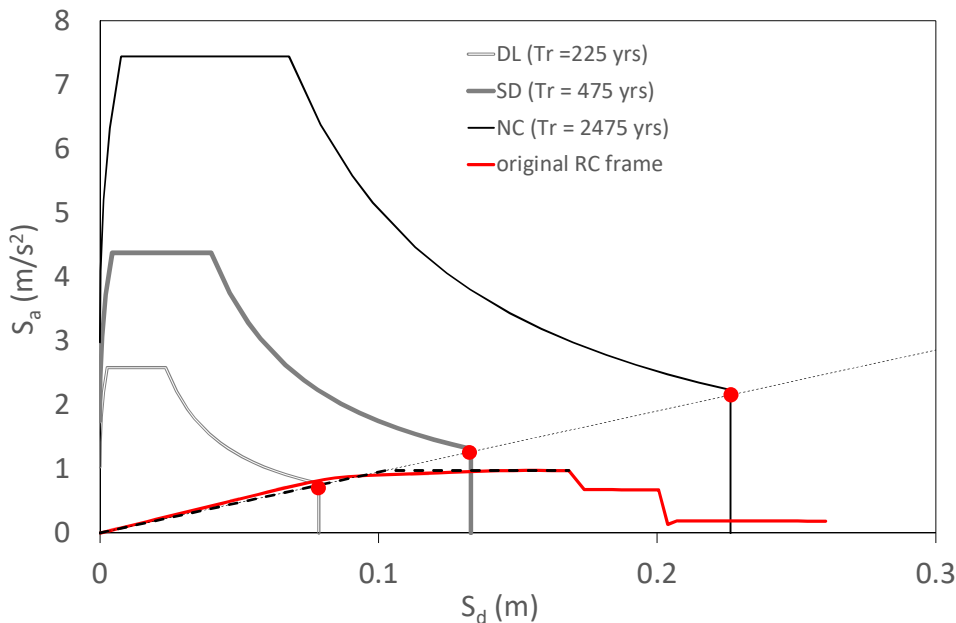


Figure 7.8: Capacity spectrum method applied for the state of art condition (x and y direction).

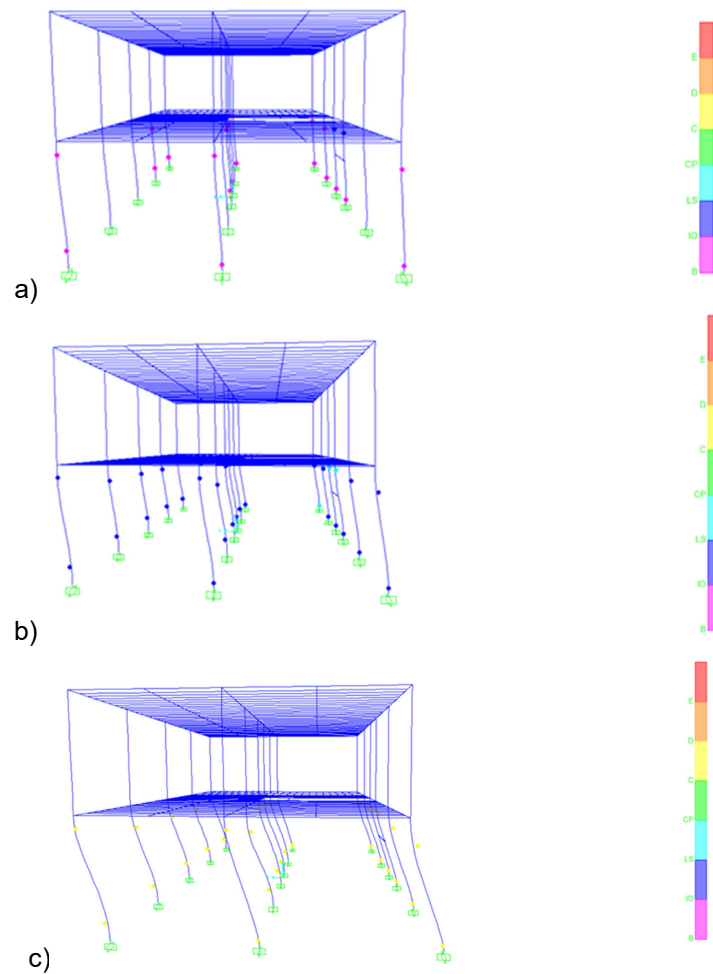


Figure 7.9: Response at DL (a), SD (b) and NC limit state (c).

### 7.3 RETROFIT OF THE EXISTING CASE STUDY BUILDING

In the examined case study the TRSH devices were designed in order to satisfy different performance at each seismic hazard level: i) at 10%/50 years the FDBF should behave in elastic field; ii) at 2%/50 years the additional dampers have to control the interstorey drift ratio demand within 2% of the storey height which should corresponds to very limited structural damage. The damage limitation (DL) limit state is verified a-posteriori in order to control that the interstorey drift ratio is lower than 0.5%. To achieve these goals an iterative procedure based on the use of capacity spectra has been adopted.

In particular, the response of a RC frame equipped with RSTHs can be schematically idealized as a simple system consisting of two inelastic springs connected in parallel, namely the RC frame and the TRSH system, similarly as shown for BRBs by El-Bahey and Bruneau [5]. As shown in Figure 7.10 the response curves of the RC frame and TRSH system are given by bi-linear curves, while the response curve of the strengthened frame is the tri-linear obtained by summing the effective stiffness of the two springs if the interaction between the bracing system and the RC frame is

negligible. This implies that the TRSH stiffness and strength should be chosen to limit the demand on the structure such that the system displacement demand at the performance point for the design seismic hazard level is less than or equal the yield displacement of the MRF.

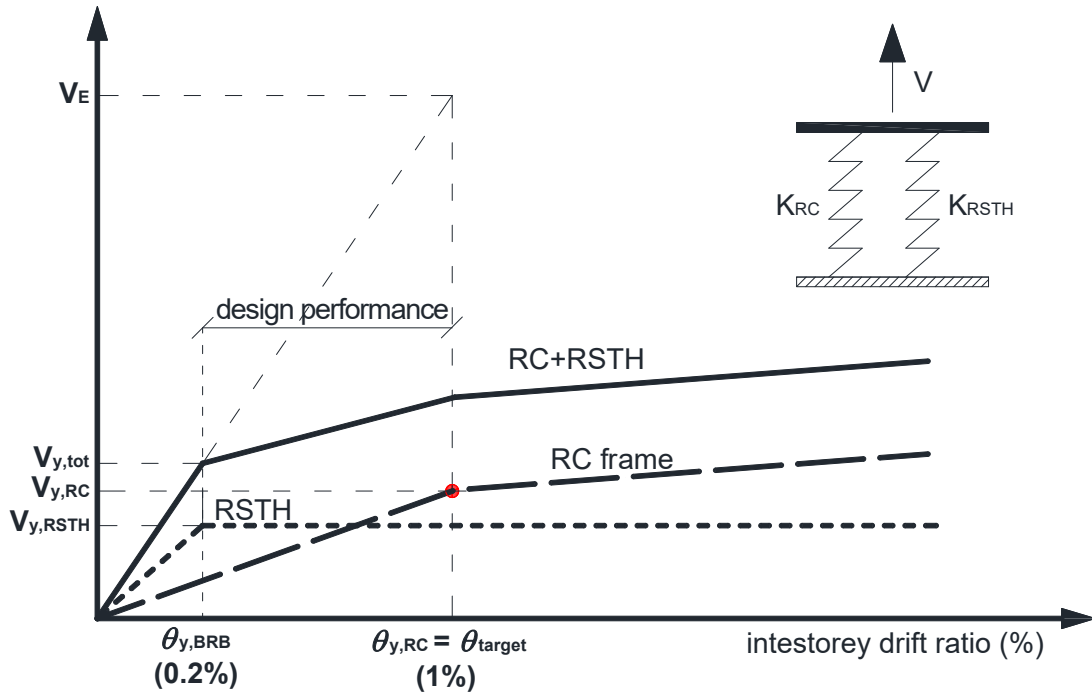


Figure 7.10: Design response curves of the retrofitting system.

For the structural fuse concept, RSTH system should absorb most of the seismic energy through additional dampers while maintaining the elasticity of the main structure. This design target can be achieved when the RSTH yield displacement,  $\theta_{y,RSTH}$ , is less than the yielding displacement of the frame,  $\theta_{y,RC}$ . This implies that the RSTH stiffness and strength should be chosen to limit the demand on the structure such that the system displacement demand for the design earthquake is less than or at least equal to  $\theta_{y,RC}$ . In this concept, assuming the target performance as the achievement of first yielding in RC frame it is possible to obtain the minimum ductility that the RSTH should guarantee to behave as a structural fuse by the following:

$$\mu_d = \frac{\theta_{target}}{\theta_{y,RSTH}} = \frac{\theta_{y,RC}}{\theta_{y,RSTH}} \quad (1)$$

Since in the most of RC frames the infill walls are made of masonry panels the yield drift for RSTH system can be designed to occur when the infill walls start to crack. Early studies [6] on the RC structure examined in this paper showed that it is possible to assume that the mean value of interstorey drift ratio corresponding to the

first cracks in masonry infill walls is about 0.2%. Hence, this value is assumed for  $\theta_{y,RSTH}$ .

Moreover, these previous studies showed that the yielding of the examined RC frame occurs at 1% of interstorey drift ratio. On the basis of these assumptions, the

RSTH design ductility was given by  $\mu_d = \frac{\theta_{target}}{\theta_{y,RSTH}} = \frac{1\%}{0.2\%} = 5$ .

Since  $\theta_{target}$  is in the constant velocity region of the spectrum, the shear strength of the building with RSTH was estimated using the equal displacement theory as

$V_{RC+RSTH} = \frac{V_E}{\mu}$ , where  $V_E$  is the elastic base shear, defined as the seismic demand on

the total system if the system behaved elastically. Hence, the minimum strength of the RSTH can be easily derived as follows:

$$V_{RSTH} = \frac{V_E}{\mu} - V_{RC} \quad (2)$$

On the basis of Eq. (2) it is possible to determine the number of devices once fixed the type of the TRSH. In this example it was assumed as elementary dissipative fuse the triangular shape reported in the informative brochure [1], see Figure 7.11.

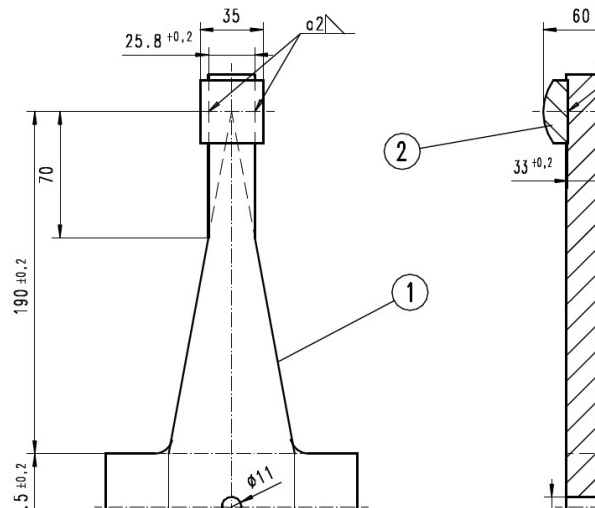


Figure 7.11: Considered TRSH element.

Let assume a maximum strain  $\varepsilon_u = 0,04$ , the yielding  $F_y$ , damping force  $F$ , elastic  $k_1$  and post yielding  $k_2$  stiffness are:

$$F_y = \frac{b \cdot t^2}{4 \cdot h} \cdot \sigma_y = \frac{70 \cdot 35^2}{4 \cdot 190} \cdot 424 = 47,8 \text{ [kN]}$$

$$F = \frac{b \cdot t^2}{4 \cdot h} \cdot \sigma \cdot \left(1 + \frac{2}{(h+c)^2} \cdot s\right) = \frac{70 \cdot 35^2}{4 \cdot 190} \cdot 424 \cdot \left(1 + \frac{2}{(190+70)^2} \cdot 35,7^2\right) \cdot 10^{-3} = 49,6 \text{ [kN]}$$

$$k_1 = \frac{b \cdot t^3}{4 \cdot h \cdot (h^2 - c^2)} \cdot E_1 = \frac{70 \cdot 35^3}{4 \cdot 190 \cdot (190^2 - 50^2)} \cdot 70000 = 8227,1 \text{ [N/mm]}$$

$$\begin{aligned} k_2 &= \frac{b \cdot t^3}{4 \cdot h \cdot (h^2 - c^2)} \cdot E_2 + \frac{2}{(h+c)^2} \cdot F_y \cdot s \cdot \left(1 + \frac{\varepsilon_y}{\varepsilon_u}\right) \\ &= \frac{70 \cdot 35^3}{4 \cdot 190 \cdot (190^2 - 70^2)} \cdot 758 + \frac{2}{(190+70)^2} \cdot 47800 \cdot 35,7 \cdot \left(1 + \frac{0,0061}{0,04}\right) \\ &= 107,6 \text{ [N/mm]} \end{aligned}$$

For design purposes, the curved force- displacement response curve of the RSTH system has been approximated by a bilinear hysteresis envelope with an initial stiffness  $k_1$ , a yielded stiffness  $k_2$  and a yield force  $F_y$ .

On the basis of these mechanical features it is necessary to use 8 TRSH at first storey, namely 4 per side of the building, and 4 TRSH at second level, namely 2 per side of the building.

Figure 7.12 show the comparison between the obtained pushover curves and their corresponding bilinearized curves of the original RC structure and that equipped with the designed TRSH system.

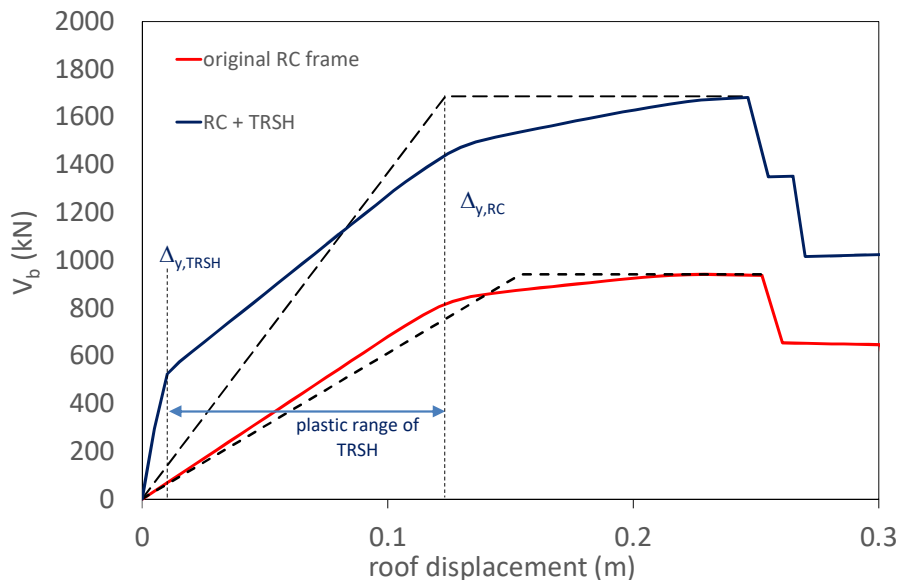


Figure 7.12: Original RC vs RC+RSTH pushover curves.

The plots showing the performance points obtained for both TRSH and original RC at the three design seismic hazard levels are given in Figure 7.13, where it can be

directly observed that the design objectives at SD and NC are satisfied, namely the seismic displacement demand of the structure equipped with TRSH is smaller than the yield displacement of the RC response curve at SD and lower than 2% at NC. In addition, even the DL is satisfied, being the drift ratio at first storey lower than 0.5%.

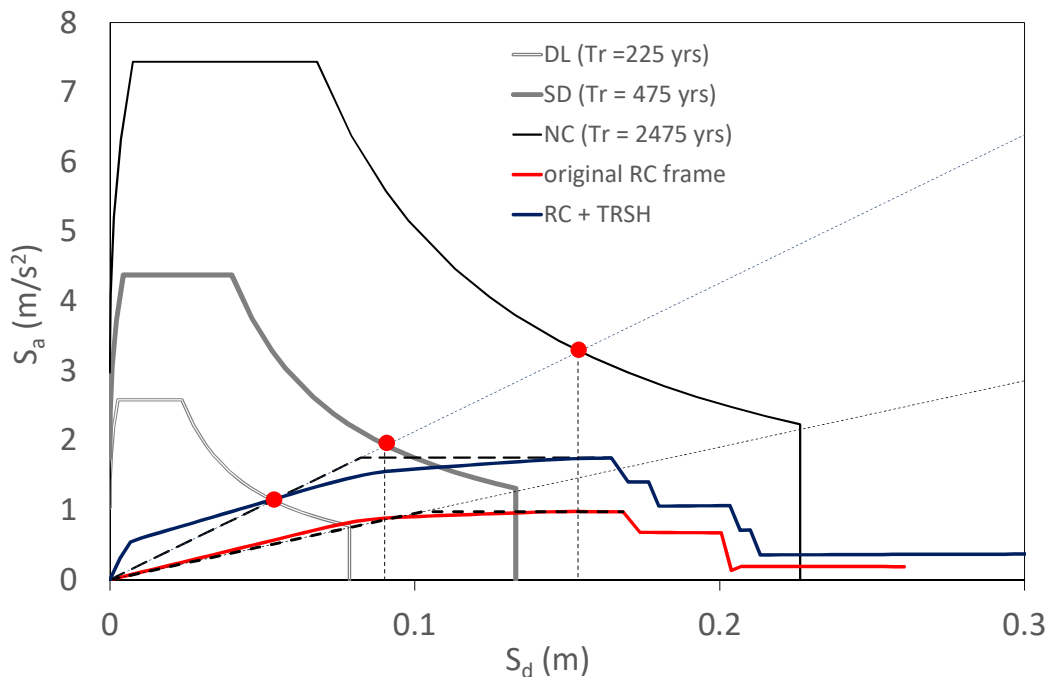


Figure 7.13: Original RC vs RC+RSTH pushover curves.

The analysis of the condition of structural elements evidenced that the RC frame is elastic at DL limit state, with plastic deformations into the RSTH only (see Figure 7.14,A). At SD limit state slight damage into some columns of the RC building can be observed (see Figure 7.14,b), thus confirming the effectiveness of the RSTH system as well as the adopted design strategy. The RC structure is severely damaged at NC (see Figure 7.14,c), but the plastic hinges of RC elements still have residual deformation capacity and strength. In addition, it can be noted that limited interaction between the RC structure and the RSTH system can be recognized. Hence, no local interventions are necessary to increase the strength of single structural elements.

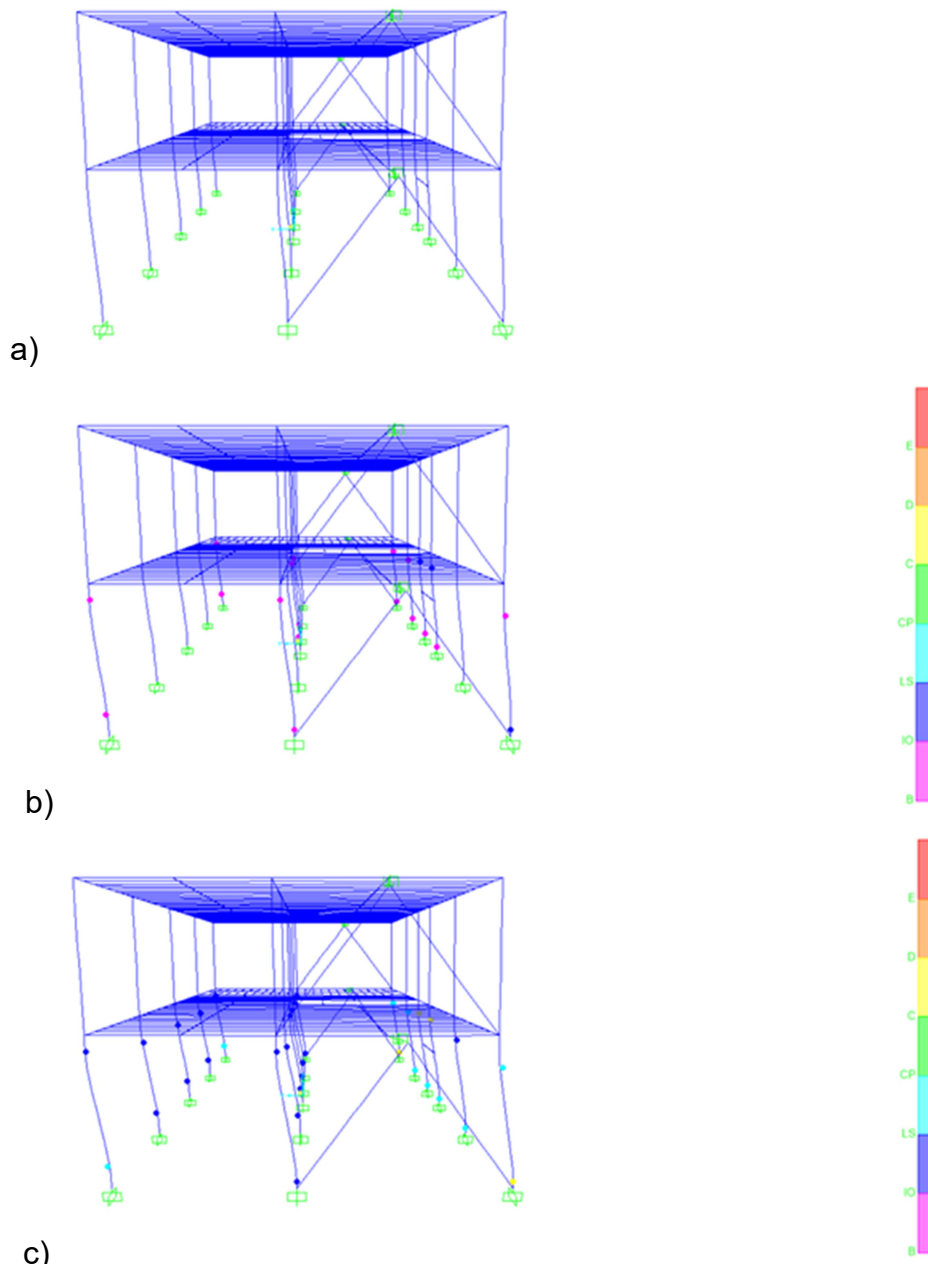


Figure 7.14: Response at DL (a), SD (b) and NC limit state (c).

## 7.4 CONCLUSIONS

The TRSH has been designed based on the use of N2 method to derive the appropriate strength and stiffness to limit the displacement demand into the RC frame.

The static pushover analysis was executed on a nonlinear model with concentrated plasticity globally and it confirmed the effectiveness of the design assumptions. The designed system also satisfies the safety checks. The analysis shows that no local

interventions are necessary, thus being very promising for such a type of RC buildings.

## 7.5 REFERENCES

- [1] Ioannis Vayas editor. Innovative anti-seismic devices and systems 1st edition, 2017. European Convention for Constructional Steelwork, ISBN: 978-92-9147-136-2
- [2] FEMA 356 (2000). Prestandard and commentary for the Seismic Rehabilitation of Buildings. Building seismic safety Council for the Federal Emergency Management Agency, Washington
- [3] EN1998-3:2005 - *Eurocode 8 –Design of structures for earthquake resistance, Part 1: Assessment and retrofitting of buildings.*
- [4] NTC (2008) Norme tecniche per le Costruzioni. Gazzetta Ufficiale n. 29, February 4, 2008, Suppl. Ordinario n.30, Italy. (in Italian)
- [5] El-Bahey S., Bruneau M., (2011). Buckling restrained braces as structural fuses for the seismic retrofit of reinforced concrete bridge bents *Engineering Structures* 33, 1052–1061
- [6] Della Corte, G., Fiorino, L., Mazzolani, F.M., (2008). Lateral loading tests on a real RC building including masonry infill panels with and without FRP strengthening. *Journal of Materials in Civil Engineering*, ASCE, Vol. 20, No. 6.

## 8 SEISMIC RETROFIT OF AN EXISTING INDUSTRIAL STEEL BUILDING USING MOON SHAPED HYSTERETIC DEVICES

### 8.1 INTRODUCTION

This case study refers to the seismic retrofitting of an existing industrial steel building through the moon shaped hysteretic devices. Steel buildings are, indeed, more suitable to be retrofitted using hysteretic devices thanks to the intrinsic deformability of the structure itself. Such lateral deformability allows to dissipate an important ratio of the seismic energy through hysteretic cycles, maximizing the efficiency of the device. The seismic vulnerability of the case study presented within this chapter has been studied in its current (un-retrofitted) state by both static and dynamic non-linear analyses in [1]. In this study, taking into account the results of the seismic vulnerability analysis in the current state, the retrofitting of the structure is designed. The retrofitting consists in the introduction of the innovative Moon Shaped Hysteretic elements (MSSH) in the end of brace elements. Given the strong nonlinear behavior of such system, non-linear static analyses are used.

### 8.2 DESCRIPTION OF CASE STUDY BUILDING

The case study building (see Fig. 8.1) is an existing steel silo characterized by a large mass placed at high altitude and different typologies of horizontal forces resisting systems. It has the function of filtering the gasses coming from the steelwork and can be schematized as made up of a supporting structure, the silos containing the filtered material and the roof.

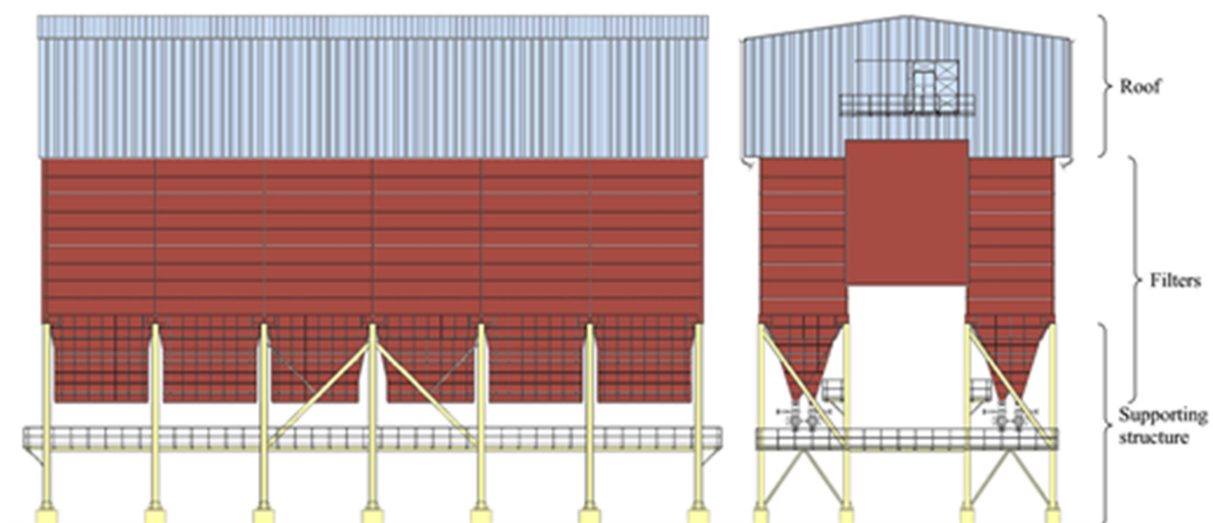


Fig. 8.1: Front (left) and side (right) views of the case study

The building has a regular plan, with overall dimensions 37.80 m x 16.94 m and total height 29.64 m. The supporting structure, with a total height of about 10.80 m, has six bays in the longitudinal (X) direction and three in the transversal (Y) one. As is typical of industrial buildings, where the functionality issues often prevaricate the rules for an optimized structural design, different horizontal resisting systems (Fig. 8.2) can be individuated such as moment resisting frames (X direction - ground floor), inverted V bracings (Y direction - ground floor) and diagonal bracings (X and Y directions - first floor).

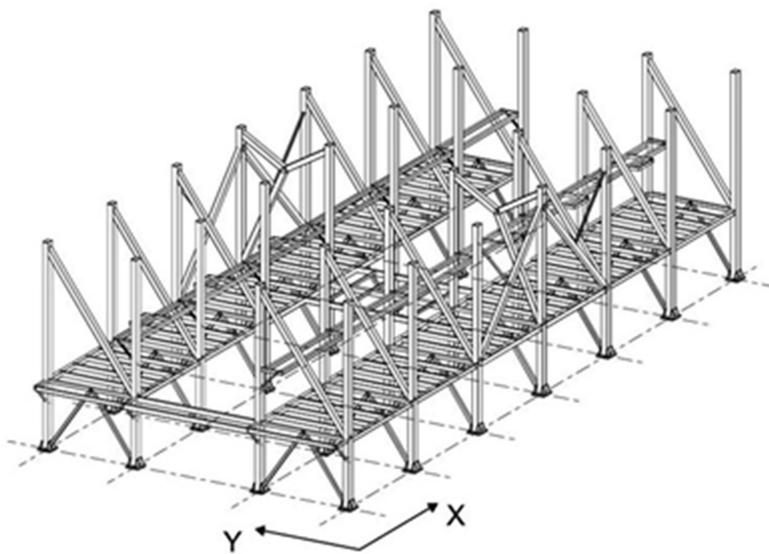


Fig. 8.2: 3D view of the supporting system

The silos are realized with thin (4 mm) walls stiffened with a close series of horizontal UPN and vertical HEA profiles. The total mass of the silo (23700 kN), considering the structural elements and the infill material, represents the 86% of the total mass (27650 kN). The roof is connected directly to the filter walls and its contribution is considered only in terms of vertical load and mass.

## 8.3 ANALYSIS OF THE CASE STUDY

### 8.3.1 Linear and non-linear modelling

A preliminary comparison between a full-comprehensive linear model (Fig. 8.3) and a geometrically-simplified (

Fig. 8.4) model was carried out given the need to simplify the structural scheme to obtain a reliable and time-saving nonlinear model. The infill material was modelled as five different lumped masses connected to the silo wall by elastic springs whose stiffness was evaluated on the base of the edometric modulus of the infill material.

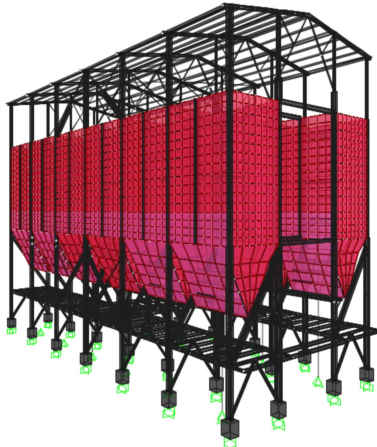


Fig. 8.3: "Complete" linear model global view

The "complete" linear model highlighted a structural behavior similar to that of a single degree of freedom, where the great part of the displacement demand is located in the supporting structure. The silos and the roof acted as a rigid body and the resultant stresses were far below the yielding or buckling threshold. It was therefore assumed that the structural behavior could be represented by the simplified model shown in

Fig. 8.4. In this model the roof was considered simply as dead load and mass, while the silos were substituted by an elastic trusses system, whose characteristics were evaluated to obtain the same first period and modal shape of the "complete" model. In the simplified model, used to perform nonlinear analyses, each frame was modelled, in OpenSEES [3] using fiber elements and the material was assumed to be elasto-plastic, see

Fig. 8.5:b and

Fig. 8.5.c.

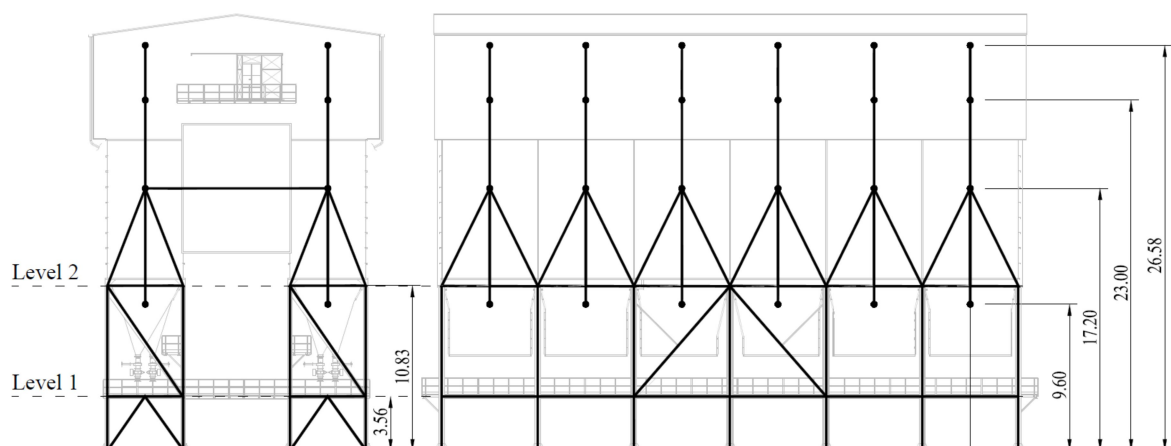


Fig. 8.4: Case study simplified model geometry

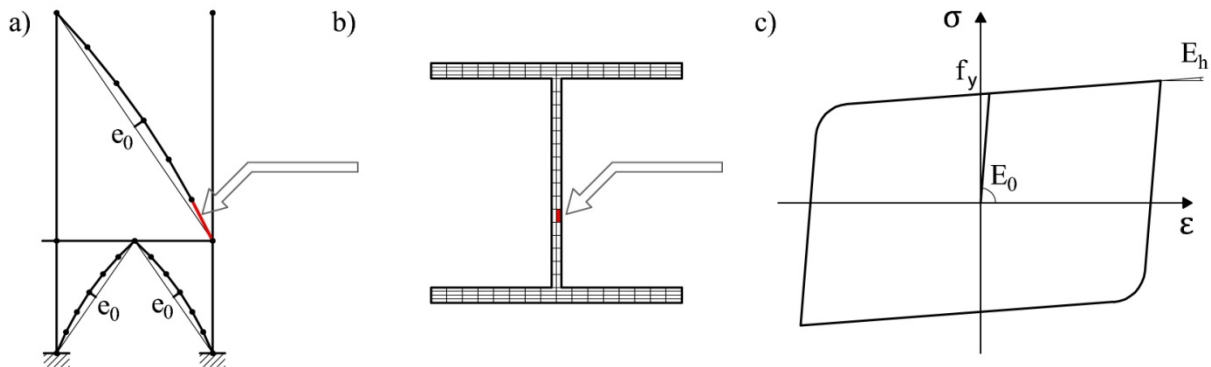


Fig. 8.5: Scheme of a braced frame modelling: a) bracings initial bow imperfection; b) subdivision of section into fibers; c) elasto-plastic stress-strain relationship (OpenSEES Steel02 material [3]) associated to each fiber

The nonlinear behavior in shear of the structural elements was not directly considered and only the elastic de-formability was taken into account. To check the goodness of such modeling approach, an automatic procedure for the assessment of the elastic behavior in shear was used, checking at the end of each nonlinear analysis that all the structural elements did not yielded in shear.

The global second-order effects were explicitly taken into account assuming a corotational geometric transformation for the bracings and a P-Delta geometric transformation for the columns. The corotational geometric transformation updates the stiffness matrix as a function of the deformed shape at each step of integration [3] and it is therefore suitable for large displacement problems, even though it requires higher computational efforts. The P-Delta method performs a linear geometric transformation of the element stiffness and resisting force considering second-order P-Delta effects [3].

To simulate the post-buckling behavior of the bracings, they were modelled introducing an initial local bow imperfection,  $e_0$ , equal to  $L/300$ , where  $L$  is the length of the bracing, following the indications of Eurocode 3 [4] in order to consider their post-critic behavior when subjected to compression forces, see

Fig. 8.5. Such modeling approach has been already used and its validity assessed by other researches [5] [6]. Within this research it was assessed that, for each bracing element, the maximum compressive load evaluated considering the local bow imperfection and the buckling load,  $N_{b,Rd}$ , evaluated according to Eurocode 3 [4] did not differ more than 5%, see Fig. 8.6.

The soil-structure interaction phenomena were neglected and the columns bases were modelled as fixed in the X direction and perfectly hinged in the Y direction.

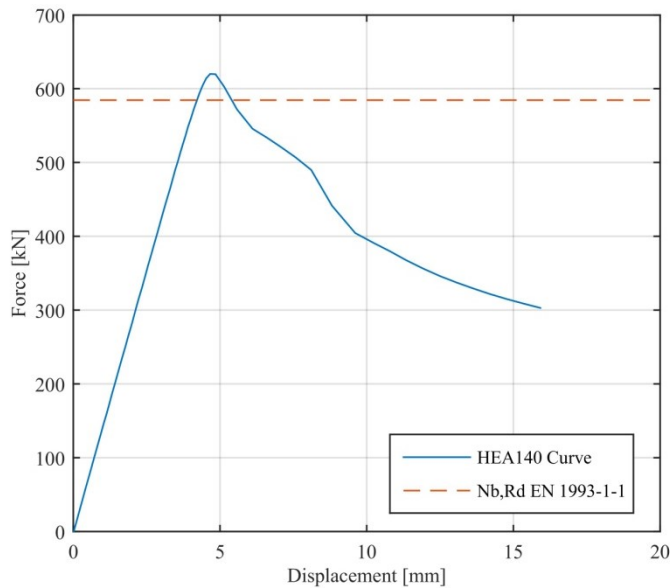


Fig. 8.6: Comparison between the force-displacement curve obtained for a HEB140 brace with the local bow imperfection (continuous line) and the buckling load evaluated according to Eurocode 3.

### 8.3.2 Nonlinear static analyses

The structural assessment of the building in its current un-retrofitted state was executed through nonlinear static (pushover) analysis, determining the capacity curve of the building (base shear/displacement); the structural capacity was compared to the effective seismic demand, determining the effective performance of the structure and evidencing the eventual need of retrofit interventions.

Table 8.1 resumes the Ultimate Limit States considered during the structural analysis. Such Limit States were obtained following the recommendations of Eurocode 8 [7].

Table 8.1: Ultimate Limit States considered during the analysis

ULTIMATE LIMIT STATE	ELEMENT	CHECK	STANDARD
Shear resistance	Columns/beams	$V_{Ed} / V_{pl,Rd} \leq 0.50$	EN 1998-1:2004
Plastic rotation capacity	Columns	$\phi < \phi_u$	EN 1998-3:2005
Plastic rotation capacity	Beams	$\phi < \phi_u$	EN 1998-3:2005
Axial deformation capacity in tension	Bracings	$\Delta L < \Delta L_y$ (tension)	EN 1998-3:2005

It is worth noting that no deformation limits were considered for the bracing in compression, assuming that the introduction of the initial local bow imperfection is able to correctly reproduce the buckling phenomena.

The capacity curves reported in Fig. 8.7, where the definition of the levels is shown in Fig. 8.4, clearly show the differences of the structural nonlinear behavior in the two directions. For a better understanding of the structural behavior, the curves are reported assuming as control point both the baricenter of the first and second floor. The force distribution adopted is the one assuming a uniform acceleration. It should be noted that, due to the concentration of practically the whole structural mass in correspondence of the silo, the force distribution proportional to the first modal mode is practically the same. In the X direction, given that the structure is characterized by moment resisting frames at the ground floor level and by diagonal concentric bracings at the first level, the curves show a more flexible and ductile behavior with a smooth transition between the elastic and the plastic ranges and a softening post-yielding behavior. The latter is mainly due to second order effects. In the Y direction, the behavior is completely different and the ductility is limited due to the buckling of the inverted V diagonal bracings causing a fast drop of the global resistance.

The following aspects of the structural behavior can be highlighted:

- In the X direction, the elastic and inelastic displacements tend to be distributed between the ground floor and the first one, leading to a global collapse mechanism;
- In the Y direction, the inelastic displacements tend to accumulate at the ground floor due to the buckling of the inverted V bracings. The collapse mechanism is so characterized by the formation of a soft-storey mechanism at the ground level, while the first floor remains substantially elastic;

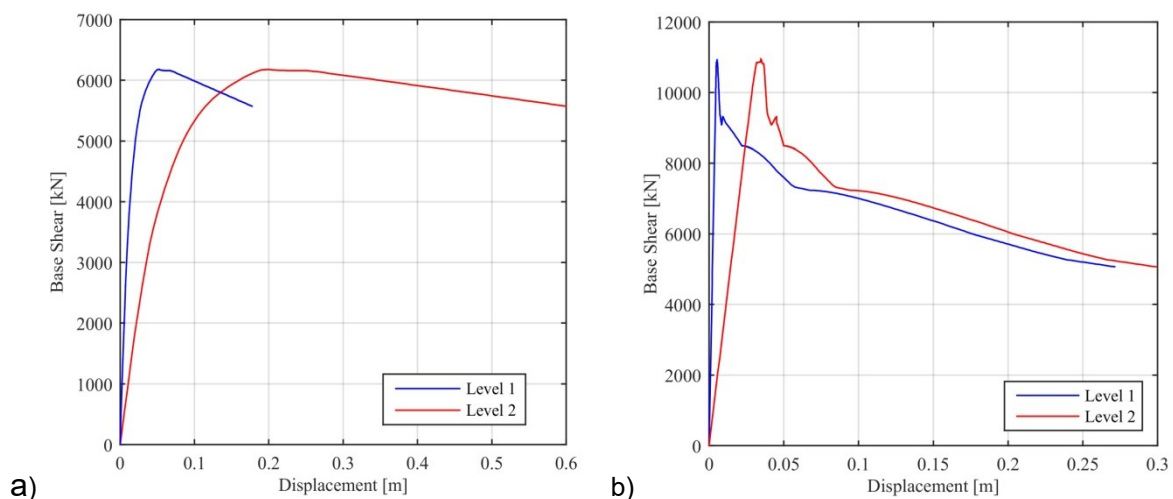


Fig. 8.7: Pushover curves associated to the uniform acceleration distribution in the a) X direction and b) Y directions

The structural performances associated to the Damage Limitation Limit State (DLS) and to the Life-Safety Limit State (LLS) were evaluated plotting the capacity curves in the Acceleration-Displacement plane together with the corresponding

Acceleration-Displacement Response Spectra (ADRS). The response spectra chosen were the Italian code NTC08 [9] Design Spectrum computed for an high Italian seismicity zone (Reggio Calabria, Lat 38.111, Long 15.647), reference period  $V_R=150$  years, with a soil type B and Probabilities of Exceedance of 63% (DLS) and 10% (LLS), which correspond to return periods of 151 and 1424 years.

The initial stiffness was assumed as the secant line passing through the axis origin and the point on the capacity curve corresponding to the 60% of the maximum base shear, see Fig. 8.8. Considering that in both X and Y direction the period evaluated adopting such initial stiffness are larger than TC, the performance points were evaluated adopting the equal displacement rule. In the X direction, the structure experiences some limited plastic deformation for the seismic action associated to the DLS (Probability of Exceedance, PoE = 63%), while it develops a complete plastic mechanism for the LLS (PoE = 10%). The expected displacement of the control point, associated to DLS limit state, is 6.2 cm while for the LLS it is 17.3 cm. In the Y direction, for the seismic action associated to the DLS, the structure does not reach the maximum strength and shows a displacement of about 2.8 cm. For the LLS, the estimated performance displacement is 8.1 cm and exceeds the capacity of the structure, corresponding to the loss of 15% of the ultimate force, highlighting that for this limit states the bracings at ground floor start to buckle.

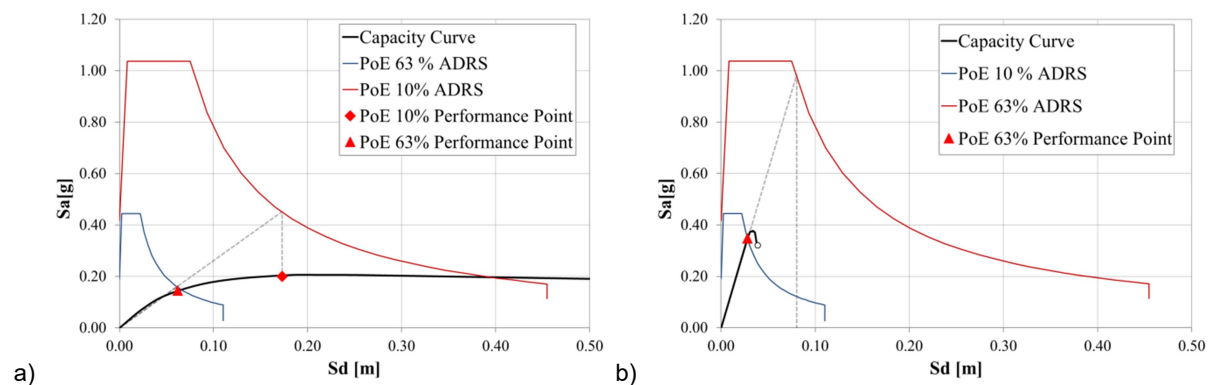


Fig. 8.8: ADRS Pushover analysis and determination of performance points for PoE 10% and 63% for the a) X and b) Y directions

## 8.4 RETROFIT OF THE EXISTING CASE STUDY BUILDING

The non-linear static analyses carried out on the current state evidenced several structural problems. The main problems affecting the building were related to the high slenderness of the bracings placed at the first floor of the Y direction, which implies an insufficiently ductile dissipating mechanism. Instead, in the X direction the building is characterized by a ductile mechanism, with seismic energy dissipation

mainly obtained through the formation of flexural plastic hinges in beams and columns.

Therefore, the proposed seismic retrofit consists in the substitution of the first floor Y direction bracing system and in the introduction of the innovative Moon Shaped Hysteretic elements (MSSH) in the end of the new brace elements.

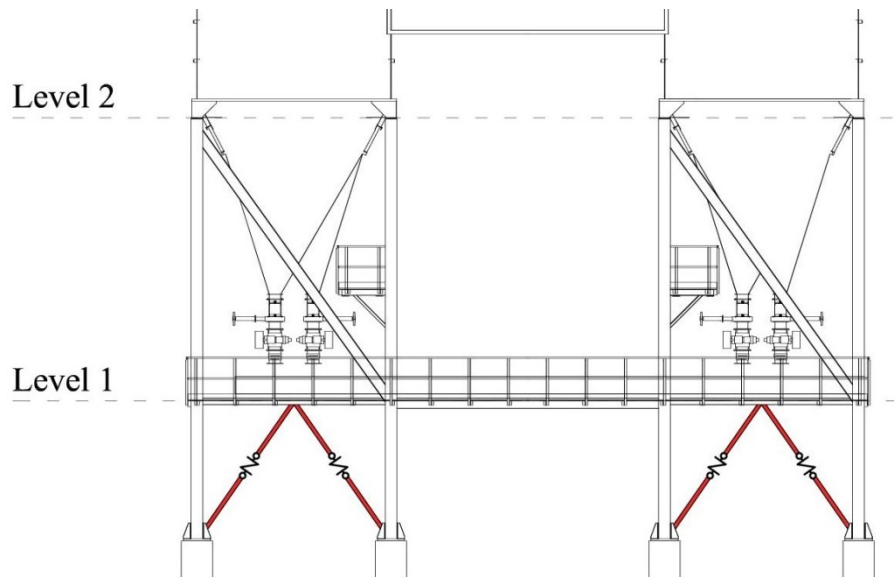


Fig. 8.9: MSSH disposition in the Y directions

The primary objective of the retrofit intervention was to increase, as much as possible, the seismic dissipation capacity and to limit the damage to the gravity structure. In order to increase the dissipation capacity, obtained through ductile mechanisms, it is necessary to avoid brittle failure mechanisms, as buckling phenomena.

With reference to Fig. 8.10, the MSSH characteristics to be defined were:

- the initial stiffness,  $k_1$ ;
- the yielding force,  $F_y$ ;
- the post-elastic stiffness,  $k_2$ ;

For the application described within this work, the characteristics of the single device were obtained from the experimental test performed, showed in Fig. 8.11 and Fig. 8.12. Starting from the characteristics reported in Table 8.2, different combination of MSSH were considered, just by varying the number of MSSH element for each brace.

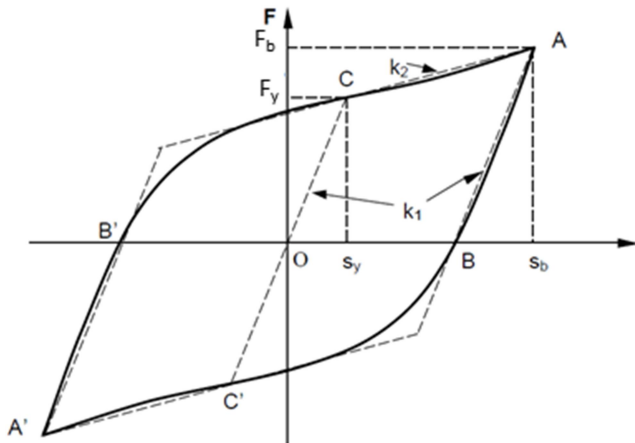


Fig. 8.10: Bilinear approximation of the hysteresis loop

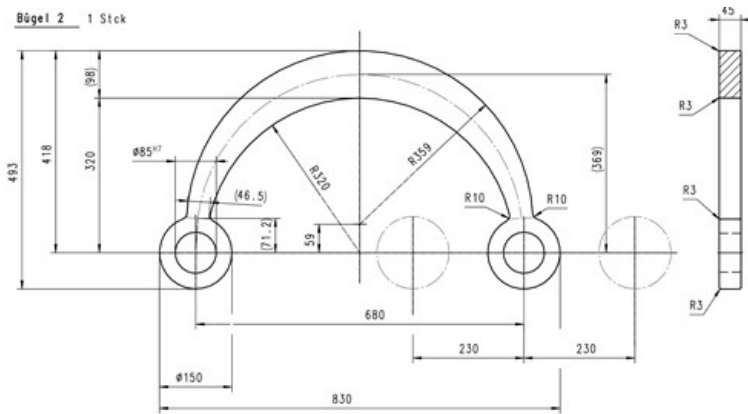


Fig. 8.11: Geometrical characteristics of the "Large" MSSH tested.

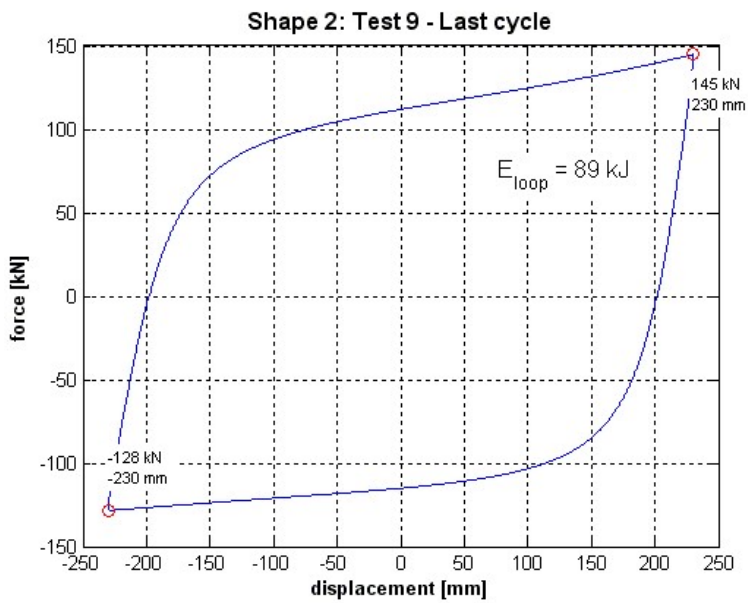


Fig. 8.12: Force-Displacement diagram of the "Large" MSSH tested.

Table 8.2: Bilinear approximation of the “Large” MSSH behavior.

$k_1$ [kNmm <sup>-1</sup> ]	$F_y$ [kN]	$k_2$ [kNmm <sup>-1</sup> ]
4.7143	115.50	0.1435

Considering the primary goal of preventing failure mechanism for the Damage Limitation Limit State (DLS), the number of MSSH elements was defined in order to assure a yielding force greater than the design one for DLS. Taking into account this limitation, at least two elements for each brace should be adopted, with the subsequent characteristics:

- $k_1 = 9.43 \text{ kNmm}^{-1}$ ;
- $F_y = 231.00 \text{ kN}$ ;
- $K_2 = 0.29 \text{ kNmm}^{-1}$ ;

Non-dissipative bracing elements were designed in capacities, taking into account the resistance of the MSSH elements. The yield strength  $N_{pl,Rd}$  of the cross section of the braces must be greater than the following value:

$$N_{Pl,Rd,brace} \geq 1.1 \cdot \gamma_{ov} \cdot N_{pl,Rd,MSSH} \quad \text{Eq. (8.1)}$$

where:

- $\gamma_{ov}$  is the over-strength factor,  $\gamma_{ov} = 1,25$  for S355 steel;
- $N_{pl,Rd,MSSH}$  is the yielding strength of the MSSH elements connected to the brace.

Braces were thus designed to resist to an axial force of 320 kN, without get into buckling. The corresponding profile, considering the length of the element, was HEA160.

Fig. 8.13: show the comparison between the capacity curves evaluated through the execution of pushover analyses on the considered building before and after the application of MSSH dissipative elements. As visible, the introduction of the innovative system in the Y direction strongly influences the global behavior of the existing building, with the following main results:

- decrease of the initial stiffness;
- decrease of the yielding strength;
- increase of the ductility and dissipation capacity;
- absence of buckling phenomena.

Indeed the curve shows a more flexible and ductile behavior with a smooth transition between the elastic and the plastic ranges and a softening post-yielding behavior. The latter is mainly due to second order effects.

Moreover, the application of the capacity spectrum method (ADSR plane) for the considered solution, shows that in the Y direction the retrofitted structure exhibited

some limited plastic deformation for the seismic action associated to the DLS (PoE = 63%), while it develops a complete plastic mechanism for the LLS (PoE = 10%). The expected displacement of the control point, associated to DLS limit state, is 5.2 cm while for the LLS it is 14.4 cm.

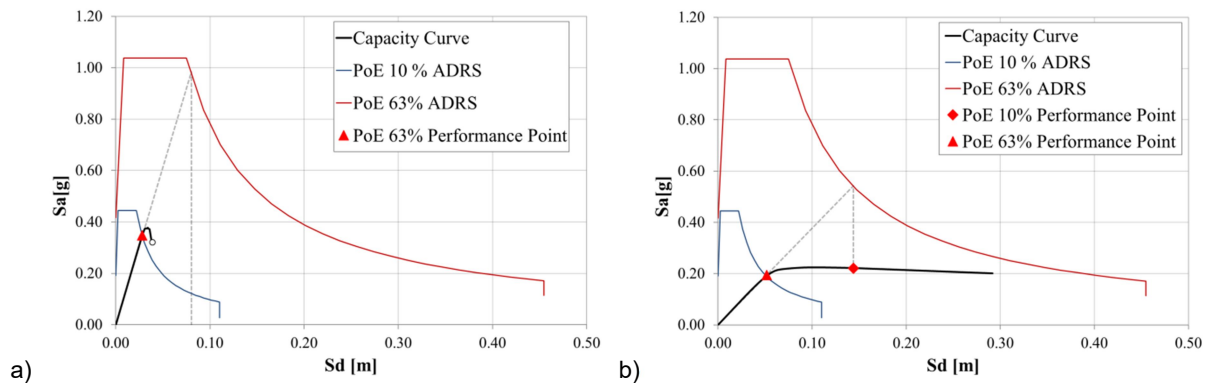


Fig. 8.13: ADRS Pushover analysis and determination of performance points for PoE 10% and 63% for the Y direction in a) current state and b) retrofitted state

It is worth noting that the application of the proposed hysteretic device allows to avoid the execution of local element strengthening, due to the decreasing of the global lateral strength. Such situation is particularly convenient when it is important to avoid any intervention on the foundations or any interruption of activities within the building.

## 8.5 CONCLUSIONS

The vulnerability analysis of the existing case study building executed with non-linear static analysis highlighted several structural problems. In particular the structure exhibited different behavior in the two main directions, with a ductile mechanism in X direction and a brittle mechanism in the Y one. In the latter, the presence at the ground floor of under-sized inverted-V bracing system caused the occurrence of buckling phenomena, resulting in the brittle failure before reaching the performance point for the Life Safety Limit State.

The design of retrofit interventions were then concentrated in the Y direction. The application of the innovative MSSH (Moon Shaped Hysteretic Device) was then analyzed to evaluate the influence on the global structural behavior of the building. The mechanical characteristics of the device resulted by the executed experimental tests, and the number of elements were defined to avoid the damage of the element for the Damage Limitation Limit State.

The introduction of the dissipative devices allowed a more flexible and ductile mechanism, avoiding the buckling phenomena, and the decrease of the solicitations in correspondence of the existing gravity structure elements.

## 8.6 REFERENCES

- [1] Morelli F., Piscini A., Salvatore W. (2017). Seismic behavior of an industrial steel structure retrofitted with self-centring hysteretic dampers. *Journal of Constructional Steel Research* 139 (2017) 157-175. <https://doi.org/10.1016/j.jcsr.2017.09.025>
- [2] Braconi A., Morelli F., Salvatore W. *Development, design and experimental validation of a steel self centering device (SSCD) for seismic protection of buildings*. *Bulletin of Earthquake Engineering* 10 (6), 1915-1941, 2012.
- [3] S. Mazzoni, F. McKenna, M. H. Scott, G. L. Fenves, et al. *Open System for Earthquake Engineering Simulation (OpenSEES), OpenSEES Command Language Manual*, Pacific Earthquake Engineering Research (PEER) Center, 2007.
- [4] European Committee for Standardization. *Eurocode 3: Design of steel structures - Part 1-1: General rules and rules for buildings*. En1993-1-1, August 2005.
- [5] A. Braconi, S. Caprili, H. Degee, M. Guendel, M. Hjjaj, B. Hoffmeister, S.A. Karamanos, Efficiency of Eurocode 8 design rules for steel and steel-concrete composite structures, *J. Constr. Steel Res.* 112 (2015) 108–129. doi:10.1016/j.jcsr.2015.04.021.
- [6] M. Badalassi, A. Braconi, L. Cajot, S. Caprili, M. Gündel, M. Hjjaj, B. Hoffmeister, Influence of variability of material mechanical properties on seismic performance of steel and steel–concrete composite structures, *Bull. Earthq. Eng.* (2016). doi:10.1007/s10518-016-0033-2.
- [7] European Committee for Standardization, *Eurocode 8: Design of structures for earthquake resistance - Part 1: General rules, seismic actions and rules for buildings*. EN 1998-1, December 2004.
- [8] ATC-40, 1996 Applied Technology Council 1996, ATC40, *Seismic evaluation and retrofit of concrete buildings*, California Seismic Safety Commission, Proposition 122, Seismic Retrofit Practices Improvement Program, Report SSC 96.
- [9] *Norme Tecniche per le Costruzioni*, D.Min. Inf. 14 gennaio 2008, *Gazzetta Ufficiale* n. 29 of february 4th 2008 - Suppl. Ordinario n. 30. In Italian.